SAPIENZA
UNIVERSITÀ DI ROMA

Topology of local information dynamics during motor decision in the premotor cortex of primates.

Facoltà di Medicina e Psicologia

Dottorato di Ricerca in Neuroscienze del Comportamento
curriculum: Behavioural Neurophysiology – XXXIII Ciclo

Candidate

Giampiero Bardella
ID number 1326633

Thesis Advisor

Prof. Stefano Ferraina

2019/2020

Thesis defended on 22/02/2021

Evaluation: Ottimo

Topology of local information dynamics during motor decision in the premotor cortex of primates.
Ph.D. thesis. Sapienza – University of Rome

© 2020 Giampiero Bardella. All rights reserved

This thesis has been typeset by LaTeX and the Sapthesis class.

Author's email: giampiero.bardella@uniroma1.it

Contents

Preface

"To develop the skill of correct thinking is in the first place to learn what you have to disregard. In order to go on, you have to know what to leave out: this is the essence of effective thinking".

K. Goedel, *Letter to Hao Wang, 15th March 1972*

"I know. But I do not have the proof. I don't even have clues".

Pier Paolo Pasolini, *Corriere della Sera, 14th November 1974*

Comoplex systems are very large systems comprising millions of agents interacting with each other and whose collective behaviour cannot be understood from the elementary features. In this sense the brain is the complex system *par excellence*: hundreds of billions of densely packed electrically excitable cells called neurons with hundred of millions of connections each. All exchanging electrochemical signals over short and long distances every few milliseconds and functionally interacting over multiple scales of time. Within this apparent chaotic bundle some deep questions arise. A single neuron is not in itself "intelligent" but a vast network of neurons can think, perceive, remember and generate the many extraordinary phenomena that they are collectively known as mind.

How the mind can emerge from the interconnection between different neurons? How can single interactions between neurons organize themselves into manifestations

collectively coherent like perception and movement? How the coordinated responses to sensory stimuli, the realization of complex movements and the organized selection and monitoring of goal-oriented actions are possible? Ultimately, how the set of processes known as *cognitive control* of behaviour are still possible? Many theoretical hypotheses have been put forward over the years in the form of neural network models but despite the increase in the availability of experimental data we are still far from finding the key of the coil.

Cognitive control is the processes by which the brain, using sensory input plus information already stored in memory, generates most of our motor actions. How the brain internally subdues these mechanisms and map them into the concerted activity of neurons is one of the challenging problems of modern science and most of the related questions are still unanswered. A vital component of cognitive control is response inhibition. Response inhibition is the ability to select among alternatives, suppress inappropriate, unsafe or no longer required actions, in response to changes in internal states or changes in the environment. To clarify the concept, let's imagine a researcher who, working late at the department, decides to take a little cigarette break. Being alone he decides to stay at doorstep of the lab. He then: (1) takes the cigarette, (2) puts it in his mouth, (3) takes the lighter out of his pocket but just a moment before lighting it, looking up, notices the no-smoking sign. He thus promptly stops and decide to go and smoke a bit farther. Cognitive control of motor activity hence determines subconsciously, and within seconds, which patterns of movement will be used together to achieve a complex goal that might itself last for many seconds. Therefore, the ability to stop actions is crucial for flexible, adaptive, goal-directed behavior and, ultimately, decision making. While understanding how the brain processes movement inhibition is of great scientific interest *per se*, the growing attention in this research area is also due to its clinical implications. Response inhibition is indeed impaired in various psychiatric disorders, such as schizophrenia (Hughes et al., 2012; Thakkar et al., 2011), attention deficit hyperactivity disorders (Lipszyc and Schachar, 2010; Oosterlaan et al., 1998; Pani et al., 2013), obsessive-compulsive disorder (OCD; Chamberlain et al., 2005 and in neurological diseases such as Parkinson's Disease (Gauggel et al., 2004; for a review see Bari and Robbins, 2013; Verbruggen and Logan, 2008) and cerebellar patients (Olivito et al., 2017). A complete understanding of inhibitory control would hence eventually help clinical research finding treatments for motor and cognitive disorders. In this thesis we will show evidence further supporting the role of a specific frontal region, the dorsal premotor cortex (PMd), in the control of arm movements, stepping

forward the knowledge on the neuronal mechanism often derived from single units approaches. More specifically, using a combined mathematical framework of graph and information theory we will depict a detailed representation of the local PMd network which will help clarify the contribution of different neuronal assemblies to decision making. In presenting the work, we decided to adopt the following structure. The Introduction consists of two main sections: a first section 1.1 in which we will contextualize the work from the point of view of behavioral neurophysiology and a second section 1.2 where we will introduce the mathematical concepts used for data analysis of Study 1 and Study 2. The last section will be devoted to Conclusions and a general discussion.

Introduction

"Science is build up of facts, as a house is with stones. But a collection of facts is no more a science than a heap of stones is a house".

H. Poincare

1.1 Neurophysiological framework

The stop-signal task

One of the main scientific questions of the neurosciences is how motor decision-making and, more in general, behavioural control are coded at the circuitry level in the brain. One of the most used behavioural paradigms in experimental and clical settings to investigate motor control is the countermanding or stop-signal task (Logan and Cowan, 1984) (for general reviews see Matzke et al., 2017; Verbruggen and Logan, 2009). The task requires subjects to promptly generate a response (typically investigated as an eye or hand movement) after the presentation of a Go signal (go or no-stop trials). Sporadically, the Go signal is followed by a Stop signal after a variable and unpredictable delay (stop signal delay, SSD) instructing subjects to withhold their ongoing response (stop trials). The performance during stop trials is well explained by the so called *race model* (Logan and Cowan, 1984). This behavioural model suggests for a race between two processes, the go process, which is triggered by the presentation of the Go signal, and the stop process, which is triggered by the presentation of the Stop signal. In stop trials, the movement will be successfully inhibited (correct stop trials) only if the stop process wins over the go process, otherwise movement will be executed (wrong stop trials) (Fig. 1.1

A). When combining the stop-signal task and the race model, two measures of the inhibitory performance can be extracted. One is the probability to respond with a movement on stop trials in relation to the difficulty of the race. Indeed, the ability to inhibit the movement is probabilistic, depending on the length of the SSD (Fig. 1.1 B). Typically, the shorter the SSD the lower (higher) the probability to respond (inhibit), reflecting the level of motor preparation when the Stop signal occurs. The second measure is the covert latency of the stop process: The Stop-Signal Reaction Time (SSRT, Fig. 1.1 C), i.e the time it takes for subjects to successfully inhibit a planned movement. The SSRT has been demonstrated being a key measure of the behavioral and neuronal processes involved in the inhibitory control (Aron and Poldrack, 2006; Logan and Cowan, 1984; Logan et al., 2014; van den Wildenberg and van der Molen, 2004), in the development and decline of inhibitory ability across the life span(Chevalier et al., 2014; Williams et al., 1999), in neurological disorders (Brunamonti et al., 2012; Brunamonti et al., 2011; Pani et al., 2013) and impulsive behaviours(Ersche et al., 2012; Schachar and Logan, 1990; Whelan et al., 2012). Typically, the longer the average SSRT, the more impaired (or less developed) the inhibitory process.

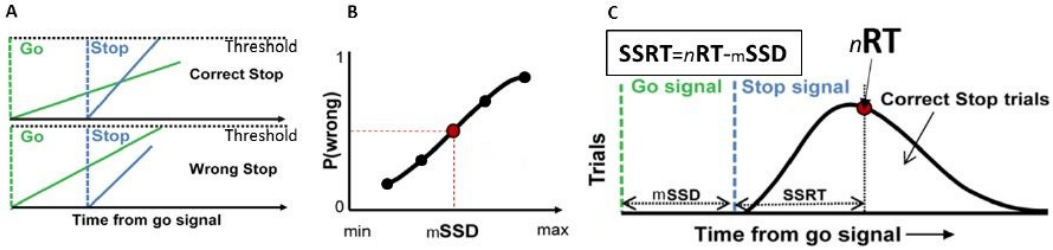

Figure 1.1. Stop Signal Task. A) Graphical representation of the race model; B) probability of responding on stop trials as a function of the SSD duration. C) The SSRT is estimated by setting 3 variables: the no-signal trials RTs, the probability of responding, $P(wrong)$, to the Stop signal, and the mean SSD (mSSD). The SSRT corresponds to the nth no-signal RT, where n results from the mathematical product of the distribution of ordered no-signal RTs and the overall probability of responding. The SSRT can then be calculated by subtracting the mean SSD from the nth no-signal RT.

Where inhibition arise from?

The neural circuitry of response inhibition: what is known

Although the neural source of inhibitory control (if it exists in the strict sense) is still unknown at the cellular level, important insights into mechanisms involved in motor inhibition have come from studies on the oculomotor system (for a review see Ersche

et al., 2012; Schall et al., 2017). The employment of a saccade stop-signal task led to the identification of two different neuronal populations in the frontal eye field (FEF; Hanes et al., 1998), a prefrontal oculomotor area, and superior colliculus (SC; Paré and Hanes, 2003) in the midbrain, whose activities control saccade generation and inhibition. The different activity patterns of these neurons have been described as reflecting, at the neuronal level, the go process (movement neurons) and stop process (fixation neurons) of the race model (Boucher et al., 2007; Paré and Hanes, 2003). Movement neurons are active during saccade preparation and execution, while fixation neurons are active while gaze is held steady. More extensively, the stop-signal performance in the oculomotor system involves a fronto basal ganglia and superior colliculus network (Schall et al., 2017), in which some neurons in FEF and SC, substantia nigra pars reticulate (SNr, an output of the basal ganglia) and in the brainstem can be considered as "inhibitory gates" for producing eye movements (for further details about the input/output connection of this network please see Stuphorn, 2015). Studies in the FEF and SC of monkeys performing the saccade version of the stop-signal task has been crucial in establishing criteria that neuronal activity must satisfy to be defined as directly involved in the inhibitory control. First, the activities must modulate differently during movement execution (go trials) and inhibition (stop trials). Second, the difference in the modulation must occur before the end of the SSRT, i.e. the time required to inhibit the movement (see previous paragraph). If a difference occurs after the SSRT, the activity it is not directly linked to the inhibitory process, but rather to other processes, like performance monitoring (Sajad et al., 2019; Stuphorn and Schall, 2006).

While advanced knowledge have been reached about the neuronal mechanisms that rule eye movement and inhibition, including clearly defined input-output connectivity patterns of single neurons, the same cannot be said for the inhibitory processes in the skeletomotor system. This is partially due to the higher level of bio-mechanical complexity of the skeletomotor system compared to the oculomotor system. Indeed, eye movements are controlled by only six muscles and have limited features variability (like speed or amplitude) while an higher muscle complexity is required in the skeletomotor system. Just to give an idea, think about the level of neuro-muscular synergy required to perform a correct tennis serve or the level of coordination of a drummer playing a solo. Also everyday tasks which we unconsciously perform, such as reaching a glass of water, writing or even talking can only be performed via an harmonious, smooth and progressive control of a broad spectrum of muscles (for a review see Scott et al., 2015 and Archambault et al.,

2015). The stop-signal task applied to the arm reaching movement in humans and monkeys, together with variations applied to rats, has provided precious insights into the neuronal mechanisms underlying movement inhibition in the skeletomotor system. Evidence suggest that the ability to control movements requires the integrity of a complex cortico-basal ganglia pathway that includes frontal regions such as the inferior frontal cortex (IFC), medial frontal areas such as supplementary (SMA) and pre-supplementary (pre-SMA) motor areas, premotor cortex (PM), primary motor cortex (M1)(see Battaglia-Mayer et al., 2014 for a review about the role of cortical regions) and subcortical structures such as striatum, pallidum, thalamus and the subtalamic nucleus (STN) (see Stuphorn, 2015 for a general review). IFC, especially in the right hemisphere, has been proposed as one of the main frontal lobe regions regulating this network in primates. Neuroimaging studies showed an increased involvement of the IFC during inhibition (Aron and Poldrack, 2006; Rubia et al., 2003). Patients with damage to the IFC showed an impairment of their inhibitory ability proportional to the damage extension (Aron et al., 2003). In line with this finding, the temporary inactivation of the IFC by transcranial magnetic stimulation (TMS) impaired the ability to inhibit but not to execute the movement (Chambers, Bellgrove, et al., n.d.; Chambers et al., 2007). Despite this evidence, the specific function of the IFC in stopping is still debated and different roles have been attributed to it. The direct role of IFC is debated, some argue for a direct role of IFC in response inhibition (Aron et al., 2003), others have suggested for a role of this region in either guiding attention to events relevant to the task goal (Corbetta and Shulman, 2002; Sharp et al., 2010), or in encoding behaviorally task rules (Koechlin et al., 2003). It is also possible that sub-regions of IFC are responsible for each of the aforementioned functionalities, giving rise to its heterogeneous roles in cognitive control of movement inhibition (Levy and Wagner, 2011). In fact, a more dorsal and posterior region, in or near the inferior frontal junction may have more stimulus processing and attention functions, while more ventral and anterior portions are more likely involved in inhibiting or changing behavioral responses (Chikazoe et al., 2009; Sebastian et al., 2017; Verbruggen and Logan, 2009). In this scenario has been shown from Floden and Stuss (Floden and Stuss, 2006) that damages of right superior medial frontal areas, specifically supplementary and pre-supplementary motor areas, impairs the inhibitory control in the stop-signal task. The authors hypothesized that the superior medial and lateral regions of the right frontal lobe participate in response inhibition depending on task requirements: superior medial regions are crucial for rapid inhibitory control, whereas the right lateral region allows

for a more controlled stop signal performance (Aron et al., 2003, involving attentional factors (Bellgrove et al., 2004; Floden and Stuss, 2006). Similar conclusions can be drawn from the functional magnetic resonance (fMRI) study of Sharp et al. (2010), in which healthy subjects were presented with a version of the stop-signal task that allowed to separate the contributions of frontal regions to attentional capture, response inhibition, and error processing. It is worth stressing that the superior medial regions have the potential to influence the generation and control of movement and to act as a possible inhibitory gate since directly project to the spinal cord (Dum and Strick, 1991). The above demonstrates that the contribution of prefrontal regions to the inhibitory functions is still debated.

Much clearer evidence instead attributes a pivotal role in arm movement inhibition to basal ganglia structures (see Stuphorn, 2015 for a review). The most plausible scenario is that the cortical areas implicated in response inhibition would send a stop command to basal ganglia structures, which would interrupt the go process (likely at the level of the internal globus pallidus, GPi), decreasing the excitability of the thalamo-cortical projections necessary for the movement execution (Aron, Durston, et al., 2007; Li et al., 2008) and acting on motor cortices. The resulting hypothesis is that competing pathways within the basal ganglia would reflect the go and stop processes of the race model (Aron, Durston, et al., 2007; Aron and Poldrack, 2006; Schmidt et al., 2013). One of the most important component of the basal ganglia, necessary for movement inhibition, is the subthalamic nucleus (STN; Aron and Poldrack, 2006; Forstmann et al., 2012; Hikosaka and Isoda, 2010; Li et al., 2008; Munakata et al., 2011). The STN receives inputs from the pre-SMA and the IFC through the "hyperdirect" pathway (Nambu et al., 1996; Nambu et al., 2002) and through a direct pathway as confirmed by tractography study in humans (Aron, Behrens, et al., 2007). It has been proposed that either the right IFC or the pre-SMA projections to the STN, would allow for fast inhibition of ongoing actions by increasing inhibitory signals from the GPi, also receiving input from the STN, thus suppressing basal ganglia output (Nambu et al., 2002; Coxon et al., 2006). Moreover, fMRI and lesion studies (Aron and Poldrack, 2006; Eagle et al., 2008; Obeso et al., 2014; Rieger et al., 2003), together with deep-brain stimulation of the STN in patients with Parkinson's disease (Van Den Wildenberg et al., 2006), support the crucial role of these areas in response inhibition. Of outstanding interest are the results observed by Schmidt et al. (Schmidt et al., 2013) in animal models. They recorded single-unit activity from multiple basal ganglia nuclei of rats, including STN and substantia nigra pars reticulata (SNr), which is the analogous of GPi in

rodents for head control and a key structure for eye movement control in primates (Hikosaka et al., 2000). In STN, neurons increased their activity quickly in response to the Stop signal on both successful and failed stop-signal trials, confirming its involvement in action inhibition. In contrast, SNr neurons were activated after the Stop signals only in trials with successful inhibition, supporting the role of these areas in motor inhibition and the race model assumption: to suppress a response, Stop signal information must be transmitted from STN to SNr/GPi before increased striatal inhibitory projections to SNr/GPi allow to start the movement. These results strongly support the key role of basal ganglia in movement generation and inhibition, as well as the hypothesis that the motor output on stop trials, i.e either the movement execution or inhibition, relies on a competing race between the go and stop processes.

Even it is not yet a standard view, it is undoubtedly worth spending some lines on the role played by a structure with which the basal ganglia is densely connected: the cerebellum (see Bostan and Strick, 2018 for a review). Recent neuroanatomical findings using viral transneuronal tracers have indeed shown that the latter could be involved in processes traditionally associated with the former (Bostan et al., 2013). It is considered that the interplay between the cerebellum and the basal ganglia could contribute to fine executive control of motor generation: frontal cortical areas send movement-related commands both to the cerebellum and to the basal ganglia; both of these subcortical regions send signals back to the primary motor cortex (M1) via the thalamus, allowing the execution of the action or its suppression (Alexander and Crutcher, 1990; Aron and Poldrack, 2006; Brunamonti et al., 2014). Only recently a neuropsychological study administered the stop-signal task to patients with focal cerebellar damage (Brunamonti et al., 2014). It was found that cerebellar patients did not experience deficits in the duration of the stop process (i.e. similar SSRTs values observed between cerebellar and control subjects). Nevertheless, they had specific inhibitory deficits, failing more often than controls in triggering the stop process, and requiring an increased time to adjust their behavior after the stop trial presentation. These data suggest that the cerebellum could contribute to executive control of voluntary actions, influencing the cortical-basal ganglia-cortical loops.

In this picture, a staple is the role of motor cortices. Indeed, it is widely accepted that the activation of corticospinal neurons in M1 and in dorsal premotor cortex (PMd), lead to muscle contraction (Aron, Behrens, et al., 2007; Cheney and Fetz, 1980; Fetz and Cheney, 1980) either through the direct or indirect (through interneurons)

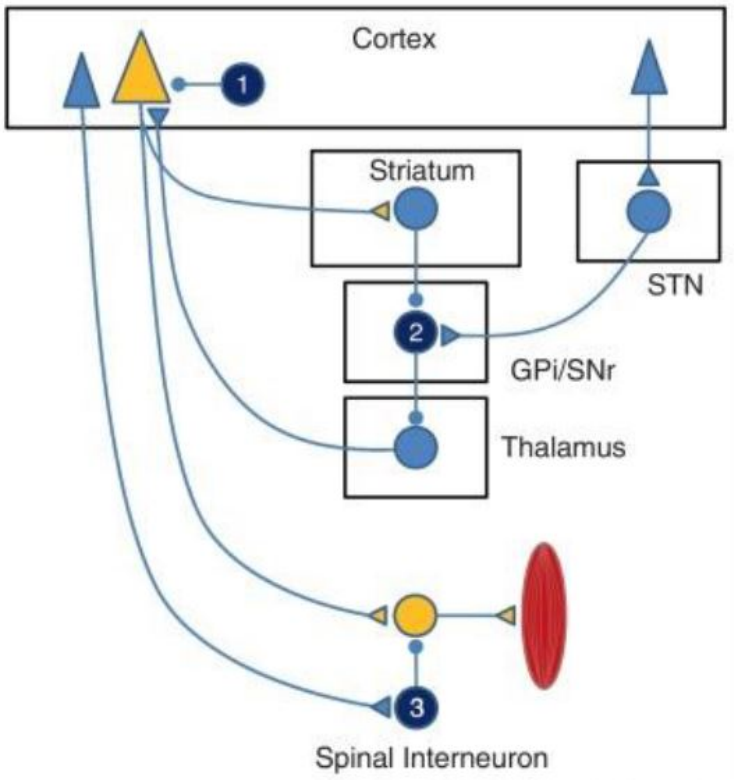

Figure 1.2. Potential mechanisms through which cortico-basal ganglia interactions control movement inhibition in the skeletomotor system (from Stuphorn, 2015). Three possible mechanisms for inhibiting the movement generation. **Upper panel**: The activity of the corticomotor neuron could be suppressed by direct inhibitory connections from cortical interneurons (indicated by the dark blue neuron 1). **Middle panel**: The motor cortex sends connections to the basal ganglia through the direct pathway to lift the tonic inhibition of the globus pallidus internal/substantia nigra pars compacta (GPi/SNr) (dark blue arrow 2). Activation of neurons in the subthalamic nucleus (STN) through the hyperdirect pathway could reactivate the GPi/SNr neurons and so reduce activity in the motor cortex via recurrent connections through the thalamus. **Bottom panel**: Other corticospinal neurons could activate inhibitory interneurons in the spinal cord (dark blue arrow 1) that suppress the activity of motor neurons.

activation of motor neurons in the spinal cord. When the movement is inhibited, the excitability in corticospinal neurons of M1 must be modulated. This modulation can be obtained at the cortical level by recruiting inhibitory interneurons, by targeting interneurons at the level of the spinal cord, by involving subcortical pathways looping back toward M1 (see Figure 1.2). Strongly connected to M1 is the area objective of the thesis, the PMd, which has been repeatedly hinted as crucial for inhibitory control.

The injection of GABA antagonists to the PMd of monkeys reduces their ability to inhibit movements (Sawaguchi et al., 1996), suggesting that in the PMd, also participating to the movement execution through corticospinal neurons, GABAergic inhibition is responsible of the movement suppression. Some TMS studies on M1 and PMd in humans, have shown a reduction of cortical excitability when the movement was inhibited (Coxon et al., 2006; Duque et al., 2012; Parmigiani and Cattaneo, 2018). Furthermore, patients with PMd lesions showed a reduction of their inhibitory performance (Picton et al., 2007). All together, these studies corroborate the role of PMd in the inhibitory process. Figure 1.3 summarizes some of the input-output connections involving PMd, also suggesting its crucial role into movement inhibition through its outputs. On one hand, PMd recives direct inputs from the posterior parietal cortex (PPC) where are believed to be the sites of evidence accumulation in decision processes and where visuospatial signals are amply represented (Gold and Shadlen, 2007; Huk and Shadlen, 2005; Kim and Shadlen, 1999). On the other, PMd also takes part in a prefrontal-BG network that might subserve both the inhibition and decision-making processes. In this network, prefrontal regions would translate visual information (in the case of the stop-signal paradigm, the stop signal) into a decision to inhibit and, in turn, would send (directly and/or through the basal ganglia) an inhibitory command to the PMd. The relationship between PMd and BG is not limited to this network but these areas establish separate key interactions. PMd receives indirect influences from different nuclei of BG such as the GPi/GPe and the SNr, also establishing mutual connections with the STN and the striatum (see Hoshi, 2013 for a review). Along these connections, BG could send to the PMd not only information related to movement execution/inhibition, promoting movement inhibition trough the indirect pathways, but they could participate in perceptual decision-making processes. Indeed, although the BG were much earlier proposed to be the central substrate for action selection and habit learning, growing evidences suggest their active participation, through cortical interactions, in perceptual decision-making (Ding and Gold, 2013; Wei et al., 2015). Thus it is legitimate to hypothesize that PMd leads to movement control by interaction with M1 local computation, basal ganglia structures and spinal cord interneurons.

Mirabella et al. in 2011 showed for the first time that single neurons in the PMd of monkeys contribute to motor initiation and suppression during the stop-signal task. The authors found the presence of two distinct neuronal populations directly related to movement inhibition, whose activities differently modulated before the end of

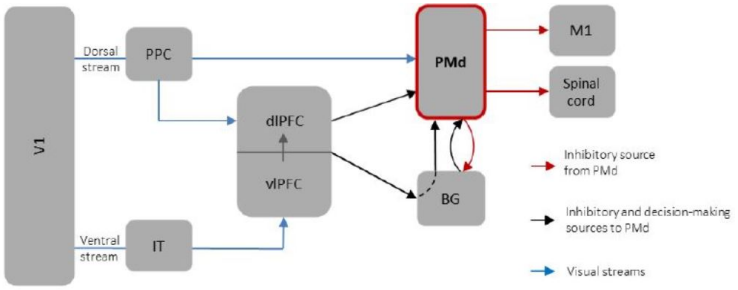

Figure 1.3. Brain network centered on the dorsal premotor cortex (PMd) potentially involved in decision-making and inhibitory processes. PPC, posterior parietal cortex; IT, inferotemporal cortex; V1, primary visual cortex; dlPFC, dorsolateral prefrontal cortex; vlPFC, ventrolateral prefrontal cortex; PMd, dorsal premotor cortex; BG, basal ganglia; M1, primary motor cortex. PMd receives direct inputs from PPC, where visuospatial signals are amply represented and where are believed to be the sites of evidence accumulation in decision processes. PMd is also part of a prefrontal-BG network that it thought to subserve both the inhibition and decision-making processes. Prefrontal regions would translate visual information (in the stop-signal task: the stop signals) into a decision to inhibit and, in turn, would send (directly and/or through the basal ganglia) an inhibitory command to the PMd. PMd itself receives indirect influences from different nuclei of BG such as the GPi/GPe and the SNr, also establishing mutual connections with the STN and the striatum. Along these connections, BG could send to the PMd not only information related to movement execution/inhibition, promoting movement inhibition trough the indirect pathways, but they could also participate in perceptual decision-making processes. Although the BG were much earlier proposed to be the central substrate for action selection and habit learning, growing evidences suggest their active participation through cortical interactions in perceptual decision-making. Thus, we could also hypothesize that PMd activity leads to movement control by interaction with M1 local computation, basal ganglia structures, and spinal cord interneurons. Blue arrows represent ventral and dorsal visual streams which convey visual information. The ventral stream conveys visual information to prefrontal cortex through the inferotemporal cortex (IT), and it is involved with object identification and recognition. The dorsal stream conveys visual information to the dorsolateral prefrontal cortex (dlPFC) and the PMd through the posterior parietal cortex (PPC), and it is involved with processing the object's spatial location. Black arrows indicate projections from prefrontal regions and BG to the PMd. These projections could be involved in the processing of both inhibitory commands and decision-making-related information. Red arrows represent interactions with the primary motor cortex (M1), BG and spinal cord interneurons for inhibitory control.

the SSRT when the movement was generated and inhibited. One population of neurons, following the Go signal, increased their activity up to a threshold necessary

for the movement generation (go trials). During stop trials, the movement was successfully inhibited only if the activity did not reach the threshold after the Stop signal presentation. Indeed, the activity of this neuronal population decreased after the Stop signal presentation during stop trials. The other population was instead associated with a greater increase of activity – after the Stop signal and before the end of SSRT – during movement inhibition (stop trials) compared to the activity during movement execution (go trials). This finding suggested that the first neuronal population, showing a movement-related activity negatively modulated in stop trials, could correspond to PMd neurons targeting interneurons in M1 or spinal cord, while the second neuronal population would represent PMd inhibitory interneurons, controlling the activity of the first neuronal population. Following this schema, the higher level of activity in the second neuronal population during movement inhibition would be necessary to prevent the increase of activity in the first neuronal population, and the corresponding movement execution. An alternative interpretation is that the decrease of activity of the first neuronal population on motor cancellation would correspond to the suppression of agonist muscles related to the movement, while the increase of the second neuronal population would correspond to the activation of the antagonist muscles. While the second interpretation is arguable, since contrasting results have been found (Kudo and Ohtsuki, 1998; Scangos and Stuphorn, 2010), evidence that further support the M1/PMd interaction comes from electroencephalographic (Swann et al., 2009) and electrocorticographic (Mattia et al., 2012) recordings from M1 and PMd cortex of epileptic patients. Hence, the prevailing hypothesis is that motor cortices more likely represent final nodes of the inhibitory network, in which inputs from other frontal and basal ganglia structures are processed.

1.2 Mathematical framework

The pioneering work of Ramon y Cajal over a century ago shaped the way modern science think about the nervous system. Indeed, since his *wiring diagrams*, that specified the direction and flow of neural signals (Garcia-Lopez et al., 2010), understanding brain functional connectivity has been a persistent ambition of neurosciences. It should certainly not be forgotten that nineteenth and twentieth century neuroscientists (Ramon y Cajal, Golgi, Meynert, Wernicke, Flechsig, and Brodmann) were well aware of the importance of connectivity and networks in understanding nervous systems but it is over the past 25 years that these concepts has been mathematically

formalized and that this research area has assumed a prominent place with the growing field of the so-called *connectome*. The term connectome was initially used to define the identification of all possible pairwise anatomical connections between cellular elements of the brain (Hagmann et al., 2007; Sporns and Kötter, 2004; Sporns et al., 2005,Fornito et al., 2016). The exponential development of research in this area combined with greater availability of data in the technological (Mahmud, Cecchetto, et al., 2018) and biological sciences has led to the development of new tools for the representation and investigations of a more general concept of the connectome. This includes the study of the anatomical connections between large-scale brain areas as well as between individual neurons, the functional interactions revealed both by the slow fluctuations of cerebral blood oxygenation measured with functional magnetic resonance imaging (fMRI, below 0.1Hz) and by the fast high-frequency neuronal oscillations detectable with invasive (over 200Hz) and noninvasive (up to 200Hz) electrophysiology. Thus, the current goal of connectomics has become quantifying, visualizing, and understanding the brain organization across multiple scales of space and time. The rise of connectomics can be better understood if we think of the great growth of the interdisciplinary fields of network science in general from the 1980s to today.

One of the first modern uses of connectomics is due to the work of White and colleagues that in 1986 mapped the complete nervous system of the nematode *C. elegans* (White et al., 1986). Their effort, which took more than 10 years to be completed, led to the creation of a large dataset on anatomical connectivity at a cellular scale that has since been a benchmark for many studies allowing for a great leap forward in the field (Chen et al., 2006; Nicosia et al., 2013; Towlson et al., 2013; Varshney et al., 2011). Indeed, the latest mathematical conceptualizations of complex networks have brought new tools to analyze and understand the most disparate complex systems: from internet to transportation networks, from interconnections between financial agents to the interaction between proteins within a cell, from microchip circuits to social interaction networks. In the next paragraphs we will give a brief overview of the state of the art of network science applied to the brain. We will also provide a quick glossary of the mathematical framework used in the thesis: graph theory coupled with information theory.

The brain as a complex network

As stated in the first sentence of the preface, all complex systems share the remarkably feature of showing properties not deductible from the behaviour of their single

components. They instead show signatures of a nontrivial organization, somewhere halfway between completely random and completely regular. Distinctive features of complex systems can be found all over the place, from the structure of societies (Facchetti et al., 2011) and economies (Tacchella et al., 2013) to infrastructural systems (Milanovic and Zhu, 2018) and molecular interactions occurring within biological organisms (Albert and Barabási, 2002; Newman, 2003). Complex networks are the most immediate mathematical representation of complex systems. Hence the brain can be modeled as such: from the smaller scales in which the connected elements are single neurons to the larger great specialized structures (van den Heuvel and Hulshoff Pol, 2010). Thus, one of the biggest challenges in studying brain networks and complex systems in general is to be able to identify an intermediate level of dynamic organization between that of the individual units and that of the system as a whole.

In representing the brain as a network several choices are possible, each of which depends on which aspect of the connections between the elements one intends to privilege. If we want to represent the synaptic junctions between individual neurons or the anatomical pathways between populations of neurons the network is called *structural*. If instead, as in the present work, the measure of interest is the correlated dynamic activity of neurons or ensemble of neurons we speak of a *functional* network. In this work we treated also another type of network, the one obtained when measuring the information exchanged between neuronal units, which is called *effective*.

The use of complex networks theory to the brain began from the large scale. Indeed, the first representation of a cortical area as an actual connected structural network is due to Felleman and van Essen (Felleman et al., 1991) who generated a connectivity matrix for the macaque visual cortex collating tract tracing data from a large number of previous studies. An year later, again from tract tracing data of macaque visual cortex, Young provided the first conscious representation of a brain network. The real turning point, however, came with the seminal work of Watts and Strogatz in 1998 which is the first methodological bridge between neuroscience, complex networks science and graph theory. The authors used graph theory tools to analyse the *C. elegans* connectome, suggesting the degree of universality of its properties as a complex network. It was around 2005 that graph theory functional measures began to be applied to studies involving humans thanks to a series of important works on humans using functional magnetic resonance imaging (fMRI), Magnetoencephalography (MEG), Electroencephalography (EEG) and diffusion magnetic resonance imaging

data (Achard et al., 2006; Eguíluz et al., n.d.; Hagmann et al., 2008; M. Kaiser and Hilgetag, 2006; Salvador et al., 2005; Sporns and Kötter, 2004; Sporns et al., 2005; Stam, 2004). Going into the details of this line of literature is beyond the scope of the thesis but it must be emphasized that this kind of works has both promoted the deepening of some aspects of complex networks theory and greatly favored its diffusion in neuroscience. Moreover, these researches have helped to translate Watts and Strogatz quantitative results by highlighting how the brain shares with many complex systems in nature some non-trivial network properties that can be generalized across different species. From what has been said it is quite clear that since the mapping of the *C. elegans* connectome the vast majority of contemporary research on brain networks has focused on macro scale analyzes. Some exceptions come from mesoscale studies on tract-tracing data from mouse, cat and macaque that mostly focused on estimation of anatomical connectivity (Kennedy et al., 2013; Markov et al., 2014; Oh et al., 2014; Scannell, 1997; Sporns and Kötter, 2004; Stephan et al., 2001; Zingg et al., 2014). On the microscale the studies have been very scarce and limited to the investigation of cellular networks of model organisms such as the *Drosophila* (Chiang et al., 2011) and zebrafish (Ahrens et al., 2013). Some progress has been made only in very recent times with the spread of the diffusion of high-density multi-electrode arrays that made possible to simultaneously record tens to hundreds of neurons. The aim of this thesis is precisely to provide a contribution to fill, even if in a small part, this gap. Indeed, in addition to representing a contribution to the study of the brain at the microscale from the point of view of complex networks theory, this work wants to provide, for the first time, experimental evidence of the detailed organization of a local cortical network *in vivo*.

Representing the brain with graph theory

The past 25 years have seen an increasing proliferation of analytical methods to model complex networks and to explore the quasi-universal principles of network organization, function, growth and evolution (Fornito et al., 2016). Principal among these general methods is graph theory. Any network built from experimental data can be indeed considered a different realization of a mathematical object called *graph*. Intuitively a graph is a way of encoding the relationship between elements of two different finite sets. If we indicate these two sets as V (vertexes or nodes) and E (edges, arcs, links or connections) we call graph the ordered pair $G = (V, E)$. As can be seen in Figure 1.4 a graph $G(n, m)$ can be represented by drawing the vertices as

points and the edges as connecting lines. Once the set of vertices and edges have been assigned, the graph is determined. We can now briefly introduce some types of graphs without giving a rigorous mathematical definition (Caldarelli, 2010):

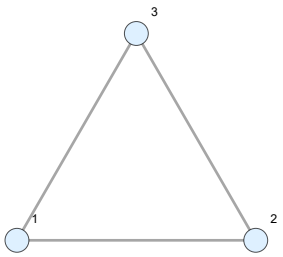

Figure 1.4. Basic example of a graph. Here $G(3,3)$, that is a graph of *order* (number of vertices) and *size* (number of edges) 3.

- *Binary undirected*: graph in which the edges are either 0 (absent) or 1 (present) and no direction is assigned from one vertex to another.
- *Binary directed*: graph in which the edges are either 0 or 1 and a direction is assigned from one vertex to another. If a vertex is connected to itself we have a *loop*. You can also have *multiple edges* when there are different edges between two same vertices. In a binary directed graph the edge (i, j) is different from the edge (j, i).
- *Undirected weighted*: graph in which each edge is assigned a weight $w \in \mathcal{R}$ and no direction is assigned from one vertex to another.
- *Directed weighted*: graph in which each edge is assigned a weight $w \in \mathcal{R}$ and a direction is assigned from one vertex to another. In a directed weighted graph we have $w_{i,j} \neq w_{j,i}$.

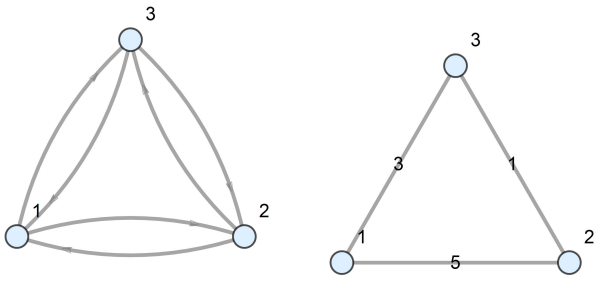

Figure 1.5. On the left a possible realization of a *directed* graph and on the right of a *weighted* graph with weights (3,1,5).

In all these contexts the graph is completely determined by a matrix called *Adjacency matrix* (A) . The adjacency matrix of a graph $G(n, m)$ is a square matrix of order n whose elements a_{ij} are 0 if the vertices i, j are not connected and 1 otherwise. In the case of undirected graphs this matrix is symmetric, while in the case of directed graphs the element a_{ij} can be different from the element a_{ji}. For weighted graphs, the elements a_{ij} of the matrix take the value w of the weight of the relative edge; in this way the adjacency matrix will be composed of real numbers for the edges present and 0 otherwise.

In the case of our studies we analysed time series from a multielectrode array of 96 channels. Interpreting each single-channel time series as a node we obtained networks with 96 nodes and (96x95)/2 possible edges (i.e. a graph or order N has at maximum N(N-1)/2 edges). As stated above, we analyzed patterns of both functional (1.2) and effective (2.5) connectivity and this corresponds to the analysis of undirected and directed weighted graphs respectively. The reasons are the following. The most used measure of functional connectivity exploits the Pearson correlation coefficient C_{ij} to estimate statistical dependencies between neural time series (Smith et al., 2011). Therefore, to build a complete map of all functional connections one must calculate the matrix of all pairwise correlation between the time series of interest. Since correlation is symmetric so will the matrix. When instead one wants to investigate patterns of information transmission, that is effective connectivity networks, a different measure must be used. Among the many available the most solid and well-founded for neuroscientific purposes is *Transfer Entropy* (TE) (Schreiber, 2000). TE quantify the information transfer between time series by defining a *driver* time series X and a *target* time series Y, hence establishing a direction for the information flow. Therefore, since TE is an asymmetric measure so will the matrix. Figure 1.6 sketches the followed procedure to build the two type of graphs analyzed in this thesis.

A concept that goes hand in hand with that of network and that will often be referred to in this thesis is that of *topology*. By definition, topology is the branch of mathematics that studies the properties of a geometric object that are preserved under deformations. In the context of graph theory it refers to all the properties and quantities that characterize the graph formation, structure and organization. Hence, all the attributes that provide information in this sense are called topological. The most basic topological quantity one could think of is the number of edges

per node, which is called the *node degree*[1]. When analyzing graphs obtained from brain data (i.e. brain graphs) topology is of particular interest since it allows to reveal properties that don't exist the physical space: i.e. the complex relationships between the dynamic activity of neurons. One could say the topology is the fifth dimension of analysis after the three dimensions of space (x,y,z) and time (Fornito et al., 2016). Topological structures with strong analogies are found in different scientific areas and it is not immediate to understand why so apparently dissimilar systems express similar features and behaviors. Moreover, in many cases, not only the global structure but also the dynamic evolution of the system is the result of self organized interactions among the individual components of the network. Currently a deep understanding of such interactions is not yet available also because in some cases, as in most biological and brain networks, the acquisition of large amount of experimental data is still problematic. To be able to give a satisfactory description of these systems, the needed approach is therefore, inevitably, statistical. In this scenario, using tools from graph theory makes possible to have a topological and statistically detailed description of real-world networks. It is in fact possible to describe, through a graph, network components also very different from each other such as the individual computers connected to the Internet network (known as WWW), economic agents or, as in the interest of the brain, neuronal ensembles ad different scales. Graph theory provides a simple and solid theoretical framework within which the topology of complex networks can be examined and, in the specific case of this work, can reveal important information on the local organization of a cortical network during a behavioural task.

[1] For details on the topological quantities analyzed in this work, please refer to the materials and methods of the individual studies 2.4 and 3.5

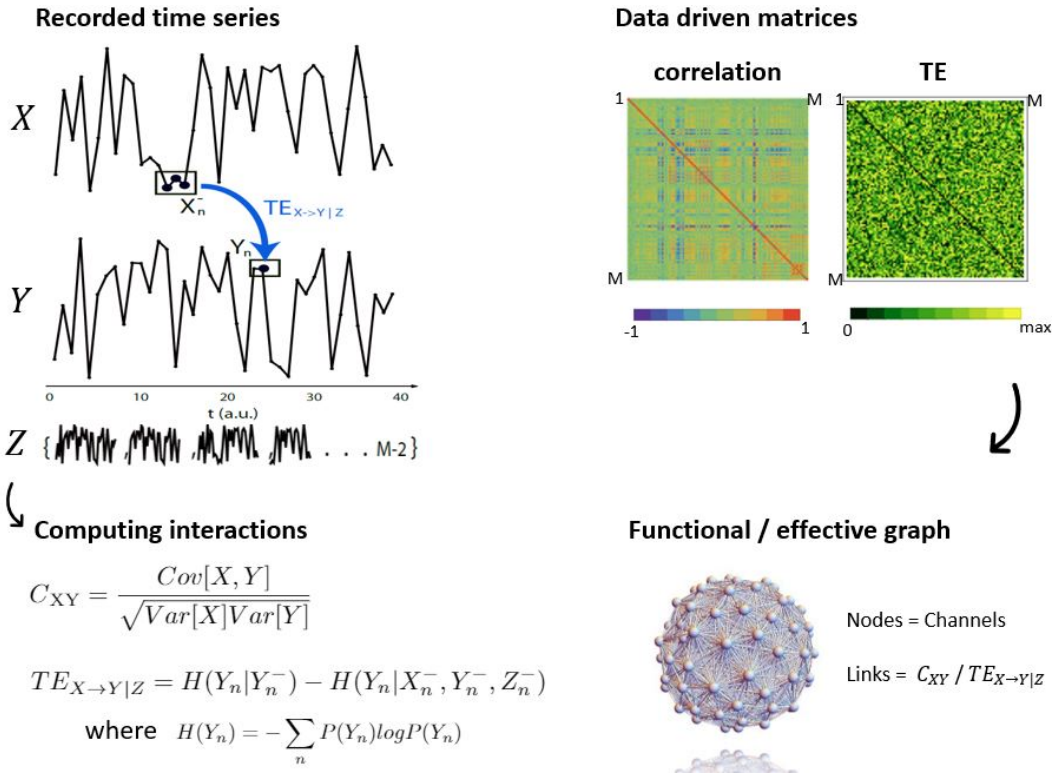

Figure 1.6. Bulding the cortical network Given an ensemble of M recorded (single-channel) time series functional and effective graphs can be built, depending on the measure used to compute the interactions. Pairwise correlation C_{XY} is a symmetric measure which gives the degree of synchrony between time series. Indeed it depends only on the present values of the couple (X,Y) via the Covariance and Variance functions. Conversely, Transfer Entropy quantifies the information transfer from a *driver* X to a *target* Y conditioned to the remaining $Z_{k=1,..,M-2}$ time series trough the variation of the entropy function $H(Y_n) = -\sum_n P(Y_n) log P(Y_n)$. Thus, for each couple (X,Y) TE depends upon the present state of Y (Y_n) and the past states of X, Y and Z (X_n^-,Y_n^-,Z_n^-) (see 3.5 for further details).

Study 1

The small scale functional topology of movement control: Hierarchical organization of local activity anticipates movement generation in the premotor cortex of primates

Abstract

How neurons coordinate their collective activity for behavioural control is an open question in neuroscience. Several studies have progressively proven, on various scales, that the patterns of neural synchronization change accordingly with behavioural events. However, the topological features of the neural dynamics that underlie task-based cognitive decisions on the small scale level are not understood. We analysed the multiunit activity (MUA) from a multielectrode (96 channels) array of the dorsal premotor cortex (PMd) in rhesus monkeys during a countermanding reaching task. Within the framework of graph theory, we found that in the local PMd network motor execution is preceded by the emergence of hubs of anti-correlation that are organized in a hierarchical manner. Conversely, this organization is absent when monkeys correctly inhibit programmed movements. Thus, we interpret the presence of hubs as reflecting the readiness of the motor plan and the irrevocable signature of

the onset of the incoming movement.

2.1 Introduction

Billions of interconnected neurons that propagate signals rapidly over short and long distances form the brain. Their interactions have been examined by two approaches: on a small scale, aiming to describe how relatively few individual neurons cooperate in a given area, using in vitro or in vivo models, and a large scale, characterizing how large populations of neurons, from different macro areas, are functionally connected. The small-scale approach has been used, for example, to examine areas of the cortico-subcortical network, which underlies the control and generation of skilled arm movements. However, for many years, neural activity has been recorded from few neurons, with limited efforts to extract a population code that can account for the interactions between neurons (Evarts, 1968; Georgopoulos et al., 1989; Wise et al., 1997). Recently, the diffusion of high-density multi-electrode arrays has made it possible to adequately study local population dynamics, thanks to the ability of simultaneously recording tens to hundreds of neurons. Using various forms of reduction complexity, the population activity in cortical motor areas has been described as a neural trajectory as a function of time, evolving in a multidimensional neuronal state space (Gallego et al., 2017; Churchland et al., 2012; Shenoy et al., 2012). These approaches, particularly when they are used to study cognitively advanced functions, have provided valuable information on how small populations of neurons cooperate during decisions, movement planning and execution. In parallel, other studies have found that simultaneously recorded neurons can display functional coupling (spike synchronization), even without undergoing any modulation in their firing rate (Fetz, 1992). Neuronal synchronization patterns change, depending on behavioural events (Vaadia et al., 1988; Hatsopoulos et al., 1998; Riehle et al., 1997; Torre, 2016), even independent of the underlying oscillatory pattern of activation (Fujisawa et al., 2008). On a larger scale, neuronal synchronization has been analysed to examine the level of interaction between areas of the entire brain network (Konig and Engel, 1995; Michaels et al., 2016). Several methods that focus on human electroencephalography (EEG) and functional-MRI (fMRI) data (Shin et al., 2013; Demuru et al., 2013; Luca et al., 2006; Liegeois et al., 2014; Bordier et al., 2018; Nicolini et al., 2017) have been successfully applied. With these approaches, analytical techniques that are derived from graph theory have shown that neuronal population interactions are organized according to a highly efficient topology, with

local and long-distance connections occasionally organised around highly functionally coupled regions (Power et al., 2013; Lutcke et al., 2013; Eguiluz et al., 2005; Vlasov and Bifone, 2017; Mastrandrea et al., 2017). Conversely, graph-based approaches have been used sparingly on data from animal models, with few exceptions (Sporns et al., 2007; Gu et al., 2019; Yu et al., 2006; Dann et al., 2016; Kiani et al., 2015; Gerhard et al., 2011; Ferraro et al., 2018; Gal et al., 2013) and, to our knowledge, not at all to describe the dynamics of local functional connectivity structures in vivo on a small scale. Thus, we wanted to study the local functional connectivity of the dorsal premotor cortex (PMd) in monkeys, preceding motor execution. We focused on the spectral estimate of the multiunit activity (MUA) signal (Mattia et al., 2013), obtained from a 96-channel array. To increase our understanding of the topology of the network, we used a percolation-based approach (Bordier et al., 2017, 2018; Nicolini et al., 2017; Vlasov and Bifone, 2017; Mastrandrea et al., 2017; Ferraro et al., 2018; Callaway et al., 2000; Gallos et al., 2012). Percolation is a powerful tool that is derived from statistical physics that allows one to inspect the self-organization of networks. Our study shows that the PMd exhibits signatures of self-organization only when the motor plan is mature, not when it is successfully cancelled. Further, the occurrence of this phenomenon correlates with the emergence of functional hubs in the network.

2.2 Results

2.2.1 Behavioural evaluation of the lead time to suppress a movement

To examine the local functional connectivity before movement execution, we recorded neuronal activity from the PMd of two monkeys (P, C) that were performing a countermanding reaching task (Fig. 2.7). At the beginning of the task, the animals were required to hold their hand over a central target that was presented on a touch screen. Two types of randomly intermingled trials were possible: no-stop trials (67%) and stop trials (33%). During no-stop trials, concurrent with the disappearance of the central target (Go signal), a peripheral target appeared on the left or right. To obtain the reward, the monkeys were instructed to reach the peripheral target. In stop trials, after the Go signal, the central target reappeared (Stop signal) after a variable delay, called the SSD (Stop signal Delay). The monkeys were then required to refrain from moving to earn the reward. If the movement is withheld, the trial is a stop-correct trial; otherwise, it is a stop-wrong trial. Generally in these trials

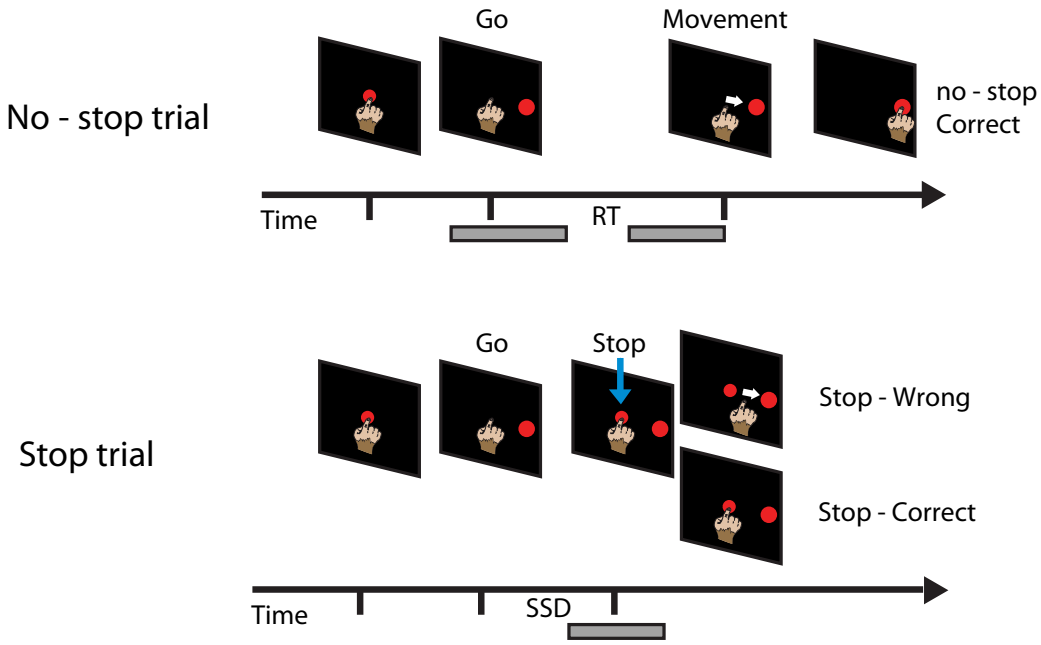

Figure 2.7. Behavioural task and epochs of analysis. No-stop and stop trials were randomly intermixed during each session. The grey horizontal rectangles under the time scale of no-stop and stop trials represent the epochs of analysis (Go epoch, Pre-Movement epoch, Stop signal epoch, respectively). RT reaction time; SSD Stop signal delay.

the monkeys detached the hand from the screen and then stopped the movement on the fly avoiding to touch the peripheral target. Immediately after the error a blank screen was displayed. Typically, in relation to the duration of the average SSD, the stop-correct trials constituted approximately 50% of stop trials.

Monkeys	RT_{ns}	RT_{ws}	SSD	SSRT	Independence test	P(r)
P	769 (110)	710 (82)	557 (115)	203	P=8.44 e-5; zval -3.9; ranksum= 7411	0.48
C	585 (92)	537 (71)	371 (110)	190	P=8.58 e-5; zval -3.9; ranksum= 9213	0.44

Table 1. Behavioral results. For each monkey mean and standard deviation are presented for RTs in no-stop (RT_{ns}) and stop-wrong (RT_{ws}) trials, and presented SSDs. The estimates of SSRT were obtained after checking for the statistical difference (Independence assumption; rank-sum test) between RT_{ns} and RT_{ws}.

The countermanding task permits one to inspect the neuronal correlates of movement execution by comparing trials in which movements are planned and then executed (no-stop trials) with those in which movements are planned and then aborted (stop-correct trials). In this comparison, it is ideal to identify the specific neuronal signature of the movement execution and determine when it occurs. Moreover, it allows one to establish when the neuronal signature that is specific for movement execution must manifest. The countermanding task makes it possible to calculate a behavioural measure that it is broadly considered an index of efficiency in movement suppression: the stop signal reaction time or SSRT. To estimate SSRT the race model (Logan and Cowan, 1984) must be applied. This model describes the behaviour in the stop trials as the result of two stochastic processes racing toward a threshold: the GO process triggered by the onset of the Go signal, which duration is represented by the RT, and the STOP process triggered by the onset of the Stop signal, which duration must be calculated. When the GO process wins the race the movement is generated (stop-wrong trial), alternatively it is withheld (stop-correct trials). The race model allows to estimate the SSRT by taking into account the duration of the GO process, the probability to respond, and the SSDs. However to make the race model applicable to study response inhibition, a central assumption must be satisfied: the GO process in the stop trials must be the same as in the no-stop trials (independence assumption). Indeed the RTs that are employed to estimate the SSRT are obtained from the no-stop trials. To broadly validate this assumption, stop-wrong RTs must be shorter than the no-stop trials (Logan and Cowan, 1984) (see Table 1). To estimate the SSRT we employed the integration method because it has been proven to be the most reliable (Band et al., 2003). It assumes that the finishing time of the Stop process corresponds to the nth no-stop RT, where n results from the multiplication of the ordered no-stop RTs distribution by the overall probability of responding, p(respond). The SSRT is then obtained by subtracting the average SSDfrom the nth no-stop RT. The SSRT can also be considered the lead time that is required to inhibit a movement, or, simply, the time that precedes the start of a movement when a Stop signal, if presented, halts the generation of the same movement approximately 50% of the time. If the Stop signal is presented after this time, it will be less effective, because the neuronal phenomena that lead to the movement generation will have already started. If the Stop signal is presented well before this time, it will be more effective in halting the movement. Consequently, the neuronal activity that is related to movement generation must occur around the time that is defined by the SSRT before the movement onset. To compute the

SSRT, we first tested data for an assumption of independence of the race model.

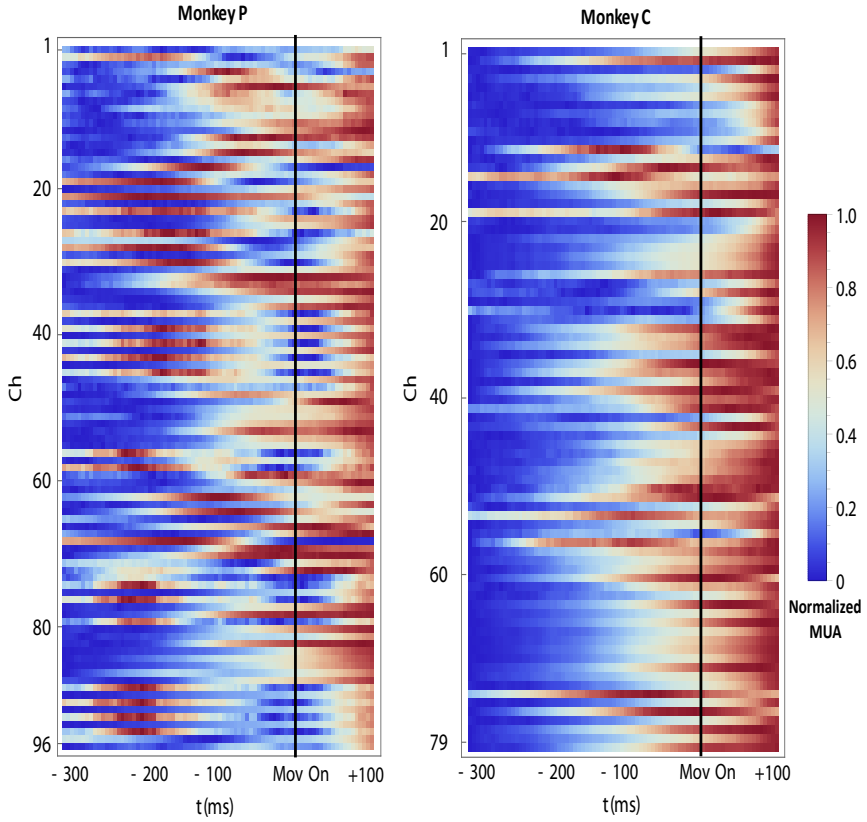

Figure 2.8. Trial-averaged single channel MUA aligned to the movement onset. Normalized MUA (no-stop trials) for every single recording channel in the two animals. Broken electrodes have been removed from the list in Monkey C.

2.2.2 In the PMd, certain recording sites show anti-correlated neuronal activity before movement generation

We focused on no-stop trials, i.e., the trials that required movement generation—to examine the organization of the functional network in the PMd in relation to movement execution. Consistent with previous approaches that have shown that important changes in single and multiunit activities and local field potentials occur in the PMd in the time before movement onset, (Mattia et al., 2013, 2010; Kaufman et al., 2016; Pani et al., 2014; Lara et al., 2018; Chandrasekaran et al., 2014), Fig. 2.8 shows that most of the recording sites in the arrays were modulated, demonstrating increased or decreased MUA activity, in the 300 ms that preceded the movement onset. We have suggested (Mattia et al., 2013) that these changes constitute a

signature of the maturation of the motor plan, achieved in cortical modules that show both positive (low-to-high) and negative (high-to-low) transitions in the MUA. We examined the level of mutual interactions among various recording sites by computing a correlation matrix between MUA time series using a sliding window approach. We modelled the evolving interactions of the network as a sequence of snapshots of correlation matrices, at the single-trial (single-trial network time series) and average levels (average network time series; see 2.4 for further details). Within this framework, each recording site can be considered a node of the functional network in the PMd, and the connections (or links) represent the amount of interaction (synchrony) between nodes. In our case, the weight of each connection was the correlation coefficient between corresponding time series. Notably, certain recording channels had a negative median value of the distribution of correlation coefficients in the 200 ms that preceded the movement onset (supplementary Figure S1), suggesting the presence of nodes with specific functions in the PMd network of both monkeys. Fig. 2.9 (and supplementary Figure S2, for the other animal) shows select snapshots of the average network time series aligned to the Go signal (top) and movement onset (bottom) in Monkey P. We found that although nothing peculiar occurred after the Go signal (Go epoch) as the time of movement generation approached (Pre-Movement epoch), positive (red regions) and negative correlations (blue regions) appeared. The marked blue lines (nodes that anti-correlate with the rest of the network) suggest that the network is more organized in the selected snapshots and that the anti-correlation is a determinant of this functional change.

2.2.3 In the functional network of the PMd, a hierarchy of hubs of anti-correlation emerges before movement generation

To quantitatively assess whether the emergence of negative correlations is the signature of the impending movement generation and to monitor the evolution of the network configurations, we performed dynamic percolation analysis. This technique allows one to inspect the network organization by iteratively removing links between nodes as a function of a control parameter. As a control parameter, which quantifies the structural characteristics of the network, we used the number of connected clusters of nodes in the network (Bardella et al., 2016) (namely, the number of connected components; see 2.4 for further details). The results of the percolation are encoded in a percolation curve, in which the number of connected components is plotted as a function of a threshold (i.e., the link weights). Thus, link weights represent the thresholds according to which network disintegration is monitored.

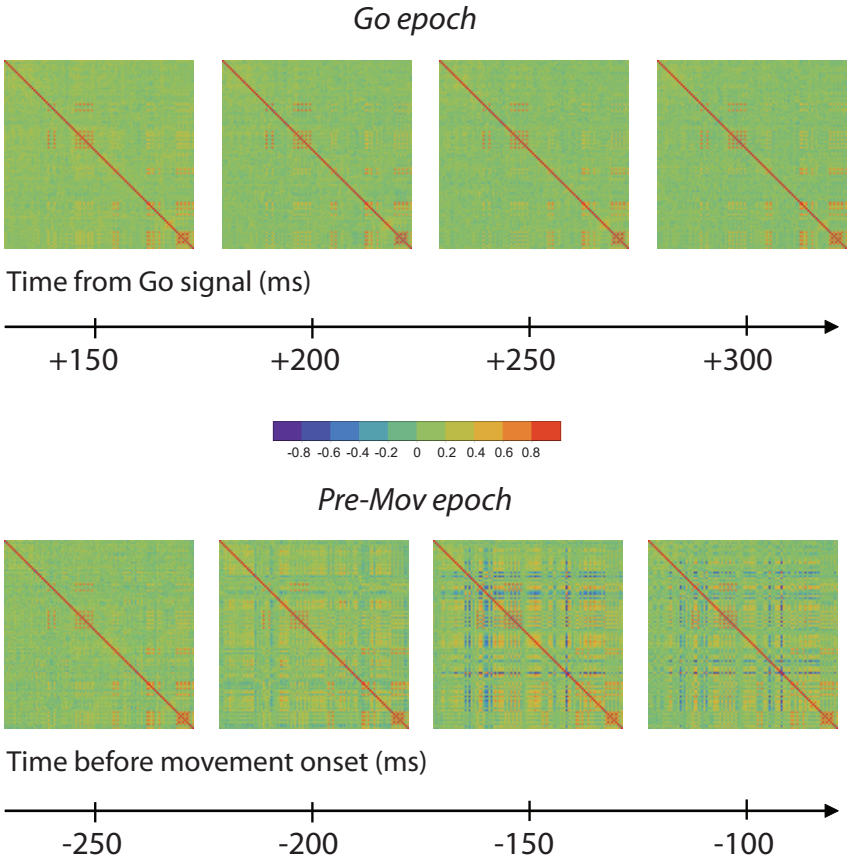

Figure 2.9. Average network series changes during RT. Snapshots of the average network time series at four different times from the Go (Go; top) and before the movement (Pre-mov; bottom) epochs of no-stop trials in monkey P. The scale bar indicates the values of correlation coefficients

Moreover, because links are removed based on the value of their weights this process reveals the presence of a hierarchical organization within the network. If the network is randomly arranged at the time of analysis, the curve is characterized by a sharp transition in the number of connected components for changes in threshold values. Thus, the network disintegrates very quickly on removal of the links, and there are no stable configurations of its constituent components. Conversely, when a hierarchical structure is present, for certain threshold values, stable clusters of nodes (number of connected components) exist, and the network is insensitive to the progressive removal of links. This yields a stepwise percolation curve in which plateaus reflect the presence of stable hierarchical configurations in the network. 2.10 shows the percolation curves (step: 5 ms; see 2.4) for negative correlations of no-stop trials, separately for each animal, starting from 300 ms before movement onset.

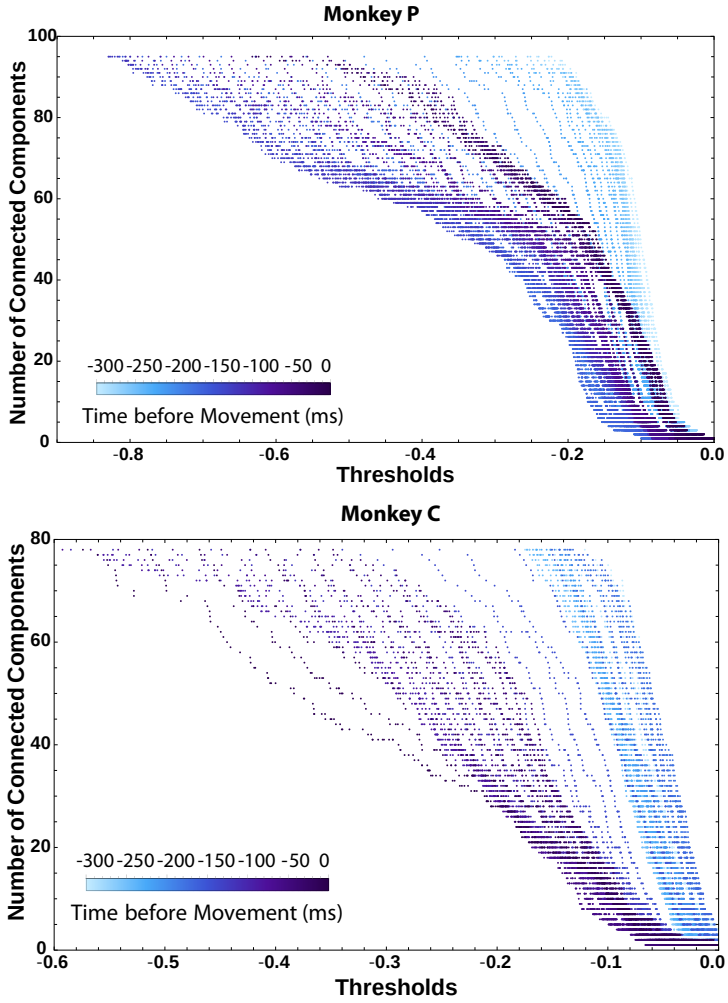

Figure 2.10. Percolation curves before Movement onset in no-stop trials. Time evolution of the percolation curves for 300 ms before the movement onset, for each monkey. Times far from the movement onset are coloured in lighter shades of blue and times close to the movement onset in darker shades of blue. Thresholds values are correlation coefficients.

In the early phase (light blue lines), the curves are characterized by the absence of plateaus and by steep transitions in the number of connected components. Later (at different times in the two animals; darker lines), the trends become more stepwise. This pattern suggests that, approaching the movement onset, the functional network of anti-correlations of the PMd evolves from a pseudo-random state toward a more organized state that is endowed with signatures of hierarchy. We calculated the slope of all percolation curves that were obtained and plotted them as a function of time (Figure 5, A) to generate a straightforward view of the evolution from pseudo-random to organized state in the pre-Movement epoch for both animals. We found that at approximately 200 ms before the movement in both animals, a transition in the average slope appeared (from roughly -600 to -200). To validate the results of the percolation analysis statistically, we proposed a null model (see 2.4) and computed the slope of each percolation curve for the experimental data and null model. We expected the experimental trend to be reproduced by the null model during the early stages of the epoch and to differ significantly when approaching the later stages. The results show that the steepness of the percolation curve did not differ significantly from the null model for times that were far from the movement onset (Figure 5B, top), whereas it lay well outside of the 95% confidence interval in the late stages (Figure 5 B, bottom).

To obtain the complete picture of the network evolution, we examined its topology in greater detail, searching for a measure of available functional connections for each node and for the presence of hubs. In percolation, the threshold immediately prior to the beginning of network disintegration (disintegration starts when the number of connected components is >1 for the first time) is critical.

Indeed, recent studies (Bordier et al., 2018; Nicolini et al., 2017) have demonstrated that at this threshold, the optimal balance between information about network organization and statistical noise is realized (see 2.4 for further details). Thus, we inspected the network topology at this threshold and found that nodes with links (measured as Vertex Degree; VD; see 2.4) that greatly exceeded the average value existed (see supplementary Figure S3), consistent with the definition of hub nodes (Albert and Barabási, 2002). Hubs are, indeed, the most important nodes in the network and, during percolation, preserve high VD values at high thresholds. Inspecting the entire sequence of thresholds — that is, climbing the ladder of the percolation curve — we unfolded the stable configurations of the network, and a hierarchy of hubs was revealed. Supplementary Figure S4 shows the configuration

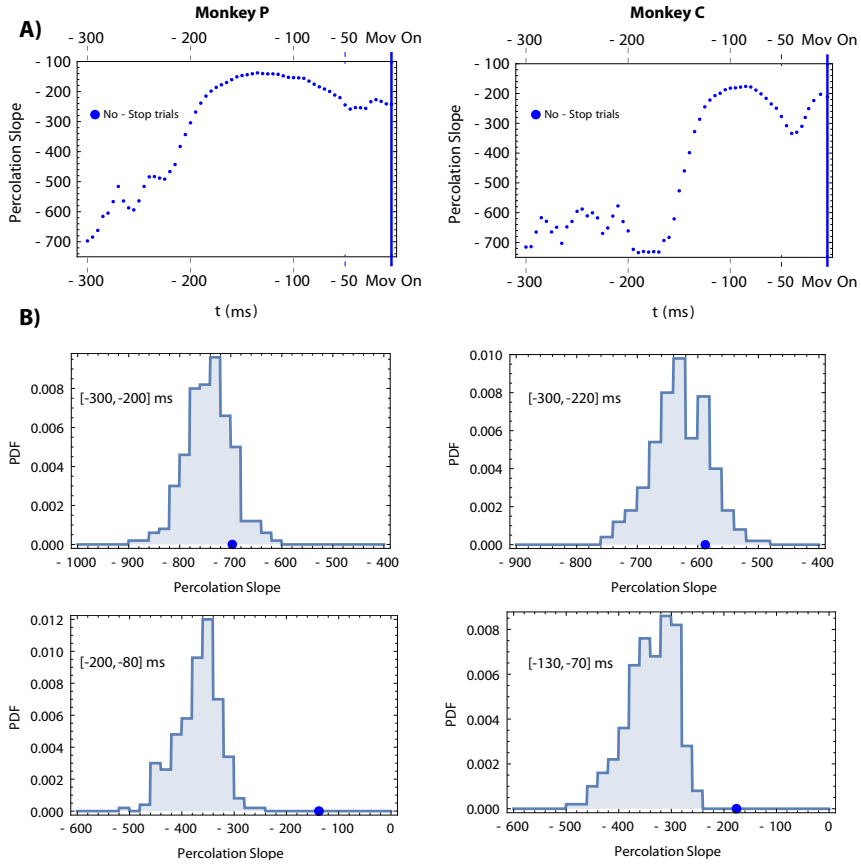

Figure 2.11. Dynamics of the percolation slopes before movement onset and comparison with null models in two sub-epochs. A) Evolution of the slope of the percolation curves during the pre-movement epoch. B) Comparison with the null model for the early (top) and the late (bottom) phases of the epoch. For the early stages we averaged the matrices of the average network time series corresponding to the interval [-300,-200] ms for monkey P and [-300, -220] ms for monkey C. For the late stages we averaged the matrices of the average network time series corresponding to the interval [-200, -80] ms for monkey P and [-130, -70] ms for monkey C. Histograms: null model data. Blue dots represent the experimental slopes obtained for each interval. PDF, probability density function.

(hubs are colour-coded) for four threshold values for Monkeys P and C before the movement onset.

2.2.4 Network dynamics when movements are cancelled

Supplementary Figure S5 shows the percolation curves and the evolution of the percolation slopes for stop-wrong trials in the pre-movement epoch. The comparison with Figures 4 and 5 suggests that the network evolves very similarly in no-stop

and stop-wrong trials. At this stage, a natural question arises: what happens to the network functional structure during stop-correct trials? If the emergence of the observed hubs is a mark of the incoming movement onset, it should be absent in stop-correct trials, when the movement execution is aborted. To this end, as we did for no-stop trials, we performed percolation analysis on the average network time series, relative to (from 100 ms before to 100 ms after) the Stop signal, for wrong and stop-correct trials (see supplementary Figure S6), calculating the corresponding slopes (Figure 6, top). To determine whether a difference in the configurations of the network between conditions existed, we computed the Euclidean distance between all slope values. We found that the maximum distance was reached approximately 25 ms before the Stop signal presentation — as a consequence of the decreasing slope values in stop-correct trials — for both animals.

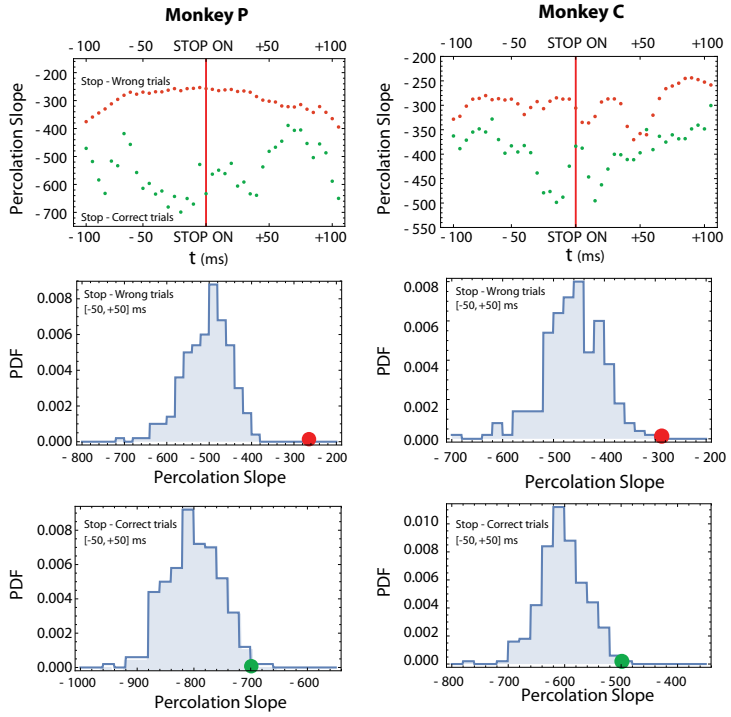

Figure 2.12. Percolation curves dynamics in stop trials. Top panels: evolution of the experimental slope of the percolation curve during the epoch for stop-wrong trials (red) and stop-correct trials (green). Bottom panels: comparison between the observed slope (colored dots; red stop-wrong trials, green stop-correct trials) and the corresponding null models (histograms). The red vertical line marks the Stop signal presentation. Other conventions and symbols as in Figure 5.

Then, we confronted the network states of stop-wrong trials to those of stop-correct

trials and found that during stop-correct trials, hubs were absent while emerged in stop-wrong trials (supplementary Figure S7), confirming the link between the emergence of hubs and movement generation. Moreover, the hubs channels were the same in stop-wrong and no-stop trials. Despite the sketch suggests an intriguing specific location for the hubs in the brain region, we avoided to link our observations to anatomical landmarks. The issue deserves future investigation. To validate this finding, we tested our results against the null model (Figure 6, bottom), averaging the correlation matrices of the average network time series that corresponded to the interval $[-50, +50]$ ms with respect to the Stop-signal (it fully contains the point of maximum distance between slopes). We then compared the experimental slope with those that were obtained from the randomization. As reported in Figure 6, the slope of the observed percolation curve for stop-wrong trials was outside of the 95% confidence interval of the null distribution for both animals. For stop-correct trials, we found that Monkey P had a slope that was well inside of the distribution of randomizations, thus confirming the hypothesis that the network is maintained in a pseudo-random configuration. For Monkey C, the slope was still reproduced by the null model but was closer to the 95% confidence interval compared with Monkey P. However, the absence of hubs led us to conclude that the state that the network expresses during a stop-correct trial is a sort of a quiescent configuration, in which the motor plan is not fully mature and thus cannot become a movement, because no hubs take the lead. If, in that window, the hubs become active, the Stop signal, even if it is presented, is ineffective. We believe that the emergence of hubs is proof of spontaneous self-reorganization of the network from a pseudo-random to more organized state in light of a forthcoming cognitive decision (moving vs not moving).

2.2.5 Topology of the functional network of the PMd before executed and cancelled movements

To complement the percolation results, we implemented an increasingly used technique in neuroscience: minimum spanning tree analysis (MST; Stam et al., 2014; see 2.4 for further details). For a given graph, MST provides a unique connected graph without cycles or loops. MST corresponds to a subnetwork, the links of which are the strongest within the set of all possible ones. MST identifies the core structure of a network and, for this study, elicits the backbone of functional connectivity of the PMd. Two extreme configurations are possible, as quantified by Leaf Number (LN; see 2.4 for further details), for the MST (Stam et al., 2014): star-like, in which one (or more) central node is connected to all others via one link only, and chain-like, in

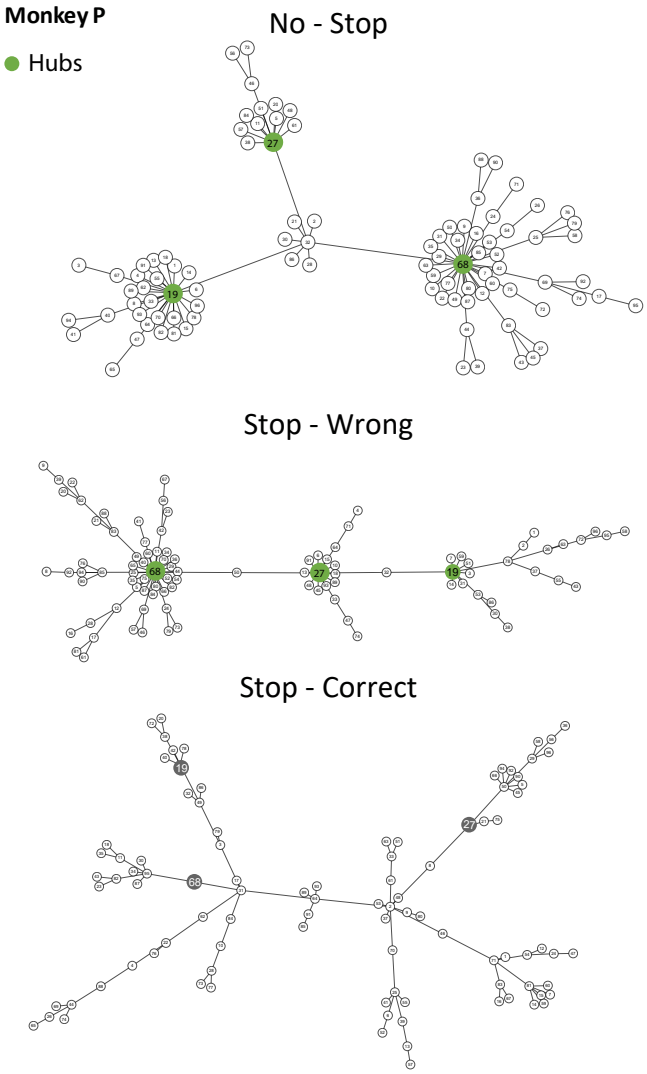

Figure 2.13. Minimun spanning tree analysis. Results from Monkey P. MST computed 150 ms before Movement onset for no-stop trials and at the time of the Stop signal presentation for correct and stop-wrong trials. Hubs are indicated by the green circles. Gray circles in stop-correct trials show the location in the MST of the same recording channels.

which all nodes (with the exception of the extremes) are connected to two others (see 2.4 for further details). In the first scenario, the central nodes are the hubs of the network. In the latter, the MST stretches out, with hubs excluded. Figure 7 (and supplementary Figure S 8, for Monkey C) shows the results of the MST analysis for the average network time series for no-stop (before the Movement onset) and wrong/stop-correct trials (at the time of the appearance of the Stop signal). To

correctly compare no-stop trials and stop-wrong trials, an equivalent time T with respect to the movement onset in both trials must be chosen. To this end we derived a time T — as an estimate of the Stop signal appearance — for the no-stop trials as: T = $\overline{RT}_{Stop}$-$\overline{SSD}_{Stop}$, where $\overline{RT}_{Stop}$ is the mean reaction time for the stop-wrong trials and $\overline{SSD}_{Stop}$ is the mean Stop signal delay.

The dynamics of the MST in the Pre-mov epoch is shown in the Supplementary Video V1 (for Monkey P) and Supplementary Video V2 (for monkey C). MST was computed every 20 ms (in the interval -300 -60 ms before movement onset). Videos show the gradual evolution in the configurations, from chain to star, as the movement time is approaching.

Although multiple hubs (green circles) are evident in no-stop trials and stop-wrong trials, they are absent in stop-correct trials where MST configuration is more chain-like, as expected. To determine the statistical significance of the findings, we used the corresponding null model (supplementary Figure S9). The results show that during no-stop and stop-wrong trials (blue and red dots), the star-like topology (average LN) of the MST was not reproduced by the null model. During stop-correct trials (green dots), the MST configuration of Monkey P was reproduced by the ensemble of randomizations, whereas for Monkey C, it was close to the 95% confidence interval. In both cases, the hubs nodes that were characteristic of no-stop and stop-wrong trials were absent, consistent with what was found by percolation analysis and confirming that during stop-correct trials, the network lies in a meta-state at the borders of randomness and is not fully mature (i.e., not organized).

To check for the stability of the functional structure observed we repeated the same analysis in one of the other available sessions with similar characteristics. The session was recorded about 9 months apart in monkey P. The results show that the described features in MUA modulation are stable, i.e., a hierarchical organized pattern of anticorrelation emerges before movement onset, together with the star like topology and hubs (see supplementary Figure S10, top). Similar features have been observed in other sessions (not shown). However, we were not able to detect the same functional organization by analyzing single units extracted see 2.4 from the same session (see supplementary Figure S10, bottom).

2.2.6 Characterization of network of positive correlations

We also applied percolation analysis to the network of positive correlations, finding that its topology was less informative than that of negative correlations because their topology does not show presence of hubs organized in a hierarchical manner. Except for the presence of the hubs that had already been identified in the analysis of negative correlations, we failed to observe other specific topological signatures (e.g., the VD distributions shows no evidence of hubs; see supplementary Figure S11). Further, we found that the hubs of anti-correlation shared high positive correlation values within themselves, forming the most important cluster in the network of positive correlations. By percolation analysis, we monitored the decomposition of this cluster (see supplementary Figure S12) concluding that the hubs of anti-correlation form a sort of 'rich-club' (Colizza et al., 2006), in which the links between hubs are positive (see supplementary Figure S13). These results show that the dynamic of the functional network of the PMd relies on the coordinated action of a small subset of neuronal populations that synchronously anti-synchronize with the rest of the network. This finding also suggests that the most notable features regarding the topological arrangement of the network are encoded in the negative weights.

2.3 Discussion

We have examined, for the first time, the premotor cortical functional network that underlies movement generation, using graph-based algorithms that were applied to simultaneously recorded MUAs (from up to 96 channels). We found that movement generation is anticipated by a clear stereotypical increase in synchronization in the form of anti-correlation between several channels and the rest of the network. These channels act as network hubs and are organized in a hierarchical manner. Notably, this phenomenon was not observed for successfully cancelled movements but remained present in trials in which movements where generated despite the command to stop. The latency of the increase in anti-correlation occurs in a window of approximately 200 ms before movement onset. This period is in the same range that is necessary to render a Stop signal effective (the SSRT): if a movement is going to be made, the Stop signal must be presented roughly 200 ms ahead of movement generation to be successful in interrupting the movement. Thus, in stop-correct trials, the effectiveness of the Stop signal is associated with the absence of hubs of anti-correlation.

Our results suggest that the emergence of hubs of anti-correlation can be identified as the neuronal computational strategy the drives the irrevocable maturation of the motor plan. The specific signature in the network topology of the PMd that we detected is characteristic of the pre-movement epoch. Previous studies have shown that before a movement is made, single units, MUA, and LFP in the motor cortices experience strong widespread modulations. They represent the largest change in neuronal activity in delayed reaching tasks (Churchland et al., 2012; Kaufman et al., 2016; Sussillo et al., 2015, Pani et. al, 2014) and as such are believed to correspond to the passage from stable preparation to movement generation. Similar phenomena, compatible with an attractor-like dynamic, have also been observed in the MUA during the same task (**Marcos**; Mattia et al., 2013) In all of these studies, the latency between the start of the population dynamic and the movement onset is 100-150 ms in a window that is compatible with the anti-correlation patterns that we detected.

In our study, neural activity was recorded at a roughly constant depth (Utah array; electrode length: 1.5 mm). A recent study (Chandrasekaran et al., 2017) found that single unit activity in the PMd is organized following a gradient from superficial to deep layers. Neurons in more superficial layers showed increasing activity during the RT epoch, correlating with behavioural parameters and thus potentially related to decision. Conversely, neurons in deeper layers showed stereotypical modulated activity solely around 150 ms before movement onset. Among these neurons, a subpopulation (approximately 15%) experienced decreased activity before movement generation. The evidence of anti-correlation between recordings in our study suggests that, thanks to the larger spread of MUA in the cortical layers, we have been able to sample activity from deep layers. However, results also suggest that the location of the tip on the electrodes array is definitively too superficial. In fact, when the network was observed more locally by analyzing single units, the topology was lacking of an organization based on the presence of different populations in anti-correlation.

The MST results suggest that the hubs of anti-correlation that we detected have a function in the computation that is necessary to send the information to subcortical structures. This possibility is supported quantitatively by several groups (Demuru et al., 2013; Dubbelink, 2014) that have recently linked MST changes, based on EEG and MEG data, to cognition and motor functions. Specifically, our results agree with the widespread concept in which most of the traffic in a weighted network flows through the MST. In this scenario, it is not surprising to observe a star-like MST, because this is the optimal configuration for efficient, fast and integrated

communication within a network. The cognitive decision of whether to perform a movement is indeed a fast computation, and the command to move could be transferred, through the star-like MST, to lower cortical, subcortical and spinal circuits that will promote muscle activation. Consequently, the information stream would only flow shortly through the hubs, thus helping prevent overloading issues in the network during the ongoing computation (Stam et al., 2014). This, however, does not imply that the PMd is the only region that participates in this form of control. Other cortical and subcortical structures (e.g., basal ganglia, prefrontal cortex) are needed to finalise this process to permit movement initiation (Battaglia-Mayer et al., 2014). Future studies should focus on several crucial aspects: Is the computation that we observed specific at this depth, or is it present across all layers? Do other structures perform similar computations? Is this signature related to specific interactions between the PMd and other brain areas?

In the neural control of movements, various computational strategies have been proposed to define the function of the PMd and MI. In the past several years, many studies have used a dynamical system approach with data from simultaneously recorded neurons. Their main finding is that in motor cortices, neuronal activity evolves smoothly across various state spaces to facilitate movement generation. Importantly, this evolution provides insights into how an entire population of neurons participates in generating movement. This approach gave rise to the idea that several subspaces of neural activity correspond to different behavioural functions. These methods, however, are based on the covariance of the simultaneously recorded neurons and, as such, are suited to account for neuronal activity at the population level, without distinguishing between specific contributions by single neurons (or recording sites) to the topology of the interactions. Our approach differs, because we provide evidence that our computational strategy is based on a hierarchy of hubs. Indeed, this was obtained by considering the mutual interaction between recording sites. By percolation analysis, we succeeded in identifying, without any *a priori* assumption (in a totally data-driven fashion), the sites that act as hubs. This corresponds to a complete characterization of the topological arrangement of network dynamics, consequently marking a substantial difference from other approaches (e.g., Chandrasekaran et al., 2017; Churchland et al., 2012; Mattia et al., 2013). The function of hubs in driving the computation emerges spontaneously from the collective behaviour as an intrinsic property of the system.

To the best of our knowledge, this report is one of the few studies that has performed

graph analysis on specific cortical areas at the small scale and mesoscale levels in vivo and during a behavioural task. Schroeter et al. (2015) examined the properties of the primary mouse hippocampal functional network via MUA in vitro, finding that hub neurons have a crucial function in shaping the synchronous dynamics during development. This result confirms the importance of this complex topological structure in coordinating the dynamics at the microcircuit level. Recently, Dann et al. (2016) — using multielectrode depth cortical recordings — examined the functional topology of three areas of the fronto-parietal network that are involved in grasping, measuring the spiking activity of single units. They found that the network had a modular topology, with hubs in all three areas. Each module was confined primarily to a single area but could also involve neurons in the other areas. Notably, the hubs were composed mainly of oscillatory spiking and synchronized units, whereas the more peripheral units were non-oscillatory. The authors proposed that the oscillator hubs allowed the coordination of functional communication between cortical areas. Further, the topology that they described was highly similar to the that at the whole-brain level using other techniques (EEG, fMRI).

In our study, we evaluated the functional topology of a small portion of the cortex: the PMd. Thus, we can not account for the functional communication between the PMd and other areas. Additional study will be necessary to test whether the anti-correlation that we observed is a phenomenon that is limited to the premotor cortex or whether it involves other areas that participate in the cortical reaching network (e.g., parietal regions). In this regard, an important difference between our study and Dann et al. (2016) is that their analysis did not distinguish between positive and negative functional connections.

With our approach, it was possible to determine whether there was synchronization between neural populations and what the sign of this synchrony was. These findings represent an advance in the field, because nearly all previous studies on the motor cortex have merely explored, in various forms, the nature of positive synchrony (Vaadia et al., 1988; Riehle et al., 1997; Hatsopoulos et al., 1998; Torre, 2016). Renart et al. (2010) and Ecker et al. (2010) provided the first evidence that positive correlations are not the only meaningful associations in micro-neuronal networks. Renart et al. (2010) found that recurrent neural networks can generate an asynchronous state due to fluctuations in the activity of excitatory and inhibitory populations. The authors proposed that the negative correlations that characterize this state prevent uncontrolled network-wide synchrony and facilitate efficient processing of informa-

tion. Their results were confirmed by in vivo recordings from the somatosensory and auditory cortices of urethane-anesthetized rats. Ecker et al. (2010) analysed neuronal recordings from the primary visual cortex of awake macaques, noting very low spike count correlations between local neurons. They also opined that the decorrelated state of the network might be crucial for hierarchical cortical processing and information routing, offering substantial advantages over communication that relies solely on positive synchrony. Our results are also supported by recent work from Gu et al. (2019), who linked the anatomical and physiological properties of local neural networks through the development of a novel circuit model. They found that highly interconnected hubs neurons emerge as a key feature of the spatiotemporal activity of local cortical circuits. As hypothesized by the authors, the presence of hub neurons in local networks accounts for the transition between dynamic cortical states. Moreover, it provides a solid framework in which the anatomical, functional and dynamic features of brain networks can be integrated. Furthermore, although the attention toward negative weighted links has grown in the past decade, most studies on brain networks have ignored anti-correlations or left them uninterpreted. Has topology that is characterized by strong anti-correlation (as we observed) been reported in large-scale studies by fMRI or EEG? Greicius et al. (2003) made one of the earliest contributions, showing a negative correlation between the default mode network (DMN) and executive function network. Subsequently, anti-correlations have been seen in the attentional network (Fox et al., 2003), sensorial regions (Tian et al., 2007), parietal and medial frontal regions (Tian et al., 2007), the infralimbic cortex (IL) and amygdala (Liang et al., 2012) and in the DMN and executive control network (Di and Biswal, 2013). Further, recent work on fMRI data has focused on the network of negative correlations (Gopinath et al., 2015; Parente et al., 2018; Parente and Colosimo, 2018). Gopinath et al. (2015) examined the anti-correlation maps of healthy patients by resting-state fMRI using a graph-based approach and found that hubs of anti-correlations were involved in important regulatory interactions between various regions, including reciprocal modulations, inhibition and during neurofeedback procedures. They hypothesized that negative links in a brain correlation network are more suitable for describing state-dependent signal couplings than anatomically constrained fluctuations. Parente et al. (2018) reported that central nodes of negative brain networks are affected in schizophrenic patients compared with controls: specifically, patients were characterized by a reduction in centrality measures. The authors speculated that central nodes have an important function in the modulation of other regions that share information with low-degree nodes.

These conclusions suggest that, also on the large-scale level, hubs of anti-correlations are likely to be pivotal in cognitive functions.

2.4 Materials and Methods

2.4.1 Subjects

Two male rhesus macaque monkeys (Macaca mulatta, Monkeys P and C), weighing 9 and 9.5 kg, respectively, were used. Animal care, housing, surgical procedures and experiments conformed to European (Directive 86/609/ECC and 2010/63/UE) and Italian (D.L. 116/92 and D.L. 26/2014) laws and were approved by the Italian Ministry of Health. Monkeys were pair-housed with cage enrichment. They were fed daily with standard primate chow that was supplemented with nuts and fresh fruits if necessary. During recording days, the monkeys received their daily water supply during the experiments.

2.4.2 Apparatus and task

The monkeys were seated in front of a black isoluminant background (<0.1 cd/m^2) of a 17-inch touchscreen monitor (LCD, 800 x 600 resolution), inside a darkened, acoustic-insulated room. A non-commercial software package, CORTEX (http://www.nimh.gov.it), was used to control the presentation of the stimuli and the behavioural responses. Figure 1 shows the scheme of the general task: a reaching countermanding task (Mirabella et al., 2011). Each trial started with the appearance of a central target (CT) (red circle, diameter 1.9 cm). The monkeys had to reach and hold the CT. After a variable holding time (400-900 ms, 100-ms increments) a peripheral target (PT) (red circle, diameter 1.9 cm) appeared randomly in one of two possible locations, and the CT disappeared (Go signal). In no-stop trials, after the Go signal the subjects had to reach and hold the PT for a variable time (400-800 ms, 100-ms increments) to receive juice. Reaction times (RTs) were defined as the time between the presentation of the Go signal and the onset of the hand movement. In Stop signal trials, the sequence of events was the same until the Go signal. Then, after a variable delay (Stop signal delay, SSD), the CT reappeared (Stop signal), and the monkeys had to hold the CT until the end of the trial (800-1000 ms) to receive the reward (stop-correct trial). Conversely, removing the hand after the Stop signal constituted a wrong response (stop-wrong trial). The same amount of juice was delivered for stop-correct and correct no-stop trials. The intertrial interval

was set to 800 ms. Stop trials represented the 25% of all trials in each session. To establish the duration of the SSDs, a staircase tracking procedure was employed. If the monkey succeeded in withholding the response, the SSD increased by one step (100 ms) in the subsequent Stop signal trial. Conversely, if the subject failed, the SSD decreased by one step.

2.4.3 Extraction and processing of neuronal data

A multielectrode array (Blackrock Microsystems, Salt Lake City) with 96 electrodes (spacing 0.4 mm) was surgically implanted in the left dorsal premotor cortex (PMd; arcuate sulcus and pre-central dimple used as references after opening of the dura; see supplementary Figure S 7) to acquire unfiltered electric field potentials (UFP; i.e., the raw signal), sampled at 24.4 kHz (Tucker Davis Technologies, Alachua, FL). Neuronal activity was recorded from animals fully trained in the task. Since animals were also trained in other motor tasks, we had different sessions with the same task but often separated in time. For the analysis performed in this work we selected one session for each animal were the trial number was sufficiently high and the behaviour was in fully adherence with the expectative of the race model (see **??**). As a measure of neuronal activity at the population level, MUA was extracted offline from the raw signal, as in Mattia et al. (Mattia et al., 2013), by computing the time-varying power spectra P(ω, t) from the short-time Fourier transform of UFP in 5-ms sliding windows. Relative spectra R(ω, t) were then obtained, normalizing P(ω t) by their average P_{ref} (ω) across a fixed window (10 to 30 minutes) for the entire recording. The spectrally estimated MUAs are the average R(ω, t) across the $\omega/2\pi$ band $[0.2, 1.5]$ kHz. As detailed in Mattia et al. (Mattia et al., 2013), this estimate relies on two hypotheses. The first is that high ω components of UFPs result from the convolution of firing rates ν(t) of neurons that are close to the electrode tip with a stereotypical single-unit waveform. R(ω, t) allows one to eliminate the Fourier transform K(ω) of such an unknown waveform, rendering R(ω,t) a good approximation of the ratio of firing rate spectra $|\nu(\omega,t)|^2$ $/|\nu(\omega,t)|_{ref}{}^2$. In the second hypotesis, high ω power $|\nu(\omega,t)|^2$ is proportional to the firing rate ν(t) itself (Mattia and Del Giudice, 2002), such that our MUA estimate is proportional to ν(t). As a last step, logarithmically scaled MUAs were smoothed by a moving average (40-ms sliding window). To analyze single units correlations we represent neuronal activity via a spike density function (SDF) obtained by convolving the spike train with an exponential function mimicking a postsynaptic potential.

As a convolution function we used the following kernel $K(t)$:

$$K(t) = [1 - exp(-t/\tau_g)] \cdot exp(-t/\tau_d) \tag{2.1}$$

where $\tau_g = 1ms$ corresponds to the growth phase of the synaptic potential, and $\tau_d = 1ms$ to the decay phase Scangos and Stuphorn, 2010.

For our analysis we selected units that showed an increase/decrease of the average firing rate before movement onset (pre-RT, from -300 ms to movement onset), compared to the 200 ms before Go signal (pre-Go) or for at least one movement direction (Wilcoxon rank-sum test $P < 0.01$).

2.4.4 Preliminary analyses

We first analysed the activity profiles of each recording site. To obtain a uniform view of the changes in MUA levels, we normalised the activity of each channel with respect to its maximum value (see Figure 2). To examine the local network organization in the PMd, we constructed a functional network that represents the synchronisation between the MUAs that were recorded by the electrodes of the array. To this end, we used the Pearson correlation coefficient C, because it is one of the best-known methods for calculating synchrony by cross-correlation and because we wanted to focus on the simplest type of relationship between the signals that were recorded from the electrodes: the linear correlation.

For two time series, $X^i(t)$ and $X^j(t)$, at times t, in a 0 lag condition the C_{ij} is calculated as follows:

$$C_{ij} = \frac{Cov[X^i, X^j]}{\sqrt{Var[X^i]Var[X^j]}} \tag{2.2}$$

,$-1 \leq C_{ij} \leq 1$ where high negative values indicate a high inverse linear correlation (anti-synchronisation), whereas high positive values reflect a high linear relation between time series (synchronisation). For our purposes, $X^i(t)$ is represented by the spectrally estimated MUA in a chosen time window (epoch of analysis: see Figure 1) of the task, which is usually defined in relation to the behavioural events (e.g., Go Signal, movement onset, etc.). The approach provides an N x N (N= recording sites) correlation matrix, the generic entry of which is the C_{ij} between the i-th and j-th channel time series in the time window.

We interpreted the correlation matrix as being the adjacency matrix of an undirected weighted graph, in which the nodes are the channels and the weighted edges are the pairwise C_{ij}. Because the purpose of this study was to characterize the network organization that supports the evolution of motor decisions in relation to behavioural

events, we needed a graph that represented the time-evolving coupling between electrodes. The simplest route to addressing this issue was to assess the dynamical connectivity between nodes using a sliding window approach to support the static measure of Pearson C_{ij}. To this end, the window width w parameter is crucial for segmenting the time series. Because the uncertainty in the correlation measure is given by $\epsilon = \frac{1}{\sqrt{2B_w W}}$, where B_w is the spectral bandwidth of the data and w is the window width (O'Neill et al., 2018), we chose a w that effected a good compromise between accurate time resolution and statistical significance. Because MUA lies in the $[0.2, 1.5]$ kHz band, we obtained $\epsilon \sim 0.06$, choosing w=100 ms.
Once w and a step of 5 ms were fixed, we then defined the following task epochs to perform our analysis: for correct no-stop trials and stop-wrong trials, we defined the Go epoch with w from -150 ms to +350 ms relative to the Go Signal and the pre-Movement epoch from -350 ms relative to the Movement onset. For correct and stop-wrong trials, we defined the Stop signal epoch, with w from -150 ms to +150 ms relative to the Stop signal. Our aim, while using the Stop signal epoch, was to compare conditions in which a movement was generated (stop-wrong trials) to those in which a movement was inhibited (stop-correct trials). This choice is due to the objective of our analyses: inspect the state of the network at the time of the Stop signal presentation and before. Indeed, in agreement with the race model (see **??**),a stop trial is wrong if the Stop signal is presented when the motor plan is already at a processing state that it can no longer be inhibited. For this reason, by the time of the Stop signal is presented we expected the network state of stop-wrong trial to differ from the one of stop-correct trials (and comparable to the one of no-stop trials). With our choice of w, each time point x_t of the epochs had boundaries of x_t $\pm$ 50 ms. Consequently, we managed to fully describe the following intervals: [-100, +300] ms for the Go epoch, [-300, 0] ms for the Pre-Movement epoch and [-100, +100] ms for the Stop signal epoch (see Figure 1).

To remove noise and outliers from our data, we excluded the trials for which the MUA showed a peak with an amplitude that exceeded the average of the activity of 2 standard deviations in the epochs of interest and for over 80% of the channels from the analysis. Moreover, for Monkey C, damaged electrodes were excluded a priori from the computation, such that its correlation matrix had dimensions of 79 x 79. We computed a correlation matrix for each window of every trial of our epochs to obtain a time course of connectivity at the single-trial level (single-trial network time series). Successively, to generate a unique average matrix for each time window,

each coefficient of the single-trial matrices at timestep t was Fisher-transformed, averaged over trials and then back-transformed, ensuring that the variance in C_{ij} was disassociated from its mean (Thompson and Fransson, 2016). As a result, we were able to reconstruct the evolving dynamics of the network as a sequence of snapshots at each time step, at the single-trial and average levels (average network time series).

2.4.5 Percolation and minimum spanning tree analysis

Fixing an appropriate threshold to study network properties is a common problem when studying brain connectivity matrices (structural or functional) with a graph-based approach. To overcome this obstacle, we adopted a solid method, called percolation. Percolation is a tool that is rooted in statistical physics and has been applied to study phase transitions of connected subgraphs in random networks (Callaway et al., 2000), the first application of which to brain networks was performed by Gallos (Gallos et al., 2012). Since then, the method has been used progressively and successfully to examine the hierarchical organization of brain networks (Nicolini et al., 2017; Vlasov and Bifone, 2017; Mastrandrea et al., 2017; Bordier et al., 2018; Ferraro et al., 2018). We performed percolation analysis to examine the organization of the network without any a priori assumptions (data-driven approach). Simply, percolation consists of the iterative removal of edges of a network and allows one to inspect the intrinsic stability of the network and the presence of a hierarchical organization simultaneously. The usual procedure is to monitor the disaggregation of the network as a function of a threshold of interest (the correlation coefficient, in our case). We used the number of connected components as a parameter to monitor disaggregation (see also Bardella et al., 2016). A hallmark of hierarchical organization is the presence of multiple disaggregation points (more formally, percolation thresholds). At each of these thresholds, the network fractures and reveals its self-organized internal structure, comprising connected subgraphs (Gallos et al., 2012), corresponding to a stepped percolation curve that is endowed with plateaus. Conversely, in a graph with random features (i.e., without organization), the number of connected components is characterized by a sharp transition (Callaway et al., 2000; Albert and Barabasi, 2002). Recent studies (Bordier et al., 2017; Nicolini et al., 2017) have shown that percolation makes it possible to find a threshold that realizes the optimal balance between the removal of spurious correlations that are induced by noise and the loss of information that might be encoded in the weaker links. This threshold is just above the fragmentation of the largest connected component of the graph. Here, although the spurious links have been removed, the

connectedness and hence, the structural fundamental characteristics of the network is preserved. Our analysis followed several steps (Bardella et al., 2016): 1) all experimentally determined correlation coefficients are listed in decreasing/increasing order; 2) starting from the greatest/lowest value, each entry in the list is chosen as a threshold; 3) all links that correspond to the correlations above/below the threshold are removed and 4) the number of connected components that characterize the remaining part of the network is computed. Thus, it is possible to analyse the network of negative and positive correlations We examined the topology of the functional network of the PMd by inspecting a well-known measure of centrality, the vertex degree. Vertex degree is the number of links to a node i: $VD_{\mathrm{i}} = \sum_{j=1}^{N} c_{\mathrm{ij}}$, where c_{ij} is the generic entry of the adjacency matrix. We computed the probability distribution of vertex degrees (i.e. the degree distribution) at the threshold just above the fragmentation of the largest connected component for each step of the average network time series. In the context of complex network theory, nodes that significantly exceeds the average network degree arise as a long tail in the degree distribution and are called hubs (Albert and Barabasi, 2002). We further studied the topological organization of the functional connections of the PMd by computing the minimum spanning tree (MST). Given an undirected weighted graph, the MST is defined as a unique subgraph that includes all nodes of the original graph and connects them, minimizing the sum of the weights of the edges without forming cycles and minimizing the number of links that are involved. As reported in Stam et al. (2014), in recent years, the use of spanning tree techniques has attracted the interest of neuroscientists, as implemented in EEG (Demuru et al., 2013; Lee et al., 2006, 2010), fMRI (Alexander-Bloch, 2010; Ciftci, 2011; Bardella et al., 2016; Mastrandrea et al., 2017) and magnetoencephalography (MEG) source space data studies (Gong et al., 2009; van Dellen et al., 2009; Dubbelink, 2014). The MST (Mieghem and van Langen, 2005; Mieghem and Magdalena, 2005) provided us with the backbone of the functional interactions in the PMd and allowed us to strengthen the results that were yielded via percolation analysis. We obtained an MST for each step of our average network time series for all epochs. In the MST approach, a tree can have two extreme topologies: path (or chain) and star. In the first case, all nodes are connected to two other nodes, apart from the nodes at either end, each of which have only one link. In the latter, there is one central node that is connected to every other node (leaves) via a single link only. With the star topology, the efficiency of communication and integration of information between nodes is optimal, harbouring the maximum possible number of leaves and the minimum average path

length. However, in this topology, the problem of overloading the central node arises easily; thus, the optimal configuration for an efficient tree would be halfway between these two extremes. Between the path and star, there exists a spectrum of many possible configurations, the characteristics of which can be described with a set of relatively simple measures, as detailed in Stam et al. (2014). Among the various measures, we chose the leaf number (LN). The leaf number is the number of nodes with only one link. With the LN, it is possible to intuitively quantify the topology of an MST. A path would have an LN of two, whereas a star of N nodes would have an $LN = N - 1$ that is, the same number of available edges. Thus, an MST that more closely resembles a path will have a lower LN than one that is more similar to a star. A shift from a path-like to star-like configuration of the MST can be interpreted as a change in the network from a less to more integrated state.

2.4.6 A statistical benchmark for PMd functional network

To properly assess the statistical significance of percolation and MST analyses, we defined a null model. The choice of a suitable null model remains a complicated issue in network and complex systems science. In this context, in addition to searching for a model that accounts for the observations, one common practice when analysing real-world networks is trying to identify properties that deviate from the null hypothesis, because it is likely that the deviations themselves encode unknown information about the network functions (for an exhaustive review on this topic see Cimini et al., 2019). Conscious of this, the core of our null model consists of an established numerical procedure for correlation matrices (Higham, 2016), which has been used successfully in other studies on brain networks (Bardella et al., 2016; Mastrandrea et al., 2017). Our procedure comprised three steps for each of the epochs under examination: 1) Calculate the empirical probability distributions of the entries of the empirical correlation matrices. Means and standard deviations of the fitted distributions were estimated by maximum-of-the-likelihood procedure. 2) Generate an ensemble of null networks by drawing correlations from the corresponding fitted distributions. We generated an ensemble of 300 synthetic matrices for each matrix of the average network time series. 3) Refine the procedure to compute the nearest correlation matrices to synthetic ones on which to apply our algorithms and compare the results. The last step is likely to be the most delicate, because it requires the procedure from (Higham, 2016) to be implemented, wherein a fast algorithm computes the nearest correlation matrix to a given, symmetric matrix. Indeed, the first two steps alone do not guarantee that true correlation matrices will be

obtained: in fact, the synthetic matrices might still have negative eigenvalues. For this reason, most standard randomization techniques are unsuitable. Generally, to be considered a correlation matrix, a matrix must satisfy several requirements: it must be symmetric, with diagonal elements equal to 1, with off-diagonal elements in the range [-1, 1], and it has to be positive semidefinite. With our procedure, we kept the spectrum distribution of the observed correlation matrix fixed, applying random orthogonal similarity transformation — which consisted of repeatedly projecting onto the positive semidefinite matrices and then the unit diagonal matrices — to the diagonal matrix of eigenvalues. This matrix was interpreted, for each epoch, as the weighted adjacency matrix that represented the functional network of the PMd. We then compared the observed percolation trend with those obtained running the procedure on the synthetic matrices. The slope of the percolation curve was computed between correlation values in correspondence of which we detected 2 and n-1 connected components respectively, where n is the number of nodes (we excluded trivial clusters that were represented by the entire network and the single channels/nodes). To test results from MST analysis, the test statistic employed for comparison is the ensemble of LN obtained from the MST computed on the randomized matrices.

2.5 Supplementary Material

For the supplementary materials for study 1 please refer to the following links:

- Supplementary Figures $S1$ to $S14$:
  https://ars.els-cdn.com/content/image/1-s2.0-S1053811919309450-mmc1.pdf
- Supplementary videos $V1$ and $V2$:
  https://ars.els-cdn.com/content/image/1-s2.0-S1053811919309450-mmc3.mp4
  https://ars.els-cdn.com/content/image/1-s2.0-S1053811919309450-mmc4.mp4

Study 2
Changing in the hierarchical organization of local information dynamics during motor decision in the premotor cortex of primates

3.1 Abstract

Despite recent works have investigated functional and effective cortical networks in animal models, the dynamical information transfer underneath most of the higher brain functions is still unknown. Here we address the issue by analysing, at the mesoscopic scale, neuronal activities from a multielectrode array in the dorsal premotor cortex (PMd) of rhesus monkeys during a countermanding reaching task, requiring motor decisions after visual instructions. We used multivariate Transfer Entropy and graph theory to quantify and describe decision-related changes in the local information patterns. We found that the highly heterogeneous activities of the PMd network could be described by 4 classes according to the information processing during the task. Moreover, we found that the observed network is hierarchically organized and exhibits topological differences between movement generation and inhibition. Interestingly, these differences were reflected in changes in the hierarchical organization among classes and paired with a decrease in the information processed when movement was cancelled after programmed. We thus propose that PMd

participates to motor decisions by readjusting the local network in relation to the contextual changes.

3.2 Introduction

The brain is a complex system formed by different interconnected modules. The definition of a module depends on the scale of analysis. At the small scale modules are single neurons, at the large scale they ae coincident with great-specialized brain areas. In between, at the mesoscale level, aggregates of populations of neurons of different dimensions (columns; single areas; etc). In the last fifty years, neuroscience has tried to describe brain computations linking neural activities to behaviour. At whatever scale, crucial to this purpose is the understanding of how different modules interact and how information is shared and processed among parts. In this context, the neurophysiological approach to brain functions with recording microelectrodes provided invaluable advances, mainly in animal models (Hong and Lieber, 2019). Indeed, the high spatial resolution of the high density recordings methods proved to be suitable for linking neurons activity to behaviour, to describe the organization of local microcircuits and, sometimes, of the over standing larger networks (Ferraina et al., 2001; Wurtz et al., 2001). Most of these studies referred to the analysis of single unit (spiking) activity (SUA), others focused more on mesoscopic signals as the local field potentials (LFP) indicating the average synaptic input to the explored area (for review see Herreras, 2016) and, to a lesser extent, on Multiunit activity (MUA) sampling the average spiking activity (output) of discrete populations (Mattia et al., 2013; Stark and Abeles, 2007; Trautmann et al., 2019).

Aiming to contribute to the understanding of the role of the dorsal premotor (PMd) cortex in arm motor control (Cisek and Kalaska, 2010; Shenoy et al., 2013; Wise et al., 1997) we studied the MUA derived from a multi-electrode array and implemented a combined information-theory and topological approach to describe how the collective activity of mesoscopic local modules is linked to motor decision-making. Indeed, it has been shown that neurons express more their contribution to complex behavioural functions either when observed as coordinated functional ensembles (Bardella et al., 2020; Fetz, 1992; Georgopoulos et al., 1986; Munoz and Wurtz, 1993; Riehle et al., 1997; Schall, 2015; Vaadia et al., 1988; Vyas et al., 2020) or described as common responses to the input they receive (e.g., the visual stimulus orientation; Hubel and Wiesel, 1962). A paradigmatic example is the interaction between fixation and movement neurons during saccade generation (Munoz and Wurtz, 1993; Schall,

2015). Here, we explored how information is managed among modules and how the local PMd network is arranged during either movement execution or cancellation. How different neuronal actors contribute to motor decisions is in fact still largely discussed, especially for brain centres involved in reaching control (Shenoy et al., 2013; Stuphorn, 2015).

We observed that modules segregate into different classes, organized around different hierarchical levels, changing in relation to the behavioural outcome. Moreover, we found the PMd network explored different configurations depending on the behavioural decision. Indeed, during movement generation, compared to movement inhibition, information transmission among modules was higher and required fewer steps. This demonstrates that the level of classes coordination is different for the two motor behaviours explored and suggests a new perspective on the view of how the local computation evolves during action decision-making.

3.3 Results

We investigated, at the mesoscopic level, the information transfer and directed connectivity patterns among discrete populations of neurons during the motor decision phase for arm movements. To this aim we extracted a spectral derived MUA (see below) from each electrode of a microelectrode array (up to 96 channels) in the dorsal premotor cortex (PMd) of two male Rhesus monkeys (Monkey P and Monkey C) while they performed a countermanding reaching task.

This task (Fig. 3.14) required to move (Go trials; 67%) toward a peripheral target (either right or left) on a touch screen but to cancel the movement (Stop trials; 33%) in case of appearance of a Stop signal. The two types of trials were randomly presented. During Go trials, after the disappearance of the central target (Go signal) the monkeys were instructed to reach the peripheral target to obtain the reward. In Stop trials, after the Go signal, the central target reappeared (Stop signal) after a variable delay, called the SSD (Stop signal delay). In these trials the monkeys were required to refrain from moving to earn the reward (correct Stop trials). If the monkey were unable to stop, the trials were classified as wrong Stop trials, and no reward was provided. Because the SSDs were varied according to a staircase procedure based on the performance, correct Stop trials constituted approximately 50% of Stop trials (see Table 3.1). This task, when the behavioural performance adheres to the race model, i.e. when wrong stop trials are faster than Go trials

(Table 3.1), allows to estimate a time window during which the decision to move (or to refrain) is taken. This time window is the stop signal reaction time (SSRT; see Table 3.1 for the values observed in the present study). Hence, the SSRT can be considered as the lead time that is required to inhibit a movement. Following the Go signal the movement is prepared is a similar manner until the presentation of the Stop signal in both Go and correct Stop trials. From the point of view of Go trials, the average SSRT ($\overline{SSRT}$, see Table 3.1) marks the time, before movement execution, that would have corresponded to the presentation of the Stop signal[2]. Consequently, when comparing time epochs between Go and correct Stop trials, every time difference that exceeds the duration of SSRT must be accounted for. As a clarification, let us examine the following example. Consider analyzing an epoch of t_{go} ms before movement execution in Go trials and having an SSRT of t_{ssrt} ms. Let us assume $t_{go} > t_{ssrt}$. The corresponding time window in correct Stop trials would be given by the interval $T = [-(t_{go} - t_{ssrt}), + t_{ssrt}]$ ms with respect to the Stop signal presentation. The amount $t_{go} - t_{ssrt}$ is precisely the excess to account for. Note that if $t_{go} \leq t_{ssrt}$ there is no excess to consider and t_{go} is fully described, in correct Stop trials, by t_{ssrt}. Thus, the countermanding task permits to investigate the neuronal correlates of motor decision by comparing, in a behaviorally relevant time window dependent from the SSRT (i.e., T), trials related to two behavioural conditions: one in which movements are prepared and then executed (Go trials); one in which movements are prepared and then aborted (correct Stop trials).

3.3.1 Neural Recordings can be grouped in classes providing different contribution to the network information dynamics

We investigated a total of 21 recording sessions (12 for monkey P and 9 for monkey C). For each of them we preliminarily checked for the adherence of the behaviour to the race model (Logan and Cowan, 1984; Verbruggen et al., 2019), then we estimated the SSRT for each recording session (see Materials and Methods and Table 3.1). As a measure of the activity of a discrete population of neurons located around the tip of each electrode, we used a spectral measure of the multiunit activity (MUA, Bardella et al., 2020; Mattia et al., 2013). From now on we refer for simplicity to these discrete populations as modules.

Fig 3.15 shows for each recording electrode of one session the MUAs for Go trials

[2]The same obviously holds from the point of view of Stop trials: $\overline{SSRT}$ marks the time, after the Stop signal presentation, that would have corresponded to the movement execution.

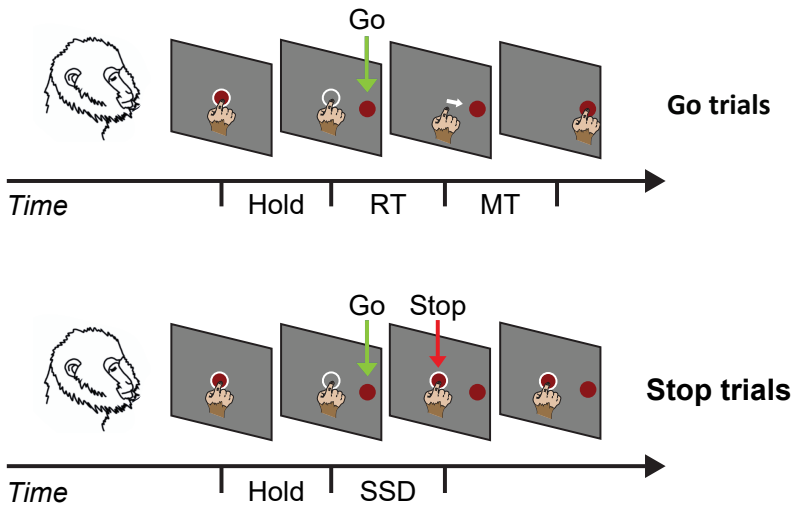

Figure 3.14. Sequence of behavioural event characterizing the task. Go and stop trials were randomly intermixed during each session. Hold, holding epoch before target presentation; RT, reaction time; SSD, Stop signal delay.

aligned to the movement onset (green lines) and Stop trials (red lines) as aligned to the Stop signal presentation. Most MUAs display a clear difference between correct Stop and Go trials after the Stop signal (i.e., during the specific SSRT) reflecting the active participation of PMd in the decision to generate or inhibit reaching movements. Several features are observable. For example, the time of divergence between the two activities for the different channels was highly variable. Moreover, in some cases (eg channels 25 and 43) the observed pattern was completely opposite (more intense activity in Stop trials than in Go trials). Similar patterns have been observed in all recording sessions. In short, the various modules seem to contribute to the control exerted on the movement to be performed by PMd in a very heterogeneous way. Of relevance, from these considerations nothing can be inferred about the information transfer and the functional relationship between different modules.

To investigate directed information transfer between the network modules we used Transfer Entropy (TE), a well-established model-free information theoretic method (Schreiber, 2000). In a given epoch TE detects asymmetric information flows among the modules, and hence it allows defining modules acting as drivers (or sources) or targets of information transfer (see Materials and Methods for further details). To evaluate whether the different behavioural conditions (moving vs withholding) were characterized by different local information dynamics we computed TE between

Behavioural Results						
Monkey P						
S	$\overline{RT}_{Go}$	$\overline{RT}_{Wr}$	$\overline{SSD}$	$\overline{SSRT}$	$P_{inhibit}$	*p-value*
1	590 ms	559 ms	273 ms	317 ms	0.52	$p < 0.05$
2	584 ms	564 ms	277 ms	307 ms	0.50	$p < 0.05$
3	575 ms	503 ms	293 ms	282 ms	0.69	$p < 0.05$
4	618 ms	592 ms	335 ms	283 ms	0.52	$p < 0.01$
5	868 ms	549 ms	675 ms	193 ms	0.58	$p < 0.01$
6	572 ms	540 ms	293 ms	279 ms	0.50	$p < 0.05$
7	643 ms	622 ms	382 ms	261 ms	0.51	$p < 0.05$
8	600 ms	568 ms	340 ms	260 ms	0.48	$p < 0.01$
9	656 ms	641 ms	445 ms	211 ms	0.37	$p < 0.01$
10	788 ms	753 ms	528 ms	260 ms	0.54	$p < 0.01$
11	674 ms	619 ms	418 ms	256 ms	0.56	$p < 0.01$
12	765 ms	721 ms	504 ms	261 ms	0.51	$p < 0.01$
Monkey C						
1	598 ms	523 ms	322 ms	276 ms	0.57	$p < 0.01$
2	539 ms	460 ms	382 ms	157 ms	0.65	$p < 0.05$
3	561 ms	522 ms	318 ms	243 ms	0.58	$p < 0.01$
4	673 ms	625 ms	424 ms	249 ms	0.60	$p < 0.05$
5	636 ms	608 ms	396 ms	240 ms	0.55	$p < 0.05$
6	575 ms	533 ms	292 ms	283 ms	0.42	$p < 0.01$
7	667 ms	620 ms	383 ms	284 ms	0.60	$p < 0.05$
8	688 ms	672 ms	413 ms	275 ms	0.43	$p < 0.05$
9	688 ms	657 ms	402 ms	286 ms	0.60	$p < 0.01$

Table 3.1. Behavioural results. S, index of the recording session. $\overline{RT}_{Go}$, mean reaction time of Go trials. $\overline{RT}_{Wr}$, mean reaction time of wrong-stop trials. $\overline{SSD}$, mean SSD of Stop trials. $\overline{SSRT}$, mean Stop Signal Reaction Time. $P_{inhibit}$ inhibition probability. The *p-values* result from the independence test between $\overline{RT}_{Go}$ and $\overline{RT}_{Wr}$ (Kolmogorov-Smirnov test).

trial-averaged time series of neuronal activity separately for Go and correct Stop trials. We considered $t_{go} = 400ms$ for Go trials and then estimated the corresponding time windows T in correct Stop trials as described in the previous paragraph. A $t_{go} = 400$ ms ensured us to exclude from the epoch the Go signal presentation by at

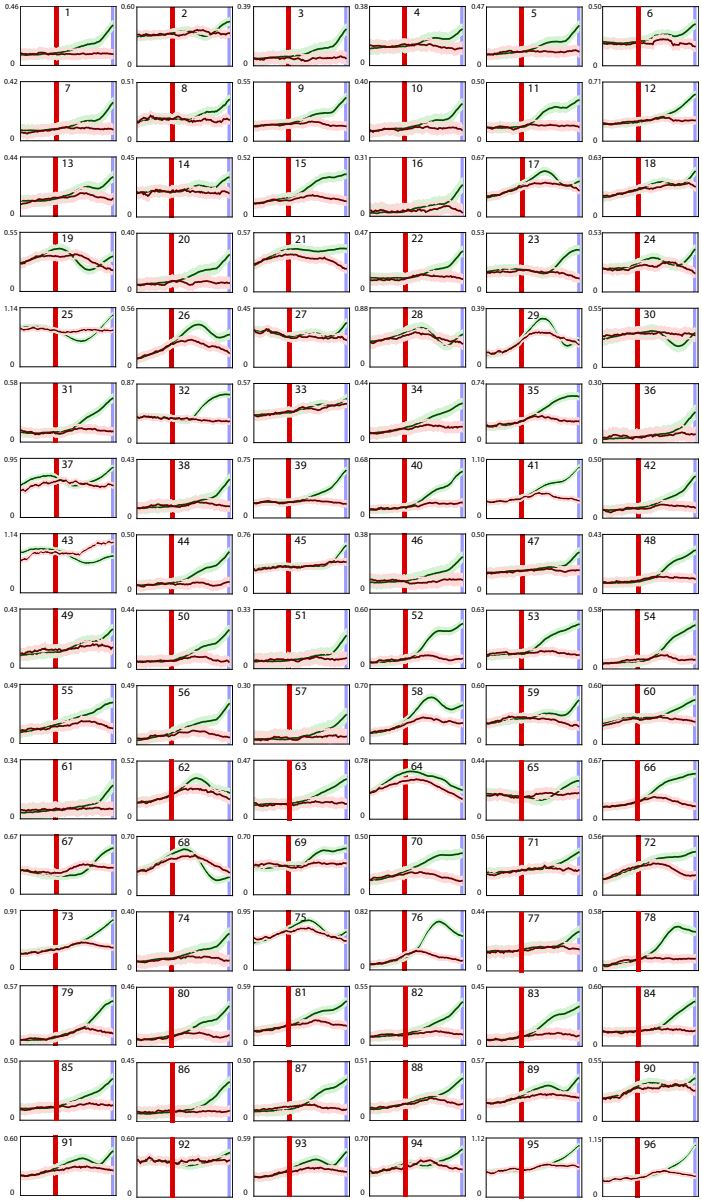

Figure 3.15. Neuronal modulation in the two behavioural conditions for all channels of a typical recording session. Green traces show the average activity during Go trials aligned to Movement onset (rightmost part of the plot). Red traces show the average activity during correct Stop trials aligned to the Stop signal presentation (red vertical line). The window between the stop signal and the movement onset is the SSRT.

least 100ms for all recording sessions for both animals. We found that some of the modules were drivers in both Go and Stop conditions (**Common_drivers**); others were drivers in one behavioural condition only (**Go_drivers** and **Stop_drivers**); others were never drivers and just targets of information flow (**Targets**) (see Table

Classes Composition	
Monkey P	$N = 96$
Class	$\boldsymbol{\mu \pm SD}$
Go_drivers	6.46 ± 2.90
Stop_drivers	13.71 ± 3.22
Common_drivers	8.62 ± 3.60
Targets	67.20 ± 4.88
Monkey C	$N = 79$
Class	$\boldsymbol{\mu \pm SD}$
Go_drivers	6.78 ± 3.93
Stop_drivers	9.56 ± 3.78
Common_drivers	7.00 ± 2.06
Targets	55.70 ± 5.29

Table 3.2. Classes composition. For each monkey the composition of classes averaged over recording sessions is reported. Composition is expressed as the average number of nodes (μ) belonging to each class. SD, standard deviation. N, the number of channels available.

3.2; see Materials and methods for further details). The presence of different classes of modules straightforwardly showed that the intrinsic composition of the PMd information network is heterogeneous, with some of the modules operating as drivers only in relation to a specific behavioral outcome (movement vs withholding). This hinted that the network configuration underlying information transmission changes according to the specific decision and behavioural output.

3.3.2 Neuronal activity classes are hierarchically organized. Common_drivers act as main hubs for information transmission within PMd. Other classes act as hubs only in relation to specific behavioural conditions

To better understand the role of the identified classes in the PMd network we investigated the topology of information transmission for each session and behavioural condition examined. In this framework each entry of the TE matrix is interpreted as a node of the network, and each link (or connection) is the information exchanged between nodes (see Materials and methods for further details). To quantify the

topology of information transmissions we resorted to different graph-based measures. We first computed the vertex degree (VD), i.e. the number of connections per module. A high value of the VD indicates that the module is connected with many others. The opposite holds for a low value of VD. Thanks to the asymmetry of TE, which defines drivers and targets, for each module it is possible to distinguish between the information directed towards other modules (VD_{out}) and the information arriving from other modules (VD_{in}). We examined the VD_{out} and the VD_{in} distributions for each recording session of both monkeys and we observed that all distributions were skewed. However, we found that only VD_{out} distributions were fat-tailed (see supplementary figures ...). The high values of VD_{out} associated to the tails thus indicate modules with a number of outwards connections that greatly exceed the average value (see Materials and Methods). These modules are network hubs (Albert and Barabási, 2002). The VD values, together with the direction of information flow detected by TE, allow defining a hierarchy among modules. Indeed, given a driver and a target the driver is hierarchically above the target. The existence of hubs means that a few modules determine the state of many others, and hence the global configuration of the network. Fig 3.16 shows the topology of PMd network in both behavioural conditions for an example session of Monkey P. Each module is assigned to a class as previously obtained from the TE analysis and coloured accordingly. The size of the dots used to identify each module (node) reflects its VD_{out} value, i.e. the number of modules on which it acts as a driver. The arrow for each connection indicates the direction (in/out) for the information path. In Go trials (top) the topology reflected a more centralized (in terms of VD_{out}) organization (star-like topology) compared to the Stop trials (bottom), confirming previous observations (Bardella et al., 2020). Indeed, in a recent study on correlation networks during the same task we showed that the presence of a star-like topology in the PMd network is the hallmark of the incoming movement. However, here, by adding the insights provided by the TE analysis, the emerging picture is of a network changing not only in the overall organization but also in the role of the components. For example, Fig 3.16 shows that Stop_drivers emerge as information spreaders in Stop trials only.

Figure 3.17 (top panels) shows that in all of the analysed sessions the Common_drivers exhibited the highest values of VD_{out} (See Table 3.3 for the corresponding statistics) compared to other classes in both Go and correct Stop trials thus resulting as the principal information-spreaders hubs across different behavioural conditions. Therefore, Common_drivers are located at a higher hierarchical level in

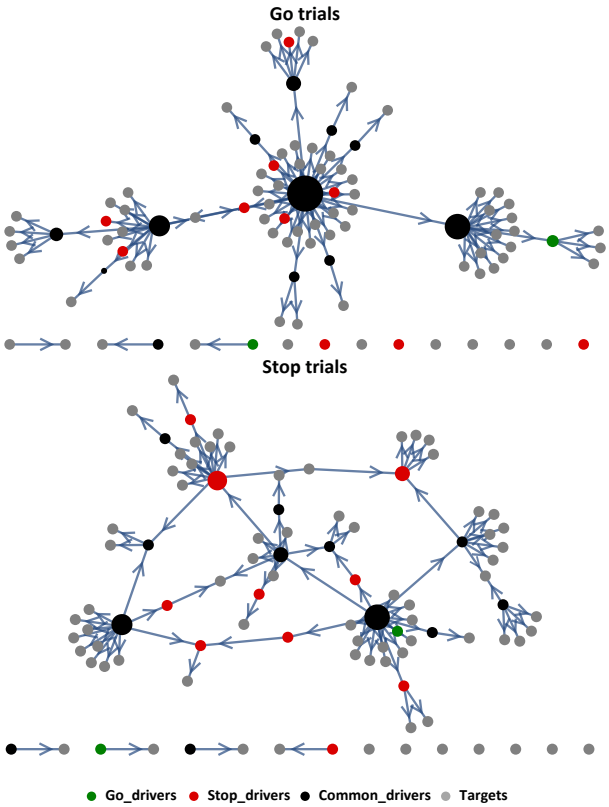

Figure 3.16. Information network of Go and Stop trials for an example session. Each node is coded accordingly to the corresponding class (see legend in the lower part of the figure). The size of the nodes is scaled according to the corresponding VD_{out}, thus bigger nodes are the information-spreaders hubs (see text for details).

the network as they regulate information transfer whatever decision, moving or stopping, is taken (see also next paragraph). Conversely, Go_drivers and Stop_drivers displayed a different role (different VD_{out} values) in Go and Stop trials, suggesting that the hierarchical organization of the network changes in relation to the motor decision process. Indeed, Stop_drivers are never hubs in Go trials and Go_drivers are never hubs in Stop trials. As a further measure of the organization of the PMd network we used betweenness centrality (Freeman, 1977; White and Borgatti, 1994) (BC). BC quantifies the influence that a given node has over the flow of information between other nodes. Therefore, it gives a measure of how a node controls communications in a network. BC is computed as the fraction of shortest paths between all nodes in the network that pass through a given node. Since we are dealing with an information network, we used BC to quantify the capability of each node to mediate and route the information traffic. An high BC value indicates that a node strongly

mediates information flow because it lies on a considerable fraction of shortest paths. Hence nodes with high BC values are topological central nodes. As reported in Fig 3.17 (panel A, bottom) and in Table 3.3, we found higher BC values during correct Stop trials compared to Go trials meaning that during correct Stop trials nodes are connected by a higher number of paths. This implies that a shift toward a less direct (and hence less centralized in terms of VD_{out}) communication between nodes occurs during Stop trials only; information is detoured through more shortest paths resulting in a more distributed and widespread transmission. An intuition can be gained by noticing the arrangement of the graphs during correct Stop trials which results more "expanded" than the optimal star-like configuration of Go trials (see Figure 3.16). Analogously to what found during the analysis of VD_{out} , Go_drivers and Stop_drivers (green and red dots in Fig 3.17) displayed a different role (different BC values) in Go and correct Stop trials respectively, confirming the specificity of these classes in relation to the behavioural conditions. The values of BC found for the Common_drivers (black dots in Fig.4) during both behavioural conditions corroborate what was found via the VD_{out} analysis: in the PMd information network they manage and distribute the information flow. Moreover, during movement inhibition the actors that collaborate the most with the Common_drivers in rerouting and reverberating communications are the Stop_drivers.

To have a compact view of the overall differences between the VD_{out} and BC measures across behavioural conditions we computed a summarising index named centralization index C (Freeman, 1977; White and Borgatti, 1994). C is the total average difference between the highest value of the centrality measure inspected (VD_{out} and BC in our case) and the values assumed by all the other nodes. High values of C indicate that nodes with high centralities with respect to the other nodes in the network exist. In this way a score with which to compare the overall organization of networks in terms of centrality measures is obtained (see materials and methods). We computed C for both measures for each recording session and then we averaged over sessions. Panel A of Figure 5 reports the average centralization indexes compared between behavioural conditions for both animals (see also supplementary figure ...). As expected, C of VD_{out} (C_{vd}) decreases from Go to correct Stop trials while the opposite holds for C of BC (C_{bc}). This confirms, at the overall level, how information processing is based on different topologies during the two behavioural conditions. We then calculated the total information processed during Go trials and correct Stop trials (Figure 5, panel B and supplementary figure ...). We found that during correct stop trials less information was processed compared to Go trials. This means that

overall changes in the topological arrangement of the the PMd network correspond to overall changes in the amount of information exchanged. More specifically, the increase in BC during correct Stop trials is accompanied by a reduction in the total amount of information elaborated. To sum up, we demonstrated with the used graph measures that classes are hierarchically organized in PMd during movement planning and suppression and that information is processed differently and to a lesser extent during correct stop trials compared to Go trials. Results revealed that the Common_drivers as the most topological central nodes in the network with the Go_drivers and the Stop_drivers playing a crucial supporting role in detouring the information during movement planning and inhibition respectively.

3.3.3 Different interactions among neuronal classes characterize behavioural conditions

To summarize the contribution of each interaction among classes we computed the average amount of information exchanged between the four classes during both behavioural conditions. To this end, we constructed a 4x4 matrix whose generic entry is given by expression (3.5.6). We then represented the matrix I as a network in which each node is now a class. This makes possible to have a compact picture of the differences between Go and correct Stop trials in terms of interactions between classes. We calculated I for both behavioural conditions of each recording session and we then averaged over sessions; results are shown in Figure 3.19 (see also Table 3.4). The Common_drivers were confirmed to be part of the high order class in the network since they transmit to other classes without receiving. Indeed, even when the Go_drivers and Stop_drivers emit information on their own, they receive from the Common_drivers. This means that the first ones are hierarchically located at a lower level. Moreover, the extent of communication of the Common_drivers with the Targets is significantly greater than that of the Go_drivers and Stop_drivers (see Table 3.4). This implies that the Common_drivers determine the global state of the network with Go_drivers and Stop_drivers playing a supporting role. It is worth noticing that the specificity of Go_drivers and Stop_drivers is confirmed by the direction of their interactions during behavioural conditions. In fact, during Go trials the Go_drivers transmit to the Stop_drivers helping the Common_drivers in the control while the opposite happens during correct Stop trials. The amount of information that the Common_drivers distribute in the network diminishes from Go to correct Stop trials. This complement and helps to better understand what said in the previous section: information is processed differently during correct Stop

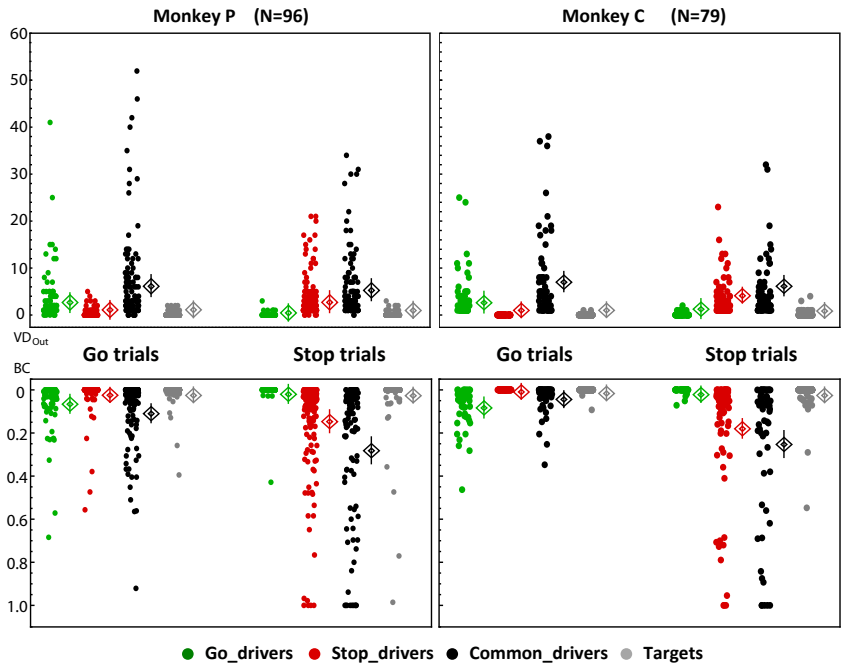

Figure 3.17. Measures for topology of information transmission. **Top panels**: VD_{out} values compared across behavioural conditions for all recording session. The Common class (black points) shows the highest values of VD_{out} compared to other classes in both behavioural conditions (for both monkeys, all adjusted p-values $Qs < 0.01$). Go_drivers and Stop_drivers show the second highest VD_{out} values during Go (for both monkeys all $Qs < 0.01$) and correct Stop (for both monkeys all $Qs < 0.01$) trials respectively. **Lower panels**: Normalized BC values compared across behavioural conditions for all recording session. Go_drivers and Stop_drivers classes have, together with the Common, the highest values of BC during Go and correct stop trials respectively (for both monkeys all $Qs < 0.01$). The Stop_driver class is the one with the greatest increase ($\Delta_{Go-Stop}$) in BC passing from Go to correct Stop trials (for both monkeys all $Qs < 0.01$). Colours reflect the neuronal classes as in Figure 3. Means and standard errors are indicated by the diamonds and related lines. Statistics is based on the adjusted p-value (Q) obtained from Kolmogorov Smirnoff tests and false discovery rate (FDR) correction. See Table 3.3 for the details.

trials where the network undergoes a less direct configuration due to an increased number of shortest paths between the nodes. Network interactions are consistent across recording sessions for both monkeys (see Table 3.4). Common_drivers are hierarchically above the other classes and orchestrate communication: they transmit information to other classes in both behavioural conditions without receiving information from the other classes of the analysed PMd network. Moreover, during

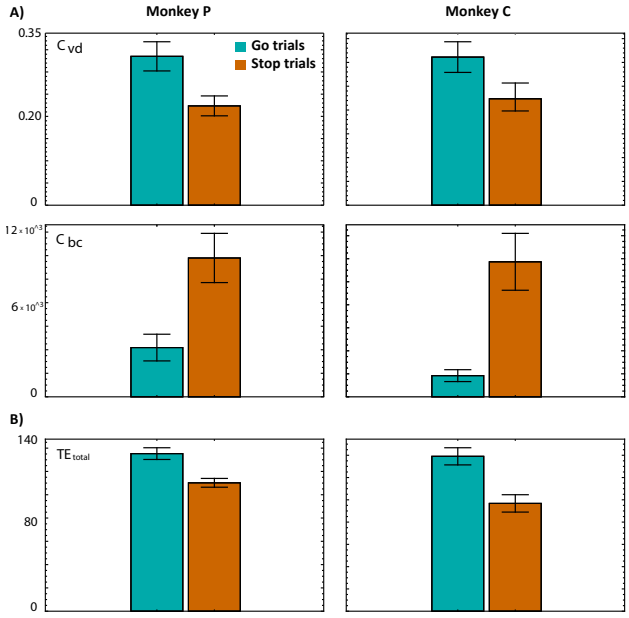

Figure 3.18. Overall network comparison between behavioural conditions. Panel A The overall centralization index C for both VD_{out} (C_{vd}) and BC (C_{bc}) measures averaged over recording sessions and compared between behavioural conditions for both monkeys. C gives an overall topological comparison of the information network compared between behavioural conditions. **Panel B** Total information processed averaged over recording sessions compared between behavioural conditions. Cyan: Go trials. Orange: correct Stop trials. Error bars are given by the standard error of the mean.

Go trials Go_drivers participate transmitting to the Targets as the Stop_drivers class does during correct Stop trials.

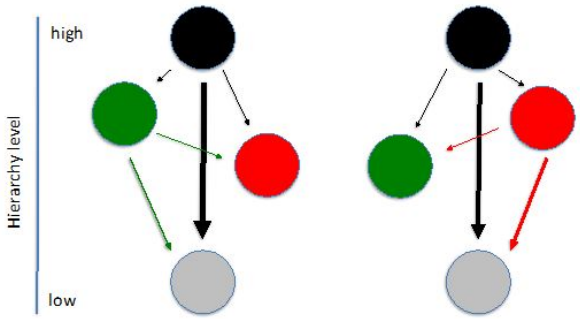

Figure 3.19. Network representation of interactions between classes in the two behavioural conditions: Colours codes for the classes are the same of the previous figures. Uncertainties are obtained via error propagation (see materials and methods).

VD_{Out}			
Monkey P			
Go trials	Go_drivers	Stop_drivers	Targets
Common_drivers	$Q < 0.005$	$Q < 0.001$	$Q < 0.001$
Stop trials	Go_drivers	Stop_drivers	Targets
Common_drivers	$Q < 0.001$	$Q < 0.01$	$Q < 0.001$
$\Delta_{Stop-Go}$			
Go_drivers	Stop_drivers	Common_drivers	Targets
−97%	+1326%	−16%	+4%
Monkey C			
Go trials	Go_drivers	Stop_drivers	Targets
Common_drivers	$Q < 0.01$	$Q < 0.001$	$Q < 0.001$
Stop trials	Go_drivers	Stop_drivers	Targets
Common_drivers	$Q < 0.001$	$Q < 0.01$	$Q < 0.001$
$\Delta_{Stop-Go}$			
Go_drivers	Stop_drivers	Common_drivers	Targets
−97%	+9828%	−29%	+950%
$Q < 0.001$	$Q < 0.001$	$Q > 0.25$	$Q > 0.25$

BC			
Monkey P			
Go trials	Go_drivers	Stop_drivers	Targets
Common_drivers	$Q > 0.05$	$Q < 0.001$	$Q < 0.001$
Stop trials	Go_drivers	Stop_drivers	Targets
Common_drivers	$Q < 0.001$	$Q < 0.001$	$Q < 0.001$
$\Delta_{Stop-Go}$			
Go_drivers	Stop_drivers	Common_drivers	Targets
-89% $Q < 0.001$	$+888\%$ $Q < 0.001$	$+157\%$ $Q < 0.001$	$+183\%$ $Q < 0.001$
Monkey C			
Go trials	Go_drivers	Stop_drivers	Targets
Common_drivers	$Q < 0.001$	$Q < 0.001$	$Q < 0.001$
Stop trials	Go_drivers	Stop_drivers	Targets
Common_drivers	$Q < 0.001$	$Q > 0.05$	$Q < 0.001$
$\Delta_{Stop-Go}$			
Go_drivers	Stop_drivers	Common_drivers	Targets
-95% $Q < 0.001$	$+5180\%$ $Q < 0.001$	$+654\%$ $Q < 0.001$	$+800\%$ $Q > 0.25$

Table 3.3. Graph metrics details.

I matrix details				
Monkey P				
Go trials	Go_drivers	Stop_drivers	Common_drivers	Targets
Go_drivers	0	1.3 ± 0.1	0	17.5 ± 0.3
Stop_drivers	0	0	0	0
Common_drivers	3.7 ± 0.1	7 ± 0.2	0	42.3 ± 0.4
Targets	0	0	0	0
Stop trials	Go_drivers	Stop_drivers	Common_drivers	Targets
Go_drivers	0	0	0	0
Stop_drivers	2.6 ± 0.2	0	0	17.5 ± 0.6
Common_drivers	2.3 ± 0.2	4.7 ± 0.4	0	25.4 ± 0.6
Targets	0	0	0	0
Monkey C				
Go trials	Go_drivers	Stop_drivers	Common_drivers	Targets
Go_drivers	0	1.1 ± 0.1	0.3 ± 0.003	21 ± 0.5
Stop_drivers	0	0	0	0
Common_drivers	3.4 ± 0.07	10.7 ± 0.2	0	45.3 ± 0.6
Targets	0	0	0	0
Stop trials	Go_drivers	Stop_drivers	Common_drivers	Targets
Go_drivers	0	0	0	0
Stop_drivers	1.9 ± 0.2	0	0	17 ± 0.6
Common_drivers	2.9 ± 0.2	1.4 ± 0.2	0	23.4 ± 0.5
Targets	0	0	0	0

Table 3.4. I matrix details.

3.4 Discussion

In this work we investigated, for the first time, the patterns of information transfer in a localized cortical network in the PMd directly involved in movement decision-making. We used combined Transfer Entropy and graph-based approaches to analyse simultaneously recorded MUAs (from up to 96 channels). Our results contribute to move forward the knowledge on the neural basis of action decision making at different levels. The first level of advancement is methodological: we employed a graph-based approach combined with information theoretic measures (specifically multivariate Transfer Entropy (TE)) to investigate neuronal interactions underlying motor control. Although TE is growing in popularity in modern neuroscience its application to invasive electrophysiological data has been so far very limited and restricted to either single neurons or in vitro (Buehlmann and Deco, 2010; Orlandi et al., 2014; Shimono and Beggs, 2015) and in silico studies (Ito et al., 2011). Shimono and BeggsShimono and Beggs, 2015 used it at the single neuron level to investigate the structure at different scale of rodent somatosensory cortex (Nigam et al., 2016; Shimono and Beggs, 2015). Timme and colleagues (N. M. Timme et al., 2016) recorded the activity of hundreds of neurons in cortico-hippocampal slice cultures and used TE to study the information transfer changes therein. An early contribution to this research topic is from Gerhard et al. (Gerhard et al., 2011). that inspected the topology of spike trains recordings from the visual system of a rhesus monkey during a fixation task. However, the authors used a different approach to measure directed connectivity. Another contribution comes from the work of Honey (Honey et al., 2007), that investigated a large-scale interregional anatomical network of the macaque cortex trough transfer entropy. An attempt to study voluntary action control through analysis of directed connectivity was made by Jahfari and colleagues (Jahfari et al., 2011) but on human MRI data. Hence, to the best of our knowledge, this report is one of the very few studies that uses graph theory to analyse the information transfer network of a specific cortical area at the mesoscale level in vivo and during a behavioural task. The level of description here obtained is more detailed compared to previous works. Indeed, we were able to specify how the decision on whether to move or to stop is implemented in PMd at the population level and who are the (key) players that perform the computations. Notably, in our framework neither any a priori assumption nor a specific neural modelling technique was needed. Our completely data-driven approach, in addition to complement the most recent models for motor generation and suppression (Boucher et al., 2007;

Lo et al., 2009), permits to overcome their main limitation which reside in the requirement of many biophysical parameters to be tweaked and tuned before fitting with acceptable accuracy the experimental data. Although is still not largely used in behavioural neurophysiological studies at the small and mesoscale, a graph-based conceptualization of neural interactions, united with information theoretic measures, can be very profitable also compared to other common approaches based on analysis of covariance between neurons or mesoscopic signals (Chandrasekaran et al., 2017; Churchland et al., 2012; Clawson et al., 2019; Kaufman et al., 2016; Mattia et al., 2013) and should be exploited more. In fact, these methods are not straightforward in distinguishing the specific contributions of single neurons (or discrete populations of neurons) to the topology of network dynamics, which is indeed the strength of our strategy. On one hand this range of methods allows for a fine temporal description of neural variability but on the other, due to their nature, are neither capable to describe the information flow between neuronal actors nor to provide quantitative insights on the topology of network connections and their hierarchical organization. Without this all spectrum of details the computational strategy underlying motor control (and neural circuitry computation in general) would be yet elusive. Recently, some authors have have started to follow the joint information theory-complex networks approach but for now, to the best of our knowledge, only on cortico-hippocampal (N. M. Timme et al., 2016), somatosensory cortex slice cultures (Shimono and Beggs, 2015) and anesthesiological (Schroeder et al., 2016) data. It is known that to fully understand the neural mechanisms behind motor control future research should focus on cortico-cortical and cortico-subcortical interactions through simultaneous recordings. In this scenario a topological information-based approach would be unquestionably necessary to gain an overall view and elicit detailed insights.

The second level of advancement concerns the novelty of our results compared to other studies, especially those that focused on the possible interaction among different classes of neurons during motor decision. We found, in the characterized PMd network, that neuronal activities could be organized around four different classes and that they actively participate, even with different roles, both in movements execution and cancellation. This constitutes a step forward in the conceptualization of the neural processes at the base of movement generation since all the widely accepted models for inhibitory control of movements (Boucher et al., 2007; Lo et al., 2009; Marcos et al., 2013; Schall et al., 2017; Verbruggen and Logan, 2008; Wei et al., 2015) are deduced from the analysis of single unit firing rates and are

based on the interaction of only two modules (or class of neurons) often reported as Go and Stop units. We instead demonstrated that information is hierarchically transferred between more than two actors with the Common class nodes acting as network hubs. This reflects the existence of a high-order complexity in functional communications and organization at the population level, even in small portions of the cortex, during behavioural control regardless of which the nature of neurons in each class might be (i.e. excitatory or inhibitory neurons etc..). Indeed, based only on the information emitted by each recording site we managed to isolate both condition-specific and nonspecific neuronal classes. It is worth stressing that we drew our conclusion on the heterogeneity of neuronal classes in a completely data-driven and model-free fashion, and this strengthens the result. Additionally, we showed the details of how this transfer occurs at the population level and to what extent it depends on behavioural conditions. Our picture substantially integrates the current view because besides specific classes involved in the generation (Go_drivers) and inhibition (Stop_drivers) of movements, it establishes the existence of a high order class (Common_drivers) not proposed in other works. This highlights, for the first time at the mesoscale resolution, the existence of a fine-grained organization of neural assemblies at the population level that handle intra-area information flow. It is worth pointing out that usual methods of studying neural activity profiles are not sufficient to infer all aspects of such architecture. The Common_drivers are higher in hierarchy with respect to the others for two reasons. The first is because they transmit information to the whole network without receiving from inside the same network (see Figure 3.17). From the information theoretic point of view this indeed means that the state of the other classes can be better predicted by the state of the Common compared to the other classes. Thus, the state of the whole local network depends on the state of the Common_drivers. The second one is topological, being the Common_drivers the most widespread hubs across behavioural conditions. The found subdivision in classes, the presence of hubs and topological central nodes deputed to the rerouting of communications reveal that the cortical information dynamics behind motor control is extremely rich and cannot be entirely explained by the current proposed models. The found topology also implies that the presence of high-degree nodes is a constituent feature of neural processing in a cortical network directly involved in cognitive control, as is the PMd. This is consistent with our previous study (Bardella et al., 2020) in which we pointed out how the functional PMd network organization differs between movement generation and inhibition in terms of hierarchy and centrality of nodes. It is also in

agreement with other works that found fat-tailed degree distributions in silico (Gu et al., 2019), in cortical and hippocampal in vitro networks (Gal et al., 2017; Perin et al., 2011; Schroeter et al., 2015; Shimono and Beggs, 2015; N. Timme et al., 2014), in vivo (Dann et al., 2016) and structural networks (Honey et al., 2007). We found that the arrangement of the PMd information network depends on the behavioural condition, passing from a centralized star-like state during movement planning to a different one during movement inhibition characterized by high values of betweenness centrality and a minor transfer of information. We interpret this reorganization as the execution in the local network of a command originating from other regions. Indeed, as known, the PMd is part of a larger network surbserving motor control based on frontal, parietal, subcortical and spinal structures. Is reasonable to think that during Go trials the hubs serve to convey the command to move to other (and possibly lower) cortical, subcortical, and spinal circuits that will eventually promote muscle activation. In this picture, the state observed during correct stop trials could reflect the PMd collective reaction to the incoming inhibitory thalamic input that prevents the execution of the programmed movement. In this scenario the volition to inhibit is locally implemented as 'the attenuation of the movement state', which seems convenient ad easy to implement at the network level detouring information flow through an higher number of shortest paths between nodes and decreasing the amount of information involved. Future studies will be necessary to investigate to whom the hubs project to. One weakness of this study is that we cannot account for the information dynamic between PMd and other structures of the reaching network. Therefore, additional research will be needed to unambiguously clarify these interactions. Lo et al. (Lo et al., 2009) also introduced a certain degree of hierarchical organization in the form of a top-down control regulating the activation of the Go and Stop unit. However, as also stated in Schall et al.(Schall et al., 2017), the control unit embodied in their model resembled an external homunculs endowed with the ability to tune the parameters to appropriately obtain the desired results. This marks a considerable difference with our report, in which, since our approach is completely data-driven, we did not need to adjust any external modelling unit to obtain the results. Conversely, we used it conceptually to contextualize our results in a wider circuitry frame. Lastly, our findings clearly show that hierarchical control is not only external but is also implemented locally by a specific neuronal class (the Common_drivers) over the others. Through the years, much evidence has been brought to support the idea that the brain is hierarchically organized both globally and locally on a spatial (Bardella et al., 2016; Bardella et al., 2020; Felleman et al.,

1991; C. C. Hilgetag and Kaiser, 2004; C. Hilgetag et al., 2000; M. Kaiser et al., 2007; M. Kaiser, 2010; Sporns et al., 2007; Sporns et al., 2005; Tononi et al., 1994; Watanabe et al., 2014; Zamora-López, 2010; Zeki and Shipp, 1988) (for a detailed review see Hilgetag et al., 2020 C. C. Hilgetag and Goulas, 2020) and temporal scale (Fox et al., 2005; He, 2011; Morcos and Harvey, 2016; Shine et al., 2016; Vidaurre et al., 2017; Zalesky et al., 2014). As far as we know, this is the first work that deeply investigates the local hierarchy of a single cortical area known to have a crucial role in the motor system. These conclusions suggest that the collective network organization found in this work represents the neural implementation of decision making for the voluntary motor control at the PMd level.

3.5 Materials and methods

3.5.1 Subjects

Two male rhesus macaque monkeys (Macaca mulatta, Monkeys P and C), weighing 9 and 9.5 kg, respectively, were used. Animal care, housing, surgical procedures and experiments conformed to European (Directive 86/609/ECC and 2010/63/UE) and Italian (D.L. 116/92 and D.L. 26/2014) laws and were approved by the Italian Ministry of Health. Monkeys were pair-housed with cage enrichment. They were fed daily with standard primate chow that was supplemented with nuts and fresh fruits if necessary. During recording days, the monkeys received their daily water supply during the experiments.

3.5.2 Apparatus and task

The monkeys were seated in front of a black isoluminant background ($< 0.1cd/m2$) of a 17-inch touchscreen monitor (LCD, 800 x 600 resolution), inside a darkened, acoustic-insulated room. A non-commercial software package, CORTEX (http://www.nimh.gov.it), was used to control the presentation of the stimuli and the behavioural responses. Fig. 1 shows the scheme of the general task: a reaching countermanding task (Mirabella et al., 2011). Each trial started with the appearance of a central target (CT) (red circle, diameter 1.9 cm). The monkeys had to reach and hold the CT. After a variable holding time (400–900 ms, 100-ms increments) a peripheral target (PT) (red circle, diameter 1.9 cm) appeared randomly in one of two possible locations and the CT disappeared (Go signal). In no-stop trials, after the Go signal the subjects had to reach and hold the PT for a variable time ($400\tilde{}800ms$,

$100ms$ increments) to receive juice. Reaction times (RTs) were defined as the time between the presentation of the Go signal and the onset of the hand movement. In Stop signal trials, the sequence of events was the same until the Go signal. Then, after a variable delay (Stop signal delay, SSD), the CT reappeared (Stop signal) and the monkeys had to hold the CT until the end of the trial (800–1000 ms) to receive the reward (correct stop trial). Conversely, removing the hand after the Stop signal constituted a wrong response (wrong stop trial). The same amount of juice was delivered for correct stop and correct no-stop trials. The intertrial interval was set to 800 ms. Stop trials represented the 25% of all trials in each recording session. To establish the duration of the SSDs, a staircase tracking procedure was employed. If the monkey succeeded in withholding the response, the SSD increased by one step (100 ms) in the subsequent Stop signal trial. Conversely, if the subject failed, the SSD decreased by one step.

3.5.3 Behavioural considerations

In the countermanding task is of crucial importance the identification of the neuronal signature of the movement execution and its time of occurrence. The task makes possible to calculate a behavioural measure that it is broadly considered an index of efficiency in movement suppression: the stop signal reaction time or SSRT. To estimate SSRT the race model (Logan and Cowan, 1984) is the accepted paradigm. This model describes the behaviour in the stop trials as the result of two stochastic processes racing toward a threshold: the GO process triggered by the onset of the Go signal, which duration is represented by the RT, and the STOP process triggered by the onset of the Stop signal, which duration must be calculated. When the GO process wins the race the movement is generated (stop-wrong trial), alternatively it is withheld (correct Stop trials). The race model allows to estimate the SSRT by considering the duration of the GO process, the probability to respond, and the SSDs. However, to make the race model applicable to study response inhibition, a central assumption must be satisfied: the GO process in the stop trials must be the same as in the go trials (independence assumption). Indeed, the RTs that are employed to estimate the SSRT are obtained from the Go trials. To broadly validate this assumption, stop-wrong RTs must be shorter than the correct go trials (Logan and Cowan, 1984). To estimate the SSRT we employed the integration method because it has been proven to be the most reliable (Band et al., 2003). It assumes that the finishing time of the Stop process corresponds to the nth go RT, where n results from the multiplication of the ordered Go RTs distribution by the overall

probability of responding $p(respond)$. The SSRT is then obtained by subtracting the average SSD from the nth Go RT. The SSRT can also be considered the lead time that is required to inhibit a movement, or, simply, the time that precedes the start of a movement when a Stop signal, if presented, halts the generation of the same movement approximately 50% of the time. If the Stop signal is presented after this time, it will be less effective, because the neuronal phenomena that lead to the movement generation will have already started. If the Stop signal is presented well before this time, it will be more effective in halting the movement. Consequently, the neuronal activity that is related to movement generation must occur before movement onset around the time that is defined by the SSRT. The aim of our study was to compare conditions in which a movement was planned and then generated (Go trials) to those in which a movement was planned and then inhibited (correct Stop trials). To this end we defined, for each recording session, two epochs of interest: the pre-Movement epoch for correct Go trials and the Stop signal epoch for correct Stop trials. To correctly compare the two behavioural conditions, a time window T equivalent for both trial types must be defined. Assuming that a time t_{go} ms before movement onset is chosen and an SSRT of t_{ssrt} ms is estimated, T in correct Stop trials is given by $T = [-(t_{go} - t_{ssrt}), + t_{ssrt}]$ ms with respect to the Stop signal presentation. Notice that T accounts for any time difference with respect to the SSRT trough the term $(t_{go} - t_{ssrt})$. In this study we fixed $t_{go} = 400$ ms and estimated the window to be taken in correct Stop trials trough T. MUA activities of Figure 3.14 are plotted during T. Behavioural parameters for the recording sessions of the two monkeys analyzed in this study are reported in Table 3.1.

3.5.4 Extraction and processing of neuronal data

A multielectrode array (Blackrock Microsystems, Salt Lake City) with 96 electrodes (spacing 0.4 mm) was surgically implanted in the left dorsal premotor cortex (PMd; arcuate sulcus and pre-central dimple used as references after opening of the dura) to acquire unfiltered electric field potentials (UFP; i.e., the raw signal), sampled at 24.4 kHz (Tucker Davis Technologies, Alachua, FL). As a measure of neuronal activity at the population level, MUA was extracted offline from the raw signal, as in Mattia et al. (Mattia et al., 2013), by computing the time-varying power spectra P(ω, t) from the short-time Fourier transform of UFP in 5-ms sliding windows. Normalizing P(ω, t) by their average P_{ref} (ω) across a fixed window (30 minutes) for the entire recording. Relative spectra R(ω, t) were then obtained. Thus, the average R(ω, t) across the $\omega/2\pi$ band $[0.2, 1.5]$ kHz represent the spectral estimated MUAs. As

better detailed in Mattia et al. (Mattia et al., 2013), such estimate relies on two hypotheses. The first is that high ω components of UFPs result from the convolution of firing rates ν(t) of neurons that are close to the electrode tip with a stereotypical single-unit waveform. The Fourier transform K(ω) of such an unknown waveform is canceled out in R(ω, t), which is therefore a good approximation of the ratio of firing rate spectra $|\nu(\omega,t)|^2$ $/|\nu(\omega,t)|_{\text{ref}}{}^2$. The second hypothesis is that high ω power $|\nu(\omega,t)|^2$ is proportional to the firing rate ν(t) itself (Mattia and Del Giudice, 2002), such that our MUA estimate is proportional to ν(t). As a last step, logarithmically scaled MUAs were smoothed by a moving average (40 ms sliding window, 5ms step).

3.5.5 Quantifying information dynamic with Transfer Entropy

We first analysed the single-trials activity profiles of each recording site of each recording session for both animals. To remove noise and outliers from our data, we excluded from the analysis the trials for which the MUA showed peaks with an amplitude that exceeded the average of the activity by 2 standard deviations in the epoch of interest and for over 80% of the channels. This ensures that artifacts caused by non-physiological oscillations are excluded from the analysis. To examine the local information dynamic in the PMd, we then computed a trial-average time series for each of the MUAs recorded by the electrodes of the array for each behavioural condition of each recording session. We then constructed the information transfer network using multivariate Transfer Entropy (*TE*). The choice is due to the fact that TE is indicated (especially in its multivariate formulations) as more accurate compared to other metrics and is known to capture non-linear interaction in the system dynamic without assuming any particular model. Moreover, this measure is of growing interest in neuroscience and there is a thriving literature on it (Ramos and Macau, 2017; Vicente et al., 2011; Wibral et al., 2011; Wollstadt et al., 2014; Xiong et al., 2017). For its computation we used the Matlab *MUTE* toolbox (Montalto et al., 2014).

Given an ensemble of M time series, the multivariate information transfer from a *driver* time series X to a *target* time series Y, conditioned to the remaining $Z_{\,k=1,..,M-2}$ time series, can be quantified taking into account the present values of the target and the past values of both the driver and the Z (Faes et al., 2015; Montalto et al., 2014; Xiong et al., 2017) through:

$$TE_{X\to Y\,|\,Z} = H(Y_n \mid Y_n^-, Z_n^-) - \; H(Y_n \mid X_n^-, Y_n^-, Z_n^-)\;, \tag{3.3}$$

where Y_n is the vector that represent the present state n of Y, $X_n^- = [X_{n-1}, X_{n-2}, ...]$, $Y_n^- = [Y_{n-1}, Y_{n-2}, ...]$ and $Z_n^- = [Z_{n-1}, Z_{n-2}, ...]$ are the vectors that represent the past of X, Y and Z respectively. The vertical bar stands for conditional probability, e.g. $H(Y_n \mid Y_n^-, Z_n^-)$ is the entropy of the present state of Y conditioned to the knowledge of the past of Y and to the past of the remaining Z. H is the Shannon entropy (Shannon, n.d.), which in the case of Y is given by:

$$H(Y_n) = -\sum_n P(Y_n)\, log P(Y_n)\ , \tag{3.4}$$

where P indicates the probability density. Hence, using equation 3.4 expression 3.3 becomes

$$TE_{X \to Y \mid Z} = -\sum_n P(Y_n, Y_n^-, Z_n^-)\, log \frac{P(Y_n \mid X_n^-, Y_n^-, Z_n^-)}{P(Y_n \mid Y_n^-, Z_n^-)} \tag{3.5}$$

In this formulation TE grows if the past of the driver increases the information about the present of target more than the past of target itself and more than any other series contained in Z. Since the past of the driver is used to predict the present of the target, TE is not symmetric (i.e. $TE_{X \to Y} \neq TE_{Y \to X}$) and defines a direction in the information trasfer. A crucial issue in estimating TE is the approximation of the vectors representing the past of the time series, a procedure known as *embedding*. The optimal embedding would be the one that include only the components of X_n^-, Y_n^- and Z_n^- that are most informative in describing Y_n. Montalto et al. (Montalto et al., 2014) described in details both different procedures for embedding and to evaluate the probability distribution functions needed to compute the entropy terms. We opted for a non-uniform embedding scheme (Faes et al., 2014) paired with the computation of H based on kernels estimators[3]. In few words the embedding method we chose iteratively selects components of the systems past based on a criterion for maximum relevance and minimum redundancy. In this context, maximum relevance means most significant in the sense of predictive information. Non-uniform embedding selects from the past of X, Y and Z only the components that are the most informative for the present of the target variable Y progressively pruning non informative terms. The maximum number of past values, or maximum lag l, to consider for the pruning is fixed at the beginning of the procedure. Cycling through the components of the past up to l, the statistical significance is then progressively assessed through the comparison with an null distribution built from the empirical values via a randomization procedure (Montalto et al., 2014). The component of the

[3]For the complete description of the embedding methods and estimators for computation of H, which is beyond the scope of this study, see the works of Faes et al. (Faes et al., 2015; Faes et al., 2014; Faes et al., 2011) and references therein.

past of X,Y and Z are thus selected as statistical significant if they are significant above a desired level α. In our case the null distribution was obtained by 100 random shuffling of empirical values and we fixed $\alpha = 0.01$. Non-uniform embedding represents a convenient and more reliable (Xiong et al., 2017) alternative to the common used approach known as uniform embedding; this would indeed select the past values X_n^-, Y_n^- and Z_n^- *a priori* and separately for each time series (Montalto et al., 2014). The probability density P needed for the computations of H was then calculated using kernel functions which weight the distance to the reference point to any other point in the time series and then average across all points. Such approach computes probabilities exploiting a local exploring of the state space and, importantly, has been proven to be more robust against unreliable estimations (Xiong et al., 2017). Therefore, if at least one component from the past is selected by the non-uniform embedding procedure, the resulting $TE_{X \to Y \mid Z}$ is positive and statistically significant. When instead none of the components of the past provide statically significant information about the target the $TE_{X \to Y \mid Z}$ is exactly 0 and assumed non significant (Montalto et al., 2014). To avoid any further bias in the selection of the past values, we initially fixed l=50 ms, but, as expected, only a recent past was selected by the procedure, in line with similar studies (Shimono and Beggs, 2015; N. M. Timme et al., 2016). Indeed, for each MUA time series, a past no older than 10ms for each n of equation 3.4 was ever selected by the optimal embedding procedure.

3.5.6 Graph theoretical measures

In our context the time series were the MUAs recorded by the electrodes of the array. We computed $TE_{X \to Y \mid Z}$ (and $TE_{Y \to X \mid Z}$) with $Z_{k=1,..,M-2}$, for each pair of (X,Y) in the epochs defined in Section 1 so to obtain a TE matrix[4] for each behavioural condition (Go trials and correct Stop trials) for both monkeys. Since the purpose of this study was to investigate the topology of information processing within the PMd cortical network during motor planning and inhibition, we interpreted the asymmetric TE matrix as the adjacency matrix of a directed weighted network, in which the nodes are the channels and the weighted edges are the $TE_{X \to Y \mid Z}$ (and $TE_{Y \to X \mid Z}$) with $Z_{k=1,..,M-2}$. To simplify the picture we considered only the off-diagonal elements of the matrix and thus excluding self-loops from the networks. Figure 3.20 reports a sketch of the construction of the local TE-based information

[4] 96x96 for all recording sessions for Monkey P; for some recording sessions of Monkey C damaged channels were removed from the analysis and therefore a 79x79 matrix was obtained.

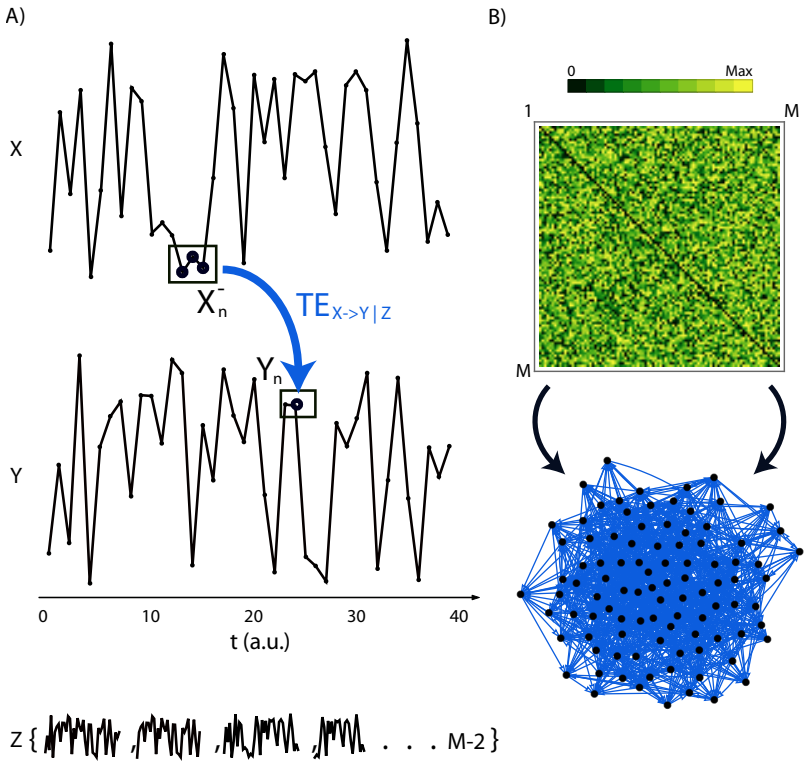

Figure 3.20. Sketch of the construction of the local TE-based network given the ensemble of the MUA time series. Panel A: key steps for the computation of the information transfer. For each couple (X,Y) of the ensemble of M time series, $TE_{X\to Y\mid Z}$ quantifies the information transfer from a *driver* X to a *target* Y conditioned to the remaining Z time series, with $Z_{k=1,..,M-2}$ (the same holds for each (Y,X) couple and $TE_{Y\to X\mid Z}$). If $TE_{X\to Y\mid Z}\neq 0$ the past of the driver X_n^- gives more knowledge about the present Y_n of the target than the past of the target itself and the remaining Z time series, i.e. give statistical significant contribution to the prediction of the present of the target. In this sketch the past of the driver comprises 3 time steps backwards with respect to the reference point and thus $X_n^- = [X_{n-1}, X_{n-2}, X_{n-3}]$. **Panel B:** an asymmetric transfer matrix MxM can be built computing the terms $TE_{X\to Y\mid Z}$ and $TE_{Y\to X\mid Z}$ for each X and Y of the ensemble. We take the TE matrix to be the adjacency matrix of a directed weighted graph in which the nodes are the channels and the weighted edges are the TE values (for simplicity diagonal elements are taken to be 0 and thus self-loops are excluded).

network. As an initial skimming of the contribution of each recording site to the exchange of information in the network we analyzed the empirical TE distributions. We found a mean $\mu \sim 10^-2$ for all recording sessions of both behavioural conditions for both animals (see supplementary figure S.. ??). Subsequently, we grouped channels

according to the trial type in which they significantly exchanged information with respect to the others. To this end we selected from the empirical TE distribution the values $> \mu + 2\sigma$ for each behavioural condition (with σ standard deviation). This selection identified the neuronal classes. As an example if node i drives node j with a TE value $> \mu + 2\sigma$ (i.e. there is a strong link directed from i to j) in Go trials but not in correct Stop trials, i would belong to the Go_drivers. Interestingly we identified two peculiar classes: nodes that emitted significant amount of information during both behavioural conditions (Common_drivers) and nodes that never emitted information in any behavioral condition (Targets). In our framework the TE values represented the strength of the connections between network nodes and hence the above classes are defined based of how much and during which behavioural condition nodes spread information trough the local PMd network.

To properly inspect the contribution of each node we needed a set of measures from graph theory. The first was Vertex Degree (VD). Vertex degree is the number of links to a node i:

$$VD(i) = \sum_{j=1}^{N} a_{\mathrm{ij}} \ , \tag{3.6}$$

where a_{ij} is the generic entry of the adjacency matrix and N is the number of nodes. In directed networks one can distinguish between in-degree (the number on inward links) and out-degree (the number of outward links). We computed the probability distribution of both vertex degrees (i.e. the in/out degree distribution) for each behavioural condition of each recording sessions for both animals. If the variance of the degree distribution is significantly larger than its mean tails in the distribution arise and network hubs are identified. Hubs are thus nodes that significantly exceeds the average degree of the network (Albert and Barabási, 2002).

We further studied the topology of the PMd information network by computing the Betweenness CentralityFreeman, 1977; White and Borgatti, 1994 (BC) of each node. For each node, BC measure the proportion of shortest paths between other couple of nodes s and t that pass through it and is defined as (Freeman, 1977):

$$BC(i) = \sum_{s \neq v \neq t} \frac{\sigma_{\mathrm{st}}(i)}{\sigma_{\mathrm{st}}} \ , \tag{3.7}$$

, where $\sigma_{\mathrm{st}}(i)$ is the number of shortest paths between s and t that pass through i and σ_{st} the the number of shortest paths between s and t. High BC scores indicate that a node lies on a considerable fraction of shortest paths connecting pairs of

vertices in the graph. Thus, such a node is considered topological central node since it plays a crucial role in passing and spreading information trough the network.
As an overall measure of comparison we used the centralization index C. Given a graph measure, C is the total average difference between the maximum of that measure and the values taken by all other nodes in the network. I.e., the centralization index of VD_{out} reads:

$$C_{vd} = \frac{1}{N-1}\sum_{i=1}^{N}[Max(VD_{out}) - VD_{\mathrm{out}}{}^{i}] \ , \tag{3.8}$$

where VD^{i}_{out} is the vertex out degree of node i, $Max(VD_{out})$ is the maximum VD_{out} value for the examined graph and N is the number of nodes. The same holds for BC. We computed C for both VD^{i}_{out} and BC for each recording session and each behavioural condition for both animals and then averaged over sessions.
In order to compute the total magnitude of information exchanged between the neuronal classes we constructed the following interaction measure I:

$$I_{\mathrm{ij}} = \rho\sum_{i}^{M}\sum_{j}^{M}\sum_{(m,n)} TE_{\,C_{\mathrm{i}}{}^{\mathrm{n}} \rightarrow C_{\mathrm{j}}{}^{\mathrm{n}}} \ , \tag{3.9}$$

where C is the neuronal class, M is the number of the classes (M=4) and m and n run over the all possible combinations of nodes within each class. $\rho = \frac{dim\ (C_{\mathrm{i}}{}^{\mathrm{n}} \rightarrow C_{\mathrm{j}}{}^{\mathrm{m}})}{dim\ (C_{\mathrm{j}})}$ is a normalization factor that accounts for the heterogeneous number of nodes within each of the classes. Therefore, our $\mathrm{I_{ij}}$ is a normalized node strength computed on the graph formed by the 4 classes (i.e. in a weighted graph the strength of a node is the sum of weights of links connected to the node). The higher are the number of nodes a class transmits information to, the higher is I. Hence, high I values reflect an high position in the hierarchy of the network communications for that class. All the interactions described by the empirical TE matrix were thus enclosed in a 4x4 matrix that represents a network of interactions in which now each node is a neuronal class. We computed I for each recording session and each behavioural condition and then we averaged over sessions for both animals. The uncertainty in estimating each element I_{ij} for each recording session was given by the standard error. Thus, the sessions-averaged element $\overline{I}_{\mathrm{ij}}$ is estimated with an error obtained via the error propagation formula for the average of n measures.

A null model

To properly assess the statistical significance of the results obtained via the graph theoretical analysis we defined a null model. As extensively detailed in a recent work (Cimini et al., 2019), the choice of a suitable null model remains a complicated issue in network and complex systems science. One common practice when analysing real-world networks such the one inspected in the present work, is try to identify properties that deviate from the null hypothesis being likely that the deviations themselves encode information about the network functions. We proceeded by initially using the most general constraints and then progressively tightening them. Firstly, we tested that results were not attributable to the distribution of MUA values. To this end we generated, for each behavioural condition and recording session, a synthetic pool of N time series with same length of the empirical ones (with N number of channels available for the corresponding animal and recording session) by random sampling from the empirical MUA distribution. We then derived a TE matrix for for each synthetic pool. This situation is the most general, since assumptions of any kind are made on the connectivity patterns and the weight distributions of the synthetic networks. We then compared the empirical graph measures with the ones obtained on the ensemble of 500 randomizations As a second null hypothesis, we tested that the topology observed in the experimental data were not attributable to the empirical TE distribution (i.e., the weight distribution of the network). We generated, for each behavioural condition and each recording session, an ensemble of 1000 synthetic TE matrices with the same distribution of real data. We then compared the empirical graph measures with the one obtained from the ensemble of randomizations.

Conclusions

In this work we used graph and information theory to analyse the activity of population of neurons recorded from a multielectrode array in PMd of rhesus monkeys during the execution and cancellation of visually guided arm movements. We observed that the local PMd network is finely organized with hierarchical hubs that emerge and with the topological arrangement of the information transmission network depending on the behavioural condition. Moreover, we showed that neuronal activities could be organized around four different classes that actively participate with different roles both in movements planning and cancellation. This reflects the existence of a high-order complexity in functional communications and organization at the population level during behavioural control regardless of which the nature of neurons in each class might be (i.e. excitatory or inhibitory neurons etc..). These results highlight, for the first time, how motor decisions are mappable in the reorganization of a local cortical network with the presence of hubs directly associabile with the readiness of the motor plan and the irrevocable signature of the onset of the incoming movement. Our results thus further strengthen the hypothesis that the computations required in movement control are implemented by neuronal ensembles at the population level. Features that cannot be deduced from the separate analysis of individual parts but can only be considered by inspecting the system in its entirety.

From the methodological perspective, the contribution of this work is to focus attention on the state-of-the-art methods of data analysis that increasingly characterize contemporary neuroscience, integrating them into a neurophysiological research protocol in order to build a bridge between the two disciplines. Indeed, whilst graph theory has been widely applied in many fields like physics, chemistry, economics, computer science, machine learning and temporal pattern recognition, i.e. bioinformatics or linguistics, its applications in neurophysiology are still surprisingly sporadic. The

common habit in electrophysiological research, especially that on primates, is in fact to rely on standard analysis techniques and to reuse existing analysis tools. This is due to the fact that a lot of effort is spent on acquiring the neural recordings. This requires a series of complex steps, such as animal training, technical management of the recording device, definition of the experimental setup, etc. In addition, the exploration of new data analysis paradigms requires scientific training that most of the time is far from the experience required in the other steps. The overall result is that a minor part of the research process is devoted to data analysis and modeling. Even more rare are the applications of graph theory in studies at the small and meso scale, in which an approach based on complex network theory has often (and probably guiltily) left aside in favor of other methods. Indeed, the effectiveness of graph theory has often been overlooked, probably because of its apparent simplicity which makes it seem less reliable. Although graphs are a merciless abstraction of the intricate neuronal interactions and can be represented in a surprisingly simple way, the mathematical foundations behind the theory are extremely rigorous. And is precisely its simplicity that makes it accessible to an interdisciplinary scientific audience such as the one that characterizes the biological sciences, in particular neuroscience. Although the origins of the theory behind these methods are not recent, there are still many technical problems to be addressed when applying these methods to local-scale datasets such as the one proposed in this thesis. This means that there is room for contributions in this area. For example, it would be of great scientific interest to characterize various parameters and network properties on such a small scale from different areas in order to produce a standardize guideline for future studies. Moreover, to fully describe the information transfer dynamics during motor control we should account for the interactions between PMd and other structures of the reaching network via simultaneous recordings (for further information see: Ding and Gold, 2013; Gold and Shadlen, 2007; Hoshi, 2013; Huk and Shadlen, 2005; Kim and Shadlen, 1999; Wei et al., 2015). In this scenario, a graph-based conceptualization of neural interactions, united with tools from information theory, would be very profitable compared to more popular approaches based on analysis of covariance between neurons or mesoscopic signals (e.g., Chandrasekaran et al., 2017; Churchland et al., 2012; Clawson et al., 2019; Kaufman et al., 2016; Marcos et al., 2013; Mattia et al., 2013) which are not straightforward in distinguishing the specific contributions of single neurons (or discrete populations of neurons) to the topology of network dynamics. Indeed, on one hand this range of methods allows for a fine temporal description of neural variability but on the other, due to

their nature, are neither capable to describe the information flow between neuronal actors nor to provide quantitative insights on the topology of network connection and its putative hierarchical organization. Without this all spectrum of details the computational strategy underlying motor control (and neural circuitry computation in general) would be yet elusive. Recently some authors have have started to follow the joint information theory-complex networks approach but for now only on cortico-hippocampal (N. M. Timme et al., 2016) or somatosensory cortex slice cultures data (Shimono and Beggs, 2015). However, we do not want to say that a complex network approach is the universal panacea for neuroscience. Despite its enormous generalizability that makes it transversal to different scientific fields, graph theory is not entirely self-sufficient. Indeed, to reach a more detailed degree of generalization, as well as reproducibility and predictability of experimental data as a function of more in-depth biologically theoretical parameters, the graph-based tools should be complemented with the historically more "classical" analytical modeling and simulation approach (e.g. Brette et al., 2007; Chicca et al., 2003; Destexhe et al., 1994; Mattia and Del Giudice, 2000, 2002; Moreno et al., 2002; Moreno-Bote et al., 2007; Segev, 1998), the most recent biologically detailed models (Amsalem et al., 2020; Gleeson et al., 2010 and references therein) and machine and deep learning techniques (e.g. Kuzovkin et al., 2018; Mahmud, Kaiser, et al., 2018; Mazzucato et al., 2015; Vahid et al., 2020; Yin and Zhang, 2018). One of the very few examples in the literature in this sense is the recent work of Gu and colleagues (Gu et al., 2019) who developed a novel circuit model and analyzed their properties through graph theory tools linking the anatomical and physiological properties of a local neural networks.

Notably, in a framework such as the one presented in this thesis neither any a priori assumption nor a specific neural modelling technique is needed. Its completely data-driven nature complements the most recent models for motor generation and suppression (Boucher et al., 2007; Lo et al., 2009) and permits to overcome their main limitation which reside in the requirement of many biophysical parameters to be tweaked and tuned before fitting with acceptable accuracy the experimental data. Given its features, the approach here presented has broad-spectrum implications, from the purely scientific side to the clinical one, *via* the technological one. Indeed, alterations of connectivity in patients suffering from diseases with motor impairment, as well as degenerative diseases such as Alzheimer's, Autism or Schizophrenia, have been observed in the literature using graph theory tools (Bordier et al., 2018; Engels et al., 2018; Lynall et al., 2010; Tessitore et al., 2019 and

references therein). Therefore, a network analysis able to identify the specific neuronal actors contributing to a correct motor control and a non-pathological cognitive condition is of great interest. This is because it can pave the way for tailor-made translational investigations aimed at investigating the biological basis of aberrant connectivity in pathological conditions and ultimately lead to clinical applications. Moreover, the flexibility of the presented approach leads to the straightforward and full characterization of network parameters and properties at all scales (from small to large, see also Bardella et al., 2016) making it perfectly suitable for many of the cutting-edge methods in motor control research. For example, graph-theory based computations can be rapidly and easily integrated in the data analysis pipeline of any optogenetic (such as in Bocchio et al., 2020) or brain-machine interface experiment (Shanechi, 2019 for a detailed review). They would provide precious (if not necessary) insights on the coordinated organization of neuronal assemblies, from ensemble of single cells to network of networks. In the same way, the topological study of the spatiotemporal patterns of neural activity would greatly facilitate the real-time analysis of communications between cortical and spinal circuits with direct applications in spinal cord injuries (Capogrosso et al., 2016), neuromorphic (Chicca et al., 2007; Gupta et al., 2016) and motor prosthetics research (Kemere et al., 2008) (for a review see Andersen et al., 2010). Furthermore, it is known that to fully understand the neural mechanisms behind motor control future research should focus on cortico-cortical and cortico-subcortical interactions through simultaneous recordings. In this scenario a topological information-based approach would be unquestionably necessary to gain an overall view and elicit detailed insights.

From the neurophysiological point of view this work further confirmed the key role of PMd in movement control, highlighting the importance of *in vivo* recordings from non-human primates as a fundamental benchmark for human motor system researches. Indeed, as showed, the ability to promptly inhibit movements in response to the environment changes relies on the concerted involvement of a wide brain network, including both cortical and subcortical structures, in which PMd plays a crucial role. Despite a detailed description of the single brain structures contribution within this network, as well as a comprehensive description of the interactions among them is still lacking, the stop-signal task has been crucial in elucidating some of the mechanisms underlying response inhibition. Here we contributed using the stop-signal paradigm to unpack the local, behavioural-dependent, organization of

the PMd, which is made up of different neuronal classes and a hierarchy of neuronal assemblies dominated by information-spreaders hubs nodes. In future studies the attention should be thus focused in investigating the interaction between PMd and other brain regions, in order to try describing, with the same topological accuracy, the connectivity patterns among structures that rule movement inhibition. The recording from multiple brain regions at the same time would be ideal to obtain a full description of these interactions, especially in terms of a well-defined temporal relationship between the activities of different brain regions. Through this approach, it would be also possible to fill some limitations of the present work. Indeed, while PMd activity clearly modulates in parallel with the behaviour under different conditions, we cannot account for the information dynamic between PMd and other structures of the reaching network. Another important limitation is the absence of EMG recordings whose unavailability limits any speculation on the cause-effect relationship between the found topological features of neural dynamics and muscle activity. However, it should be stressed that the main goal of the work was providing evidences for the principles of neuronal processing at the base of different behavioural outputs, which is not necessarily linked to muscle activation in a direct manner.

Bibliography

Achard, S., Salvador, R., Whitcher, B., Suckling, J., & Bullmore, E. (2006). A resilient, low-frequency, small-world human brain functional network with highly connected association cortical hubs. *Journal of Neuroscience*, *26*(1), 63–72. https://doi.org/10.1523/JNEUROSCI.3874-05.2006

Ahrens, M. B., Orger, M. B., Robson, D. N., Li, J. M., & Keller, P. J. (2013). Whole-brain functional imaging at cellular resolution using light-sheet microscopy. *Nature Methods*, *10*(5), 413–420. https://doi.org/10.1038/nmeth.2434

Albert, R., & Barabási, A.-L. (2002). Statistical mechanics of complex networks. *Reviews of Modern Physics*, *74*(1), 47–97. https://doi.org/10.1103/RevModPhys.74.47

Alexander, G. E., & Crutcher, M. D. (1990). Functional architecture of basal ganglia circuits: neural substrates of parallel processing. Trends Neurosci. https://doi.org/10.1016/0166-2236(90)90107-L

Amsalem, O., Eyal, G., Rogozinski, N., Gevaert, M., Kumbhar, P., Schürmann, F., & Segev, I. (2020). An efficient analytical reduction of detailed nonlinear neuron models. *Nature Communications*, *11*(1), 1–13. https://doi.org/10.1038/s41467-019-13932-6

Andersen, R. A., Hwang, E. J., & Mulliken, G. H. (2010). Cognitive neural prosthetics. *Annual Review of Psychology*, *61*, 169–190. https://doi.org/10.1146/annurev.psych.093008.100503

Archambault, P. S., Ferrari-Toniolo, S., Caminiti, R., & Battaglia-Mayer, A. (2015). Visually-guided correction of hand reaching movements: The neurophysiological bases in the cerebral cortex. *Vision Research*, *110*(PB), 244–256. https://doi.org/10.1016/j.visres.2014.09.009

Aron, A. R., Behrens, T. E., Smith, S., Frank, M. J., & Poldrack, R. A. (2007). Triangulating a cognitive control network using diffusion-weighted Magnetic

Resonance Imaging (MRI) and functional MRI. *Journal of Neuroscience*, *27*(14), 3743–3752. https://doi.org/10.1523/JNEUROSCI.0519-07.2007

Aron, A. R., Durston, S., Eagle, D. M., Logan, G. D., Stinear, C. M., & Stuphorn, V. (2007). Converging evidence for a fronto-basal-ganglia network for inhibitory control of action and cognition, In *Journal of neuroscience*, Society for Neuroscience. https://doi.org/10.1523/JNEUROSCI.3644-07.2007

Aron, A. R., Fletcher, P. C., Bullmore, E. T., Sahakian, B. J., & Robbins, T. W. (2003). Stop-signal inhibition disrupted by damage to right inferior frontal gyrus in humans. *Nature Neuroscience*, *6*(2), 115–116. https://doi.org/10.1038/nn1003

Aron, A. R., & Poldrack, R. A. (2006). Cortical and subcortical contributions to stop signal response inhibition: Role of the subthalamic nucleus. *Journal of Neuroscience*, *26*(9), 2424–2433. https://doi.org/10.1523/JNEUROSCI.4682-05.2006

Band, G. P., van der Molen, M. W., & Logan, G. D. (2003). Horse-race model simulations of the stop-signal procedure. *Acta Psychologica*, *112*(2), 105–142. https://doi.org/10.1016/S0001-6918(02)00079-3

Bardella, G., Bifone, A., Gabrielli, A., Gozzi, A., & Squartini, T. (2016). Hierarchical organization of functional connectivity in the mouse brain: A complex network approach. *Scientific Reports*, *6*(1), 1–11. https://doi.org/10.1038/srep32060

Bardella, G., Pani, P., Brunamonti, E., Giarrocco, F., & Ferraina, S. (2020). The small scale functional topology of movement control: Hierarchical organization of local activity anticipates movement generation in the premotor cortex of primates. *NeuroImage*, *207*. https://doi.org/10.1016/j.neuroimage.2019.116354

Bari, A., & Robbins, T. W. (2013). Inhibition and impulsivity: Behavioral and neural basis of response control. Pergamon. https://doi.org/10.1016/j.pneurobio.2013.06.005

Battaglia-Mayer, A., Buiatti, T., Caminiti, R., Ferraina, S., Lacquaniti, F., & Shallice, T. (2014). Correction and suppression of reaching movements in the cerebral cortex: Physiological and neuropsychological aspects. Elsevier Ltd. https://doi.org/10.1016/j.neubiorev.2014.03.002

Bellgrove, M. A., Hester, R., & Garavan, H. (2004). The functional neuroanatomical correlates of response variability: evidence from a response inhibition task. *Neuropsychologia*, *42*, 1910–1916. https://doi.org/10.1016/j.neuropsychologia.2004.05.007

Bocchio, M., Gouny, C., Angulo-Garcia, D., Toulat, T., Tressard, T., Quiroli, E., Baude, A., & Cossart, R. (2020). Hippocampal hub neurons maintain distinct connectivity throughout their lifetime. *Nature Communications*, *11*(1), 1–19. https://doi.org/10.1038/s41467-020-18432-6

Bordier, C., Nicolini, C., Forcellini, G., & Bifone, A. (2018). Disrupted modular organization of primary sensory brain areas in schizophrenia. *NeuroImage: Clinical*, *18*, 682–693. https://doi.org/10.1016/j.nicl.2018.02.035

Bostan, A. C., Dum, R. P., & Strick, P. L. (2013). Cerebellar networks with the cerebral cortex and basal ganglia. Trends Cogn Sci. https://doi.org/10.1016/j.tics.2013.03.003

Bostan, A. C., & Strick, P. L. (2018). The basal ganglia and the cerebellum: Nodes in an integrated network. Nature Publishing Group. https://doi.org/10.1038/s41583-018-0002-7

Boucher, L., Palmeri, T. J., Logan, G. D., & Schall, J. D. (2007). Inhibitory control in mind and brain: An interactive race model of countermanding saccades. *Psychological Review*, *114*(2), 376–397. https://doi.org/10.1037/0033-295X.114.2.376

Brette, R., Rudolph, M., Carnevale, T., Hines, M., Beeman, D., Bower, J. M., Diesmann, M., Morrison, A., Goodman, P. H., Harris, F. C., Zirpe, M., Natschläger, T., Pecevski, D., Ermentrout, B., Djurfeldt, M., Lansner, A., Rochel, O., Vieville, T., Muller, E., … Destexhe, A. (2007). Simulation of networks of spiking neurons: A review of tools and strategies. NIH Public Access. https://doi.org/10.1007/s10827-007-0038-6

Brunamonti, E., Ferraina, S., & Paré, M. (2012). Controlled movement processing: Evidence for a common inhibitory control of finger, wrist, and arm movements. *Neuroscience*, *215*, 69–78. https://doi.org/10.1016/j.neuroscience.2012.04.051

Brunamonti, E., Chiricozzi, F. R., Clausi, S., Olivito, G., Giusti, M. A., Molinari, M., Ferraina, S., & Leggio, M. (2014). Cerebellar Damage Impairs Executive Control and Monitoring of Movement Generation (N. P. Holmes, Ed.). *PLoS ONE*, *9*(1), e85997. https://doi.org/10.1371/journal.pone.0085997

Brunamonti, E., Pani, P., Papazachariadis, O., Onorati, P., Albertini, G., & Ferraina, S. (2011). Cognitive control of movement in down syndrome. *Research in Developmental Disabilities*, *32*(5), 1792–1797. https://doi.org/10.1016/j.ridd.2011.03.008

Buehlmann, A., & Deco, G. (2010). Optimal information transfer in the cortex through synchronization. *PLoS Computational Biology*, *6*(9), 1000934. https://doi.org/10.1371/journal.pcbi.1000934

Caldarelli, G. (2010). *Scale-Free Networks: Complex Webs in Nature and Technology* (Vol. 9780199211). Oxford University Press. https://doi.org/10.1093/acprof:oso/9780199211517.001.0001

Capogrosso, M., Milekovic, T., Borton, D., Wagner, F., Moraud, E. M., Mignardot, J. B., Buse, N., Gandar, J., Barraud, Q., Xing, D., Rey, E., Duis, S., Jianzhong, Y., Ko, W. K. D., Li, Q., Detemple, P., Denison, T., Micera, S., Bezard, E., ... Courtine, G. (2016). A brain-spine interface alleviating gait deficits after spinal cord injury in primates. *Nature*, *539*(7628), 284–288. https://doi.org/10.1038/nature20118

Chamberlain, S. R., Blackwell, A. D., Fineberg, N. A., Robbins, T. W., & Sahakian, B. J. (2005). The neuropsychology of obsessive compulsive disorder: the importance of failures in cognitive and behavioural inhibition as candidate endophenotypic markers. *Neuroscience & Biobehavioral Reviews*, *29*(3), 399–419. https://doi.org/https://doi.org/10.1016/j.neubiorev.2004.11.006

Chambers, C. D., Bellgrove, M. A., Stokes, M. G., Henderson, T. R., Garavan, H., Robertson, I. H., Morris, A. P., & Mattingley, J. B. (n.d.). *Executive "Brake Failure" following Deactivation of Human Frontal Lobe* (tech. rep.).

Chambers, C. D., Payne, J. M., & Mattingley, J. B. (2007). Parietal disruption impairs reflexive spatial attention within and between sensory modalities. *Neuropsychologia*, *45*(8), 1715–1724. https://doi.org/10.1016/j.neuropsychologia.2007.01.001

Chandrasekaran, C., Peixoto, D., Newsome, W. T., & Shenoy, K. V. (2017). Laminar differences in decision-related neural activity in dorsal premotor cortex. *Nature Communications*, *8*(1), 1–16. https://doi.org/10.1038/s41467-017-00715-0

Chen, B. L., Hall, D. H., & Chklovskii, D. B. (2006). Wiring optimization can relate neuronal structure and function. *Proceedings of the National Academy of Sciences of the United States of America*, *103*(12), 4723–4728. https://doi.org/10.1073/pnas.0506806103

Cheney, P. D., & Fetz, E. E. (1980). Functional classes of primate corticomotoneuronal cells and their relation to active force. *Journal of Neurophysiology*, *44*(4), 773–791. https://doi.org/10.1152/jn.1980.44.4.773

Chevalier, N., Chatham, C. H., & Munakata, Y. (2014). The Practice of going helps children to stop: The Importance of context monitoring in inhibitory control. *Journal of Experimental Psychology: General*, *143*(3), 959–965. https://doi.org/10.1037/a0035868

Chiang, A. S., Lin, C. Y., Chuang, C. C., Chang, H. M., Hsieh, C. H., Yeh, C. W., Shih, C. T., Wu, J. J., Wang, G. T., Chen, Y. C., Wu, C. C., Chen, G. Y., Ching, Y. T., Lee, P. C., Lin, C. Y., Lin, H. H., Wu, C. C., Hsu, H. W., Huang, Y. A., … Hwang, J. K. (2011). Three-dimensional reconstruction of brain-wide wiring networks in drosophila at single-cell resolution. *Current Biology*, *21*(1), 1–11. https://doi.org/10.1016/j.cub.2010.11.056

Chicca, E., Badoni, D., Dante, V., D'Andreagiovanni, M., Salina, G., Carota, L., Fusi, S., & Del Giudice, P. (2003). A VLSI Recurrent Network of Integrate-and-Fire Neurons Connected by Plastic Synapses With Long-Term Memory. *IEEE Transactions on Neural Networks*, *14*(5), 1297–1307. https://doi.org/10.1109/TNN.2003.816367

Chicca, E., Whatley, A. M., Lichtsteiner, P., Dante, V., Delbruck, T., Del Giudice, P., Douglas, R. J., & Indiveri, G. (2007). A multichip pulse-based neuromorphic infrastructure and its application to a model of orientation selectivity. *IEEE Transactions on Circuits and Systems I: Regular Papers*, *54*(5), 981–993. https://doi.org/10.1109/TCSI.2007.893509

Chikazoe, J., Jimura, K., Asari, T., Yamashita, K. I., Morimoto, H., Hirose, S., Miyashita, Y., & Konishi, S. (2009). Functional dissociation in right inferior frontal cortex during performance of go/no-go task. *Cerebral Cortex*, *19*(1), 146–152. https://doi.org/10.1093/cercor/bhn065

Churchland, M. M., Cunningham, J. P., Kaufman, M. T., Foster, J. D., Nuyujukian, P., Ryu, S. I., Shenoy, K. V., & Shenoy, K. V. (2012). Neural population dynamics during reaching. *Nature*, *487*(7405), 51–56. https://doi.org/10.1038/nature11129

Cimini, G., Squartini, T., Saracco, F., Garlaschelli, D., Gabrielli, A., & Caldarelli, G. (2019). The statistical physics of real-world networks. *Nature Reviews Physics*, *1*(1), 58–71. https://doi.org/10.1038/s42254-018-0002-6

Cisek, P., & Kalaska, J. F. (2010). Neural mechanisms for interacting with a world full of action choices. Annu Rev Neurosci. https://doi.org/10.1146/annurev.neuro.051508.135409

Clawson, W., Vicente, A. F., Ferraris, M., Bernard, C., Battaglia, D., & Quilichini, P. P. (2019). Computing hubs in the hippocampus and cortex. *Science Advances*, *5*(6), eaax4843. https://doi.org/10.1126/sciadv.aax4843

Colizza, V., Flammini, A., Serrano, M. A., & Vespignani, A. (2006). Detecting rich-club ordering in complex networks. *Nature Physics*, *2*(2), 110–115. https://doi.org/10.1038/nphys209

Corbetta, M., & Shulman, G. L. (2002). Control of goal-directed and stimulus-driven attention in the brain. *Nature Reviews Neuroscience*, *3*(3), 201–215. https://doi.org/10.1038/nrn755

Coxon, J. P., Stinear, C. M., & Byblow, W. D. (2006). Intracortical inhibition during volitional inhibition of prepared action. *Journal of Neurophysiology*, *95*(6), 3371–3383. https://doi.org/10.1152/jn.01334.2005

Dann, B., Michaels, J. A., Schaffelhofer, S., & Scherberger, H. (2016). Uniting functional network topology and oscillations in the fronto-parietal single unit network of behaving primates. *eLife*, *5*(AUGUST). https://doi.org/10.7554/eLife.15719

Destexhe, A., Mainen, Z. F., & Sejnowski, T. J. (1994). Synthesis of models for excitable membranes, synaptic transmission and neuromodulation using a common kinetic formalism. *Journal of Computational Neuroscience*, *1*(3), 195–230. https://doi.org/10.1007/BF00961734

Ding, L., & Gold, J. I. (2013). The basal ganglia's contributions to perceptual decision making. NIH Public Access. https://doi.org/10.1016/j.neuron.2013.07.042

Dum, R. P., & Strick, P. L. (1991). The origin of corticospinal projections from the premotor areas in the frontal lobe. *Journal of Neuroscience*, *11*(3), 667–689. https://doi.org/10.1523/jneurosci.11-03-00667.1991

Duque, J., Labruna, L., Verset, S., Olivier, E., & Ivry, R. B. (2012). Dissociating the role of prefrontal and premotor cortices in controlling inhibitory mechanisms during motor preparation. *Journal of Neuroscience*, *32*(3), 806–816. https://doi.org/10.1523/JNEUROSCI.4299-12.2012

Eagle, D. M., Baunez, C., Hutcheson, D. M., Lehmann, O., Shah, A. P., & Robbins, T. W. (2008). Stop-signal reaction-time task performance: Role of prefrontal cortex and subthalamic nucleus. *Cerebral Cortex*, *18*(1), 178–188. https://doi.org/10.1093/cercor/bhm044

Eguíluz, V. M., Chialvo, D. R., Cecchi, G. A., Baliki, M., & Apkarian, A. V. (n.d.). Scale-Free Brain Functional Networks. https://doi.org/10.1103/PhysRevLett.94.018102

Engels, G., Vlaar, A., McCoy, B., Scherder, E., & Douw, L. (2018). Dynamic Functional Connectivity and Symptoms of Parkinson's Disease: A Resting-State fMRI Study. *Frontiers in Aging Neuroscience*, *10*. https://doi.org/10.3389/fnagi.2018.00388

Ersche, K. D., Jones, P. S., Williams, G. B., Turton, A. J., Robbins, T. W., & Bullmore, E. T. (2012). Abnormal brain structure implicated in stimulant drug addiction. *Science*, *335*(6068), 601–604. https://doi.org/10.1126/science.1214463

Facchetti, G., Iacono, G., & Altafini, C. (2011). Computing global structural balance in large-scale signed social networks. *Proceedings of the National Academy of Sciences of the United States of America*, *108*(52), 20953–20958. https://doi.org/10.1073/pnas.1109521108

Faes, L., Kugiumtzis, D., Nollo, G., Jurysta, F., & Marinazzo, D. (2015). Estimating the decomposition of predictive information in multivariate systems. *PHYSICAL REVIEW E*, *91*, 32904. https://doi.org/10.1103/PhysRevE.91.032904

Faes, L., Marinazzo, D., Montalto, A., & Nollo, G. (2014). Lag-specific transfer entropy as a tool to assess cardiovascular and cardiorespiratory information transfer. *IEEE Transactions on Biomedical Engineering*, *61*(10), 2556–2568. https://doi.org/10.1109/TBME.2014.2323131

Faes, L., Nollo, G., & Porta, A. (2011). Information-based detection of nonlinear Granger causality in multivariate processes via a nonuniform embedding technique. *Physical Review E - Statistical, Nonlinear, and Soft Matter Physics*, *83*(5), 051112. https://doi.org/10.1103/PhysRevE.83.051112

Felleman, D. J., Felleman, D. J., & Van Essen, D. C. (1991). Distributed hierarchical processing in the primate cerebral cortex. *CEREB CORTEX*, 1–47. http://citeseerx.ist.psu.edu/viewdoc/summary?doi=10.1.1.225.165

Ferraina, S., Battaglia-Mayer, A., Genovesio, A., Marconi, B., Onorati, P., & Caminiti, R. (2001). Early Coding of Visuomanual Coordination During Reaching in Parietal Area PEc. *Journal of Neurophysiology*, *85*(1), 462–467. https://doi.org/10.1152/jn.2001.85.1.462

Fetz, E. E., & Cheney, P. D. (1980). Postspike facilitation of forelimb muscle activity by primate corticomotoneuronal cells. *Journal of Neurophysiology*, *44*(4), 751–772. https://doi.org/10.1152/jn.1980.44.4.751

Fetz, E. E. (1992). Are movement parameters recognizably coded in the activity of single neurons? *Behavioral and Brain Sciences*, *15*(4), 679–690. https://doi.org/10.1017/S0140525X00072599

Floden, D., & Stuss, D. T. (2006). Inhibitory control is slowed in patients with right superior medial frontal damage. *Journal of Cognitive Neuroscience*, *18*(11), 1843–1849. https://doi.org/10.1162/jocn.2006.18.11.1843

Forstmann, B. U., Keuken, M. C., Jahfari, S., Bazin, P.-L., Neumann, J., Schäfer, A., Anwander, A., & Turner, R. (2012). Cortico-subthalamic white matter tract strength predicts interindividual efficacy in stopping a motor response. *NeuroImage*, *60*, 370–375. https://doi.org/10.1016/j.neuroimage.2011.12.044

Fox, M. D., Snyder, A. Z., Vincent, J. L., Corbetta, M., Van Essen, D. C., & Raichle, M. E. (2005). The human brain is intrinsically organized into dynamic, anticorrelated functional networks. *Proceedings of the National Academy of Sciences of the United States of America*, *102*(27), 9673–9678. https://doi.org/10.1073/pnas.0504136102

Freeman, L. C. (1977). A Set of Measures of Centrality Based on Betweenness. *Sociometry*, *40*(1), 35. https://doi.org/10.2307/3033543

Gal, E., London, M., Globerson, A., Ramaswamy, S., Reimann, M. W., Muller, E., Markram, H., & Segev, I. (2017). Rich cell-type-specific network topology in neocortical microcircuitry. *Nature Neuroscience*, *20*(7), 1004–1013. https://doi.org/10.1038/nn.4576

Garcia-Lopez, P., Garcia-Marin, V., & Freire, M. (2010). The histological slides and drawings of Cajal. Frontiers Media SA. https://doi.org/10.3389/neuro.05.009.2010

Gauggel, S., Rieger, M., & Feghoff, T. A. (2004). Inhibition of ongoing responses in patients with Parkinson's disease. *Journal of Neurology, Neurosurgery and Psychiatry*, *75*(4), 539–544. https://doi.org/10.1136/jnnp.2003.016469

Georgopoulos, A. P., Schwartz, A. B., & Kettner, R. E. (1986). Neuronal population coding of movement direction. *Science*, *233*(4771), 1416–1419. https://doi.org/10.1126/science.3749885

Gerhard, F., Pipa, G., Lima, B., Neuenschwander, S., & Gerstner, W. (2011). Extraction of Network Topology From Multi-Electrode Recordings: Is there a Small-World Effect? *Frontiers in Computational Neuroscience*, *5*, 4. https://doi.org/10.3389/fncom.2011.00004

Gleeson, P., Crook, S., Cannon, R. C., Hines, M. L., Billings, G. O., Farinella, M., Morse, T. M., Davison, A. P., Ray, S., Bhalla, U. S., Barnes, S. R., Dimitrova, Y. D., & Silver, R. A. (2010). NeuroML: A Language for Describing Data Driven Models of Neurons and Networks with a High Degree of Biological

Detail (K. J. Friston, Ed.). *PLoS Computational Biology*, *6*(6), e1000815. https://doi.org/10.1371/journal.pcbi.1000815

Gold, J. I., & Shadlen, M. N. (2007). The Neural Basis of Decision Making. https://doi.org/10.1146/annurev.neuro.29.051605.113038

Gu, Y., Qi, Y., & Gong, P. (2019). Rich-club connectivity, diverse population coupling, and dynamical activity patterns emerging from local cortical circuits. *PLoS Computational Biology*, *15*(4), e1006902. https://doi.org/10.1371/journal.pcbi.1006902

Gupta, I., Serb, A., Khiat, A., Zeitler, R., Vassanelli, S., & Prodromakis, T. (2016). Real-time encoding and compression of neuronal spikes by metal-oxide memristors. *Nature Communications*, *7*(1), 1–9. https://doi.org/10.1038/ncomms12805

Hagmann, P., Cammoun, L., Gigandet, X., Meuli, R., & Honey, C. J. (2008). Mapping the structural core of human cerebral cortex. *PLoS Biol*, *6*(7), 159. https://doi.org/10.1371/journal.pbio.0060159

Hagmann, P., Kurant, M., Gigandet, X., Thiran, P., Wedeen, V. J., Meuli, R., & Thiran, J.-P. (2007). Mapping Human Whole-Brain Structural Networks with Diffusion MRI (O. Sporns, Ed.). *PLoS ONE*, *2*(7), e597. https://doi.org/10.1371/journal.pone.0000597

Hanes, D. P., Patterson, W. F., & Schall, J. D. (1998). Role of frontal eye fields in countermanding saccades: Visual, movement, and fixation activity. *Journal of Neurophysiology*, *79*(2), 817–834. https://doi.org/10.1152/jn.1998.79.2.817

He, B. J. (2011). Scale-free properties of the functional magnetic resonance imaging signal during rest and task. *Journal of Neuroscience*, *31*(39), 13786–13795. https://doi.org/10.1523/JNEUROSCI.2111-11.2011

Herreras, O. (2016). Local Field Potentials: Myths and Misunderstandings. *Frontiers in Neural Circuits*, *10*(DEC), 101. https://doi.org/10.3389/fncir.2016.00101

Hikosaka, O., & Isoda, M. (2010). Switching from automatic to controlled behavior: cortico-basal ganglia mechanisms. Trends Cogn Sci. https://doi.org/10.1016/j.tics.2010.01.006

Hikosaka, O., Takikawa, Y., & Kawagoe, R. (2000). Role of the basal ganglia in the control of purposive saccadic eye movements. American Physiological Society. https://doi.org/10.1152/physrev.2000.80.3.953

Hilgetag, C. C., & Goulas, A. (2020). HIERARCHY IN THE ORGANIZATION OF BRAIN NETWORKS. *Philosophical Transactions of the Royal Society B:*

Biological Sciences, *375*(1796), 20190319. https://doi.org/10.1098/rstb.2019.0319

Hilgetag, C. C., & Kaiser, M. (2004). Clustered organization of cortical connectivity. Springer. https://doi.org/10.1385/NI:2:3:353

Hilgetag, C., O'Neill, M. A., & Young, M. P. (2000). Hierarchical organization of macaque and cat cortical sensory systems explored with a novel network processor (M. P. Young, Ed.). *Philosophical Transactions of the Royal Society of London. Series B: Biological Sciences*, *355*(1393), 71–89. https://doi.org/10.1098/rstb.2000.0550

Honey, C. J., Kötter, R., Breakspear, M., & Sporns, O. (2007). Network structure of cerebral cortex shapes functional connectivity on multiple time scales. *Proceedings of the National Academy of Sciences of the United States of America*, *104*(24), 10240–10245. https://doi.org/10.1073/pnas.0701519104

Hong, G., & Lieber, C. M. (2019). Novel electrode technologies for neural recordings. *Nature Reviews Neuroscience*, *20*(6), 330–345. https://doi.org/10.1038/s41583-019-0140-6

Hoshi, E. (2013). Cortico-basal ganglia networks subserving goal-directed behavior mediated by conditional visuo-goal association. *Frontiers in Neural Circuits*, *7*(OCT). https://doi.org/10.3389/fncir.2013.00158

Hubel, D. H., & Wiesel, T. N. (1962). Receptive fields, binocular interaction and functional architecture in the cat's visual cortex. *The Journal of Physiology*, *160*(1), 106–154. https://doi.org/10.1113/jphysiol.1962.sp006837

Hughes, M. E., Fulham, W. R., Johnston, P. J., & Michie, P. T. (2012). Stop-signal response inhibition in schizophrenia: Behavioural, event-related potential and functional neuroimaging data. *Biological Psychology*, *89*(1), 220–231. https://doi.org/10.1016/j.biopsycho.2011.10.013

Huk, A. C., & Shadlen, M. N. (2005). Neural activity in macaque parietal cortex reflects temporal integration of visual motion signals during perceptual decision making. *Journal of Neuroscience*, *25*(45), 10420–10436. https://doi.org/10.1523/JNEUROSCI.4684-04.2005

Ito, S., Hansen, M. E., Heiland, R., Lumsdaine, A., Litke, A. M., & Beggs, J. M. (2011). Extending Transfer Entropy Improves Identification of Effective Connectivity in a Spiking Cortical Network Model (M. Zochowski, Ed.). *PLoS ONE*, *6*(11), e27431. https://doi.org/10.1371/journal.pone.0027431

Jahfari, S., Waldorp, L., van den Wildenberg, W. P., Scholte, H. S., Ridderinkhof, K. R., & Forstmann, B. U. (2011). Effective connectivity reveals important

roles for both the hyperdirect (fronto-subthalamic) and the indirect (fronto-striatal-pallidal) fronto-basal ganglia pathways during response inhibition. *Journal of Neuroscience*, *31*(18), 6891–6899. https://doi.org/10.1523/JNEUROSCI.5253-10.2011

Kaiser, M., Görner, M., & Hilgetag, C. C. (2007). Criticality of spreading dynamics in hierarchical cluster networks without inhibition. *New Journal of Physics*, *9*(5), 110. https://doi.org/10.1088/1367-2630/9/5/110

Kaiser, M. (2010). Hierarchy and dynamics of neural networks. *Frontiers in Neuroinformatics*, *4*(AUG), 112. https://doi.org/10.3389/fninf.2010.00112

Kaiser, M., & Hilgetag, C. C. (2006). Nonoptimal component placement, but short processing paths, due to long-distance projections in neural systems (K. Friston, Ed.). *PLoS Computational Biology*, *2*(7), 0805–0815. https://doi.org/10.1371/journal.pcbi.0020095

Kaufman, M. T., Seely, J. S., Sussillo, D., Ryu, S. I., Shenoy, K. V., & Churchland, M. M. (2016). The largest response component in the motor cortex reflects movement timing but not movement type. *eNeuro*, *3*(4), 85–101. https://doi.org/10.1523/ENEURO.0085-16.2016

Kemere, C., Santhanam, G., Yu, B. M., Afshar, A., Ryu, S. I., Meng, T. H., & Shenoy, K. V. (2008). Detecting neural-state transitions using hidden Markov models for motor cortical prostheses. *Journal of Neurophysiology*, *100*(4), 2441–2452. https://doi.org/10.1152/jn.00924.2007

Kennedy, H., Knoblauch, K., & Toroczkai, Z. (2013). Why data coherence and quality is critical for understanding interareal cortical networks. *NeuroImage*, *80*, 37–45. https://doi.org/10.1016/j.neuroimage.2013.04.031

Kim, J. N., & Shadlen, M. N. (1999). Neural correlates of a decision in the dorsolateral prefrontal cortex of the macaque. *Nature Neuroscience*, *2*(2), 176–185. https://doi.org/10.1038/5739

Koechlin, E., Ody, C., & Kouneiher, F. (2003). The Architecture of Cognitive Control in the Human Prefrontal Cortex. *Science*, *302*(5648), 1181–1185. https://doi.org/10.1126/science.1088545

Kudo, K., & Ohtsuki, T. (1998). Functional modification of agonist-antagonist electromyographic activity for rapid movement inhibition. *Experimental Brain Research*, *122*(1), 23–30. https://doi.org/10.1007/s002210050487

Kuzovkin, I., Vicente, R., Petton, M., Lachaux, J. P., Baciu, M., Kahane, P., Rheims, S., Vidal, J. R., & Aru, J. (2018). Activations of deep convolutional neural networks are aligned with gamma band activity of human visual cortex.

Communications Biology, *1*(1), 1–12. https://doi.org/10.1038/s42003-018-0110-y

Levy, B. J., & Wagner, A. D. (2011). Cognitive control and right ventrolateral prefrontal cortex: Reflexive reorienting, motor inhibition, and action updating. Blackwell Publishing Inc. https://doi.org/10.1111/j.1749-6632.2011.05958.x

Li, C. S. R., Huang, C., Yan, P., Paliwal, P., Constable, R. T., & Sinha, R. (2008). Neural correlates of post-error slowing during a stop signal task: A functional magnetic resonance imaging study. *Journal of Cognitive Neuroscience*, *20*(6), 1021–1029. https://doi.org/10.1162/jocn.2008.20071

Lipszyc, J., & Schachar, R. (2010). Inhibitory control and psychopathology: A meta-analysis of studies using the stop signal task. *Journal of the International Neuropsychological Society*, *16*(6), 1064–1076. https://doi.org/10.1017/S1355617710000895

Lo, C. C., Boucher, L., Paré, M., Schall, J. D., & Wang, X. J. (2009). Proactive inhibitory control and attractor dynamics in countermanding action: A spiking neural circuit model. *Journal of Neuroscience*, *29*(28), 9059–9071. https://doi.org/10.1523/JNEUROSCI.6164-08.2009

Logan, G. D., & Cowan, W. B. (1984). On the ability to inhibit thought and action: A theory of an act of control. *Psychological Review*, *91*(3), 295–327. https://doi.org/10.1037//0033-295x.91.3.295

Logan, G. D., Van Zandt, T., Verbruggen, F., & Wagenmakers, E. J. (2014). On the ability to inhibit thought and action: General and special theories of an act of control. *Psychological Review*, *121*(1), 66–95. https://doi.org/10.1037/a0035230

Lynall, M. E., Bassett, D. S., Kerwin, R., McKenna, P. J., Kitzbichler, M., Muller, U., & Bullmore, E. (2010). Functional connectivity and brain networks in schizophrenia. *Journal of Neuroscience*, *30*(28), 9477–9487. https://doi.org/10.1523/JNEUROSCI.0333-10.2010

Mahmud, M., Cecchetto, C., Maschietto, M., Thewes, R., & Vassanelli, S. (2018). Towards high-resolution brain-chip interface and automated analysis of multichannel neuronal signals, In *5th ieee region 10 humanitarian technology conference 2017, r10-htc 2017*, Institute of Electrical; Electronics Engineers Inc. https://doi.org/10.1109/R10-HTC.2017.8289091

Mahmud, M., Kaiser, M. S., Hussain, A., & Vassanelli, S. (2018). Applications of Deep Learning and Reinforcement Learning to Biological Data. *IEEE*

Transactions on Neural Networks and Learning Systems, *29*(6), 2063–2079. https://doi.org/10.1109/TNNLS.2018.2790388

Marcos, E., Pani, P., Brunamonti, E., Deco, G., Ferraina, S., & Verschure, P. (2013). Neural variability in premotor cortex is modulated by trial history and predicts behavioral performance. *Neuron*, *78*(2), 249–255. https://doi.org/10.1016/j.neuron.2013.02.006

Markov, N. T., Ercsey-Ravasz, M. M., Ribeiro Gomes, A. R., Lamy, C., Magrou, L., Vezoli, J., Misery, P., Falchier, A., Quilodran, R., Gariel, M. A., Sallet, J., Gamanut, R., Huissoud, C., Clavagnier, S., Giroud, P., Sappey-Marinier, D., Barone, P., Dehay, C., Toroczkai, Z., ... Kennedy, H. (2014). A weighted and directed interareal connectivity matrix for macaque cerebral cortex. *Cerebral Cortex*, *24*(1), 17–36. https://doi.org/10.1093/cercor/bhs270

Mattia, M., Spadacenta, S., Pavone, L., Quarato, P., Esposito, V., Sparano, A., Sebastiano, F., Di Gennaro, G., Morace, R., Cantore, G., & Mirabella, G. (2012). Stop-event-related potentials from intracranial electrodes reveal a key role of premotor and motor cortices in stopping ongoing movements. *Frontiers in Neuroengineering*, *5*(JUNE). https://doi.org/10.3389/fneng.2012.00012

Mattia, M., & Del Giudice, P. (2000). Efficient event-driven simulation of large networks of spiking neurons and dynamical synapses. *Neural Computation*, *12*(10), 2305–2329. https://doi.org/10.1162/089976600300014953

Mattia, M., & Del Giudice, P. (2002). Population dynamics of interacting spiking neurons. *Physical Review E - Statistical Physics, Plasmas, Fluids, and Related Interdisciplinary Topics*, *66*(5), 19. https://doi.org/10.1103/PhysRevE.66.051917

Mattia, M., Pani, P., Mirabella, G., Costa, S., Del Giudice, P., & Ferraina, S. (2013). Heterogeneous attractor cell assemblies for motor planning in premotor cortex. *Journal of Neuroscience*, *33*(27), 11155–11168. https://doi.org/10.1523/JNEUROSCI.4664-12.2013

Matzke, D., Love, J., & Heathcote, A. (2017). A Bayesian approach for estimating the probability of trigger failures in the stop-signal paradigm. *Behavior Research Methods*, *49*(1), 267–281. https://doi.org/10.3758/s13428-015-0695-8

Mazzucato, L., Fontanini, A., & La Camera, G. (2015). Dynamics of multistable states during ongoing and evoked cortical activity. *Journal of Neuroscience*, *35*(21), 8214–8231. https://doi.org/10.1523/JNEUROSCI.4819-14.2015

Milanovic, J. V., & Zhu, W. (2018). Modeling of interconnected critical infrastructure systems using complex network theory. *IEEE Transactions on Smart Grid*, *9*(5), 4637–4648. https://doi.org/10.1109/TSG.2017.2665646

Mirabella, G., Pani, P., & Ferraina, S. (2011). Neural correlates of cognitive control of reaching movements in the dorsal premotor cortex of rhesus monkeys. *Journal of Neurophysiology*, *106*(3), 1454–1466. https://doi.org/10.1152/jn.00995.2010

Montalto, A., Faes, L., & Marinazzo, D. (2014). MuTE: A MATLAB toolbox to compare established and novel estimators of the multivariate transfer entropy. *PLoS ONE*, *9*(10), e109462. https://doi.org/10.1371/journal.pone.0109462

Morcos, A. S., & Harvey, C. D. (2016). History-dependent variability in population dynamics during evidence accumulation in cortex. *Nature Neuroscience*, *19*(12), 1672–1681. https://doi.org/10.1038/nn.4403

Moreno, R., de la Rocha, J., Renart, A., & Parga, N. (2002). Response of Spiking Neurons to Correlated Inputs. *Physical Review Letters*, *89*(28). https://doi.org/10.1103/PhysRevLett.89.288101

Moreno-Bote, R., Rinzel, J., & Rubin, N. (2007). Noise-induced alternations in an attractor network model of perceptual bistability. *Journal of Neurophysiology*, *98*(3), 1125–1139. https://doi.org/10.1152/jn.00116.2007

Munakata, Y., Herd, S. A., Chatham, C. H., Depue, B. E., Banich, M. T., & O'Reilly, R. C. (2011). A unified framework for inhibitory control. NIH Public Access. https://doi.org/10.1016/j.tics.2011.07.011

Munoz, D. P., & Wurtz, R. H. (1993). Fixation cells in monkey superior colliculus I. Characteristics of cell discharge. *Journal of Neurophysiology*, *70*(2), 559–575. https://doi.org/10.1152/jn.1993.70.2.559

Nambu, A., Takada, M., Inase, M., & Tokuno, H. (1996). Dual somatotopical representations in the primate subthalamic nucleus: Evidence for ordered but reversed body-map transformations from the primary motor cortex and the supplementary motor area. *Journal of Neuroscience*, *16*(8), 2671–2683. https://doi.org/10.1523/jneurosci.16-08-02671.1996

Nambu, A., Tokuno, H., & Takada, M. (2002). Functional significance of the cortico-subthalamo-pallidal 'hyperdirect' pathway. *Neuroscience Research*, *43*(2), 111–117. https://doi.org/10.1016/S0168-0102(02)00027-5

Newman, M. E. J. (2003). *The Structure and Function of Complex Networks ** (tech. rep. No. 2). http://www.siam.org/journals/ojsa.php

Nicolini, C., Bordier, C., & Bifone, A. (2017). Community detection in weighted brain connectivity networks beyond the resolution limit. *NeuroImage*, *146*, 28–39. https://doi.org/10.1016/j.neuroimage.2016.11.026

Nicosia, V., Vértes, P. E., Schafer, W. R., Latora, V., & Bullmore, E. T. (2013). Phase transition in the economically modeled growth of a cellular nervous system. *Proceedings of the National Academy of Sciences of the United States of America*, *110*(19), 7880–7885. https://doi.org/10.1073/pnas.1300753110

Nigam, S., Shimono, M., Ito, S., Yeh, F. C., Timme, N., Myroshnychenko, M., Lapish, C. C., Tosi, Z., Hottowy, P., Smith, W. C., Masmanidis, S. C., Litke, A. M., Sporns, O., & Beggs, J. M. (2016). Rich-club organization in effective connectivity among cortical neurons. *Journal of Neuroscience*, *36*(3), 655–669. https://doi.org/10.1523/JNEUROSCI.2177-15.2016

Obeso, I., Wilkinson, L., Casabona, E., Speekenbrink, M., Bringas, M. L., Álvarez, M., Álvarez, L., Pavón, N., Rodŕguez-Oroz, M. C., Maćas, R., Obeso, J. A., & Jahanshahi, M. (2014). The subthalamic nucleus and inhibitory control: Impact of subthalamotomy in Parkinson's disease. *Brain*, *137*(5), 1470–1480. https://doi.org/10.1093/brain/awu058

Oh, S. W., Harris, J. A., Ng, L., Winslow, B., Cain, N., Mihalas, S., Wang, Q., Lau, C., Kuan, L., Henry, A. M., Mortrud, M. T., Ouellette, B., Nguyen, T. N., Sorensen, S. A., Slaughterbeck, C. R., Wakeman, W., Li, Y., Feng, D., Ho, A., ... Zeng, H. (2014). A mesoscale connectome of the mouse brain. *Nature*, *508*(7495), 207–214. https://doi.org/10.1038/nature13186

Olivito, G., Brunamonti, E., Clausi, S., Pani, P., Chiricozzi, F. R., Giamundo, M., Molinari, M., Leggio, M., & Ferraina, S. (2017). Atrophic degeneration of cerebellum impairs both the reactive and the proactive control of movement in the stop signal paradigm. *Experimental Brain Research*, *235*(10), 2971–2981. https://doi.org/10.1007/s00221-017-5027-z

Oosterlaan, J., Logan, G. D., & Sergeant, J. A. (1998). Response inhibition in AD/HD, CD, comorbid AD/HD + CD, anxious, and control children: A meta-analysis of studies with the stop task. *Journal of Child Psychology and Psychiatry and Allied Disciplines*, *39*(3), 411–425. https://doi.org/10.1017/S0021963097002072

Orlandi, J. G., Stetter, O., Soriano, J., Geisel, T., & Battaglia, D. (2014). Transfer entropy reconstruction and labeling of neuronal connections from simulated calcium imaging. *PLoS ONE*, *9*(6), 98842. https://doi.org/10.1371/journal.pone.0098842

Pani, P., Menghini, D., Napolitano, C., Calcagni, M., Armando, M., Sergeant, J. A., & Vicari, S. (2013). Proactive and reactive control of movement are differently affected in Attention Deficit Hyperactivity Disorder children. *Research in Developmental Disabilities*, *34*(10), 3104–3111. https://doi.org/10.1016/j.ridd.2013.06.032

Paré, M., & Hanes, D. P. (2003). Controlled movement processing: Superior colliculus activity associated with countermanded saccades. *Journal of Neuroscience*, *23*(16), 6480–6489. https://doi.org/10.1523/jneurosci.23-16-06480.2003

Parmigiani, S., & Cattaneo, L. (2018). Stimulation of the Dorsal Premotor Cortex, But Not of the Supplementary Motor Area Proper, Impairs the Stop Function in a STOP Signal Task. *Neuroscience*, *394*, 14–22. https://doi.org/10.1016/j.neuroscience.2018.10.005

Perin, R., Berger, T. K., & Markram, H. (2011). A synaptic organizing principle for cortical neuronal groups. *Proceedings of the National Academy of Sciences of the United States of America*, *108*(13), 5419–5424. https://doi.org/10.1073/pnas.1016051108

Picton, T. W., Stuss, D. T., Alexander, M. P., Shallice, T., Binns, M. A., & Gillingham, S. (2007). Effects of focal frontal lesions on response inhibition. *Cerebral Cortex*, *17*(4), 826–838. https://doi.org/10.1093/cercor/bhk031

Ramos, A., & Macau, E. (2017). Minimum Sample Size for Reliable Causal Inference Using Transfer Entropy. *Entropy*, *19*(4), 150. https://doi.org/10.3390/e19040150

Rieger, M., Gauggel, S., & Burmeister, K. (2003). Inhibition of ongoing responses following frontal, nonfrontal, and basal ganglia lesions. *Neuropsychology*, *17*(2), 272–282. https://doi.org/10.1037/0894-4105.17.2.272

Riehle, A., Grün, S., Diesmann, M., & Aertsen, A. (1997). Spike synchronization and rate modulation differentially involved in motor cortical function. *Science*, *278*(5345), 1950–1953. https://doi.org/10.1126/science.278.5345.1950

Rubia, K., Smith, A. B., Brammer, M. J., & Taylor, E. (2003). Right inferior prefrontal cortex mediates response inhibition while mesial prefrontal cortex is responsible for error detection. https://doi.org/10.1016/S1053-8119(03)00275-1

Sajad, A., Godlove, D. C., & Schall, J. D. (2019). Cortical microcircuitry of performance monitoring. *Nature Neuroscience*, *22*(2), 265–274. https://doi.org/10.1038/s41593-018-0309-8

Salvador, R., Suckling, J., Coleman, M. R., Pickard, J. D., Menon, D., & Bullmore, E. (2005). Neurophysiological architecture of functional magnetic resonance images of human brain. *Cerebral Cortex*, *15*(9), 1332–2342. https://doi.org/10.1093/cercor/bhi016

Sawaguchi, T., Yamane, I., & Kubota, K. (1996). Application of the GABA antagonist bicuculline to the premotor cortex reduces the ability to withhold reaching movements by well-trained monkeys in visually guided reaching task. *Journal of Neurophysiology*, *75*(5), 2150–2156. https://doi.org/10.1152/jn.1996.75.5.2150

Scangos, K. W., & Stuphorn, V. (2010). Medial frontal cortex motivates but does not control movement initiation in the countermanding task. *Journal of Neuroscience*, *30*(5), 1968–1982. https://doi.org/10.1523/JNEUROSCI.4509-09.2010

Scannell, J. W. (1997). Determining cortical landscapes [8]. Nature Publishing Group. https://doi.org/10.1038/386452a0

Schachar, R., & Logan, G. D. (1990). Impulsivity and Inhibitory Control in Normal Development and Childhood Psychopathology. *Developmental Psychology*, *26*(5), 710–720. https://doi.org/10.1037/0012-1649.26.5.710

Schall, J. D. (2015). Visuomotor Functions in the Frontal Lobe. *Annual Review of Vision Science*, *1*(1), 469–498. https://doi.org/10.1146/annurev-vision-082114-035317

Schall, J. D., Palmeri, T. J., & Logan, G. D. (2017). Models of inhibitory control. *Philosophical Transactions of the Royal Society B: Biological Sciences*, *372*(1718), 20160193. https://doi.org/10.1098/rstb.2016.0193

Schmidt, R., Leventhal, D. K., Mallet, N., Chen, F., & Berke, J. D. (2013). Canceling actions involves a race between basal ganglia pathways. *Nature Neuroscience*, *16*(8), 1118–1124. https://doi.org/10.1038/nn.3456

Schreiber, T. (2000). Measuring information transfer. *Physical Review Letters*, *85*(2), 461–464. https://doi.org/10.1103/PhysRevLett.85.461

Schroeder, K. E., Irwin, Z. T., Gaidica, M., Bentley, J. N., Patil, P. G., Mashour, G. A., & Chestek, C. A. (2016). Disruption of corticocortical information transfer during ketamine anesthesia in the primate brain. *NeuroImage*, *134*, 459–465. https://doi.org/10.1016/j.neuroimage.2016.04.039

Schroeter, M. S., Charlesworth, P., Kitzbichler, M. G., Paulsen, O., & Bullmore, E. T. (2015). Emergence of rich-club topology and coordinated dynamics in development of hippocampal functional networks In vitro. *Journal of*

Neuroscience, *35*(14), 5459–5470. https://doi.org/10.1523/JNEUROSCI.4259-14.2015

Scott, S. H., Cluff, T., Lowrey, C. R., & Takei, T. (2015). Feedback control during voluntary motor actions. Elsevier Ltd. https://doi.org/10.1016/j.conb.2015.03.006

Sebastian, A., Rössler, K., Wibral, M., Mobascher, A., Lieb, K., Jung, P., & Tüscher, O. (2017). Neural architecture of selective stopping strategies: Distinct brain activity patterns are associated with attentional capture but not with outright stopping. *Journal of Neuroscience*, *37*(40), 9785–9794. https://doi.org/10.1523/JNEUROSCI.1476-17.2017

Segev, C. (1998). *CHAPTER 1 KINETIC MODELS OF SYNAPTIC TRANSMISSION* (tech. rep.). MIT Press.

Shanechi, M. M. (2019). Brain–machine interfaces from motor to mood. *Nature Neuroscience*, *22*(10), 1554–1564. https://doi.org/10.1038/s41593-019-0488-y

Shannon, C. E. (n.d.). *A Mathematical Theory of Communication* (tech. rep.).

Sharp, D. J., Bonnelle, V., De Boissezon, X., Beckmann, C. F., James, S. G., Patel, M. C., & Mehta, M. A. (2010). Distinct frontal systems for response inhibition, attentional capture, and error processing. *Proceedings of the National Academy of Sciences of the United States of America*, *107*(13), 6106–6111. https://doi.org/10.1073/pnas.1000175107

Shenoy, K. V., Sahani, M., & Churchland, M. M. (2013). Cortical Control of Arm Movements: A Dynamical Systems Perspective. *Annual Review of Neuroscience*, *36*(1), 337–359. https://doi.org/10.1146/annurev-neuro-062111-150509

Shimono, M., & Beggs, J. M. (2015). Functional clusters, hubs, and communities in the cortical microconnectome. *Cerebral Cortex*, *25*(10), 3743–3757. https://doi.org/10.1093/cercor/bhu252

Shine, J. M., Bissett, P. G., Bell, P. T., Koyejo, O., Balsters, J. H., Gorgolewski, K. J., Moodie, C. A., & Poldrack, R. A. (2016). The Dynamics of Functional Brain Networks: Integrated Network States during Cognitive Task Performance. *Neuron*, *92*(2), 544–554. https://doi.org/10.1016/j.neuron.2016.09.018

Smith, S. M., Miller, K. L., Salimi-Khorshidi, G., Webster, M., Beckmann, C. F., Nichols, T. E., Ramsey, J. D., & Woolrich, M. W. (2011). Network modelling methods for FMRI. *NeuroImage*, *54*(2), 875–891. https://doi.org/10.1016/j.neuroimage.2010.08.063

Sporns, O., Honey, C. J., & Kötter, R. (2007). Identification and Classification of Hubs in Brain Networks (M. Kaiser, Ed.). *PLoS ONE*, *2*(10), e1049. https://doi.org/10.1371/journal.pone.0001049

Sporns, O., & Kötter, R. (2004). Motifs in Brain Networks (Karl J. Friston, Ed.). *PLoS Biology*, *2*(11), e369. https://doi.org/10.1371/journal.pbio.0020369

Sporns, O., Tononi, G., & Kötter, R. (2005). The Human Connectome: A Structural Description of the Human Brain. *PLoS Computational Biology*, *1*(4), e42. https://doi.org/10.1371/journal.pcbi.0010042

Stam, C. J. (2004). Functional connectivity patterns of human magnetoencephalographic recordings: A 'small-world' network? *Neuroscience Letters*, *355*(1-2), 25–28. https://doi.org/10.1016/j.neulet.2003.10.063

Stam, C. J., Tewarie, P., Van Dellen, E., Van Straaten, E. C. W., Hillebrand, A., & Van Mieghem, P. (2014). The trees and the forest: Characterization of complex brain networks with minimum spanning trees. *International Journal of Psychophysiology*, *92*, 129–138. https://doi.org/10.1016/j.ijpsycho.2014.04.001

Stark, E., & Abeles, M. (2007). Predicting movement from multiunit activity. *Journal of Neuroscience*, *27*(31), 8387–8394. https://doi.org/10.1523/JNEUROSCI.1321-07.2007

Stephan, K. E., Kamper, L., Bozkurt, A., Burns, G. A., Young, M. P., & Kötter, R. (2001). Advanced database methodology for the Collation of Connectivity data on the Macaque brain (CoCoMac). *Philosophical Transactions of the Royal Society B: Biological Sciences*, *356*(1412), 1159–1186. https://doi.org/10.1098/rstb.2001.0908

Stuphorn, V. (2015). Neural mechanisms of response inhibition. Elsevier Ltd. https://doi.org/10.1016/j.cobeha.2014.10.009

Stuphorn, V., & Schall, J. D. (2006). Executive control of countermanding saccades by the supplementary eye field. *Nature Neuroscience*, *9*(7), 925–931. https://doi.org/10.1038/nn1714

Sussillo, D., Churchland, M. M., Kaufman, M. T., & Shenoy, K. V. (2015). A neural network that finds a naturalistic solution for the production of muscle activity. *Nature Neuroscience*, *18*(7), 1025–1033. https://doi.org/10.1038/nn.4042

Swann, N., Tandon, N., Canolty, R., Ellmore, T. M., McEvoy, L. K., Dreyer, S., DiSano, M., & Aron, A. R. (2009). Intracranial EEG reveals a time- and frequency-specific role for the right inferior frontal gyrus and primary motor

cortex in stopping initiated responses. *Journal of Neuroscience*, *29*(40), 12675–12685. https://doi.org/10.1523/JNEUROSCI.3359-09.2009

Tacchella, A., Cristelli, M., Caldarelli, G., Gabrielli, A., & Pietronero, L. (2013). Economic complexity: Conceptual grounding of a new metrics for global competitiveness. https://doi.org/10.1016/j.jedc.2013.04.006

Tessitore, A., Cirillo, M., & De Micco, R. (2019). Functional Connectivity Signatures of Parkinson's Disease. IOS Press. https://doi.org/10.3233/JPD-191592

Thakkar, K. N., Schall, J. D., Boucher, L., Logan, G. D., & Park, S. (2011). Response inhibition and response monitoring in a saccadic countermanding task in schizophrenia. *Biological Psychiatry*, *69*(1), 55–62. https://doi.org/10.1016/j.biopsych.2010.08.016

Timme, N. M., Ito, S., Myroshnychenko, M., Nigam, S., Shimono, M., Yeh, F.-C., Hottowy, P., Litke, A. M., & Beggs, J. M. (2016). High-Degree Neurons Feed Cortical Computations (J. W. Pillow, Ed.). *PLOS Computational Biology*, *12*(5), e1004858. https://doi.org/10.1371/journal.pcbi.1004858

Timme, N., Ito, S., Myroshnychenko, M., Yeh, F.-C., Hiolski, E., Hottowy, P., & Beggs, J. M. (2014). Multiplex Networks of Cortical and Hippocampal Neurons Revealed at Different Timescales (Z. Wang, Ed.). *PLoS ONE*, *9*(12), e115764. https://doi.org/10.1371/journal.pone.0115764

Tononi, G., Sporns, O., & Edelman, G. M. (1994). A measure for brain complexity: Relating functional segregation and integration in the nervous system. *Proceedings of the National Academy of Sciences of the United States of America*, *91*(11), 5033–5037. https://doi.org/10.1073/pnas.91.11.5033

Towlson, E. K., Vértes, P. E., Ahnert, S. E., Schafer, W. R., & Bullmore, E. T. (2013). The rich club of the C. elegans neuronal connectome. *Journal of Neuroscience*, *33*(15), 6380–6387. https://doi.org/10.1523/JNEUROSCI.3784-12.2013

Trautmann, E. M., Stavisky, S. D., Lahiri, S., Ames, K. C., Kaufman, M. T., O'Shea, D. J., Vyas, S., Sun, X., Ryu, S. I., Ganguli, S., & Shenoy, K. V. (2019). Accurate Estimation of Neural Population Dynamics without Spike Sorting. *Neuron*, *103*(2), 292–308. https://doi.org/10.1016/j.neuron.2019.05.003

Vaadia, E., Kurata, K., & Wise, S. P. (1988). Neuronal activity preceding directional and nondirectional cues in the premotor cortex of rhesus monkeys. *Somatosensory & Motor Research*, *6*(2), 207–230. https://doi.org/10.3109/08990228809144674

Vahid, A., Mückschel, M., Stober, S., Stock, A. K., & Beste, C. (2020). Applying deep learning to single-trial EEG data provides evidence for complementary

theories on action control. *Communications Biology*, *3*(1), 1–11. https://doi.org/10.1038/s42003-020-0846-z

Van Den Wildenberg, W. P., Van Boxtel, G. J., Van Der Molen, M. W., Bosch, D. A., Speelman, J. D., & Brunia, C. H. (2006). Stimulation of the subthalamic region facilitates the selection and inhibition of motor responses in Parkinson's disease. *Journal of Cognitive Neuroscience*, *18*(4), 626–636. https://doi.org/10.1162/jocn.2006.18.4.626

van den Heuvel, M. P., & Hulshoff Pol, H. E. (2010). Exploring the brain network: A review on resting-state fMRI functional connectivity. Eur Neuropsychopharmacol. https://doi.org/10.1016/j.euroneuro.2010.03.008

van den Wildenberg, W. P., & van der Molen, M. W. (2004). Developmental trends in simple and selective inhibition of compatible and incompatible responses. *Journal of Experimental Child Psychology*, *87*(3), 201–220. https://doi.org/10.1016/j.jecp.2003.11.003

Varshney, L. R., Chen, B. L., Paniagua, E., Hall, D. H., & Chklovskii, D. B. (2011). Structural properties of the Caenorhabditis elegans neuronal network. *PLoS Computational Biology*, *7*(2), 1001066. https://doi.org/10.1371/journal.pcbi.1001066

Verbruggen, F., Aron, A. R., Band, G. P., Beste, C., Bissett, P. G., Brockett, A. T., Brown, J. W., Chamberlain, S. R., Chambers, C. D., Colonius, H., Colzato, L. S., Corneil, B. D., Coxon, J. P., Dupuis, A., Eagle, D. M., Garavan, H., Greenhouse, I., Heathcote, A., Huster, R. J., … Boehler, C. N. (2019). A consensus guide to capturing the ability to inhibit actions and impulsive behaviors in the stop-signal task. *eLife*, *8*. https://doi.org/10.7554/eLife.46323

Verbruggen, F., & Logan, G. D. (2008). Response inhibition in the stop-signal paradigm. Elsevier Current Trends. https://doi.org/10.1016/j.tics.2008.07.005

Verbruggen, F., & Logan, G. D. (2009). Proactive Adjustments of Response Strategies in the Stop-Signal Paradigm. *Journal of Experimental Psychology: Human Perception and Performance*, *35*(3), 835–854. https://doi.org/10.1037/a0012726

Vicente, R., Wibral, M., Lindner, M., & Pipa, G. (2011). Transfer entropy-a model-free measure of effective connectivity for the neurosciences. *Journal of Computational Neuroscience*, *30*(1), 45–67. https://doi.org/10.1007/s10827-010-0262-3

Vidaurre, D., Smith, S. M., & Woolrich, M. W. (2017). Brain network dynamics are hierarchically organized in time. *Proceedings of the National Academy of Sciences of the United States of America*, *114*(48), 12827–12832. https://doi.org/10.1073/pnas.1705120114

Vyas, S., Golub, M. D., Sussillo, D., & Shenoy, K. V. (2020). Computation through Neural Population Dynamics. Annual Reviews Inc. https://doi.org/10.1146/annurev-neuro-092619-094115

Watanabe, T., Hirose, S., Wada, H., Imai, Y., Machida, T., Shirouzu, I., Konishi, S., Miyashita, Y., & Masuda, N. (2014). Energy landscapes of resting-state brain networks. *Frontiers in Neuroinformatics*, *8*(FEB), 12. https://doi.org/10.3389/fninf.2014.00012

Wei, W., Rubin, J. E., & Wang, X. J. (2015). Role of the indirect pathway of the basal ganglia in perceptual decision making. *Journal of Neuroscience*, *35*(9), 4052–4064. https://doi.org/10.1523/JNEUROSCI.3611-14.2015

Whelan, R., Conrod, P. J., Poline, J. B., Lourdusamy, A., Banaschewski, T., Barker, G. J., Bellgrove, M. A., Buchel, C., Byrne, M., Cummins, T. D., Fauth-Buhler, M., Flor, H., Gallinat, J., Heinz, A., Ittermann, B., Mann, K., Martinot, J. L., Lalor, E. C., Lathrop, M., ... Garavan, H. (2012). Adolescent impulsivity phenotypes characterized by distinct brain networks. *Nature Neuroscience*, *15*(6), 920–925. https://doi.org/10.1038/nn.3092

White, D. R., & Borgatti, S. P. (1994). *Betweenness centrality measures for directed graphs* (tech. rep.).

Wibral, M., Rahm, B., Rieder, M., Lindner, M., Vicente, R., & Kaiser, J. (2011). Transfer entropy in magnetoencephalographic data: Quantifying information flow in cortical and cerebellar networks. *Progress in Biophysics and Molecular Biology*, *105*(1-2), 80–97. https://doi.org/10.1016/j.pbiomolbio.2010.11.006

Williams, B. R., Ponesse, J. S., Schachar, R. J., Logan, G. D., & Tannock, R. (1999). Development of inhibitory control across the life span. *Developmental psychology*, *35*(1), 205–213. https://doi.org/10.1037/0012-1649.35.1.205

Wise, S. P., Boussaoud, D., Johnson, P. B., & Caminiti, R. (1997). Premotor and parietal cortex: Corticocortical connectivity and combinatorial computations. Annu Rev Neurosci. https://doi.org/10.1146/annurev.neuro.20.1.25

Wollstadt, P., Martínez-Zarzuela, M., Vicente, R., Díaz-Pernas, F. J., & Wibral, M. (2014). Efficient transfer entropy analysis of non-stationary neural time series. *PLoS ONE*, *9*(7), 102833. https://doi.org/10.1371/journal.pone.0102833

Wurtz, R. H., Sommer, M. A., Paré, M., & Ferraina, S. (2001). Signal transformations from cerebral cortex to superior colliculus for the generation of saccades. *Vision Research*, *41*(25-26), 3399–3412. https://doi.org/10.1016/S0042-6989(01)00066-9

Xiong, W., Faes, L., & Ivanov, P. C. (2017). Entropy measures, entropy estimators, and their performance in quantifying complex dynamics: Effects of artifacts, nonstationarity, and long-range correlations. *Physical Review E*, *95*(6), 1–37. https://doi.org/10.1103/PhysRevE.95.062114

Yin, Z., & Zhang, J. (2018). Task-generic mental fatigue recognition based on neurophysiological signals and dynamical deep extreme learning machine. *Neurocomputing*, *283*, 266–281. https://doi.org/10.1016/j.neucom.2017.12.062

Zalesky, A., Fornito, A., Cocchi, L., Gollo, L. L., & Breakspear, M. (2014). Time-resolved resting-state brain networks. *Proceedings of the National Academy of Sciences of the United States of America*, *111*(28), 10341–10346. https://doi.org/10.1073/pnas.1400181111

Zamora-López. (2010). Cortical hubs form a module for multisensory integration on top of the hierarchy of cortical networks. *Frontiers in Neuroinformatics*, *4*(MAR), 1. https://doi.org/10.3389/neuro.11.001.2010

Zeki, S., & Shipp, S. (1988). The functional logic of cortical connections. Nature. https://doi.org/10.1038/335311a0

Zingg, B., Hintiryan, H., Gou, L., Song, M. Y., Bay, M., Bienkowski, M. S., Foster, N. N., Yamashita, S., Bowman, I., Toga, A. W., & Dong, H. W. (2014). Neural networks of the mouse neocortex. *Cell*, *156*(5), 1096–1111. https://doi.org/10.1016/j.cell.2014.02.023